NTNU

Norwegian University of
Science and Technology

Elastic Properties of Flexure Patterns

Characterization, Classification and
Development of Design Principles by
Parametric Finite Element Analyses

Oddvin Agnalt Østmo

Master of Science in Mechanical Engineering
Submission date: June 2018
Supervisor: Nils Petter Vedvik, MTP
Co-supervisor: Martin Steinert, MTP

Norwegian University of Science and Technology
Department of Mechanical and Industrial Engineering

Abstract

A flexure pattern increases the ability of a plate to undergo large elastic deformations. It is characterized as a 2D mechanical metamaterial that consist of flexures configured in a pattern that increase the compliance compared to the bulk material of which it has been made. This work contributes to the basic understanding of flexure patterns by describing the geometry, symmetries, principle deformation mechanisms and anisotropic elastic properties, using of the computational homogenization technique. The criteria for diagonal, orthogonal, tetragonal and isogonal elasticity is categorized though the minimal symmetries found in the pattern. Various examples of auxetic (materials with negative Poisson's ratio), orthogonal and isogonal patterns are explored and the relations between geometrical parameters and elastic properties are found. A set of design principles and methods are compiled to a framework that enables creation of new patterns from a set of desired behaviors.

Sammendrag

Et bøyningsmønster øker platers evne til store elastiske deformasjoner og karakteriseres som et 2D mekanisk metamateriale som består av fleksible elementer sammensatt i et mønster som øker bøyeligheten, sammenlignet med det opprinnelige materialet det er laget av. Denne oppgaven bidrar til å øke den grunnleggende forståelsen av geometrien, symmetrien, prinsipielle deformasjonsmekanismer og de anisotrope egenskapene gjennom homogenisering og elementmetoden. Kriteriet for diagonal, ortogonal, tetragonal og isogonal elastisitet er kategorisert gjennom det laveste antallet symmetrier et mønster kan ha. Interessante eksempler av auxetiske (materialer med negativ Poisson's tall), ortogonale og isogonale mønster er vist i tillegg til effektene små endringer av geometrien kan ha for stivheten. Designprinsipper og metoder er sammenfattet til et rammeverk som kan bli brukt til å lage nye mønster med ønsket oppførsel.

Contents

List of Tables

List of Figures

Preface

When first introduced to a physical copy of a flexure pattern, it is hard not to be fascinated. The structure is particular decorative to the eye with all kinds of different symmetries which makes it easy to get lost when trying to understand under which rules the pattern repeats itself. It is also a rare case to encounter materials that are stiff and hard, but behaves flexible and that has different properties in different directions. A flexure pattern is also an effective way of integrating functionality into a material. Thus, it is a technique which has shown great potential for making sophisticated designs and to make simpler assemblies leading to reducing production costs and a more effective material use.

The qualities and properties of the technique highlighted above are some of the main reasons the topic caught my attention about a year ago. Ever since my first encounter with this concept, it has been an interesting journey to explore different aspects of flexure patterns. Perhaps the biggest surprise after being working with this topic for a year, was to find out how little is written about it. There are many related fields like the field of compliant mechanisms and meta-materials, but the lack of publications that describes it was also a great motivator for revisiting the simple concepts to describe a flexure pattern.

The path of exploring the different sides of flexure patterns starts with the geometrical aspects. The interest in patterns are as old as civilization and have fascinated the human mind ever since. Impressive geometrical patterns in mosaics and decorations found in artifacts and architecture, date back to ancient times.

Within the field of mathematics, many aspects of geometric patterns and tilings have been thoroughly studied. Kepler wrote on tilings in his book *Harmonice Mundi* in 1619, but the work was largely forgotten for many centuries. Throughout the nineteenth century, the field became popular again and is today a large field. In the case of flexure patterns, some important concepts are borrowed from this in order to describe the topology of a repetitive pattern.

Furthermore, the mechanical relations were to be investigated. Mechanics is the oldest branch of physics and is probably the most intuitive to human beings. Simple principles show the relations between different flexible members deflect and yet simple principles govern the creation of more compound flexible mechanisms.

By digitizing the knowledge and models, one can make rapid changes and produce large data sets within a short time. The efficiency of the computer was therefore the chosen tool for discovering many properties of different flexure patterns. In this way it also becomes an easy task to share the tools, so others can make use of them.

Content and organization

This thesis is written in a multiple chapter format with the following chapters: an introduction, which introduces the research topic, related concepts, as well as its relevance; a background, which review relevant literature and theories, showing how this has informed the research issue; a methodology chapter, explaining how the research has been designed and why the research methods, data collection and analysis, have been chosen. A results chapter, outlining the findings of the research itself; a discussion chapter, analyzing the findings and discussing them in the context of the literature; and lastly a conclusion.

Throughout all chapters, three topics are visited and discussed in its respective sections. These are essential to understand - and effective to describe - various aspects of flexure patterns. The topics are: the geometrical understanding of a repeating structure, the mechanical response of compliant structures and computational techniques.

Objectives

In order to facilitate the further work for utilizing flexure patterns in applications the following objectives are defined for this thesis:

1. Establish the geometry-symmetry conditions in order to (a) understand and (b) create new patterns
2. Establish a numerical model to quantify the properties of any given pattern
3. Make a tool for adjusting parameters of new flexure patterns efficiently to make it easier for people to make and utilize the patterns

Limitations

Within the topic of flexure patterns there are many things one could investigate. As a result of having a limited time span for the thesis many potentially interesting approaches are left out of. Some of the limitations are described bellow. These are however closely related to the further work proposed in 5.7.

1. *Linear elastic deformation*: the predicted behaviour of flexure patterns do not account for non-linear effects that change the stiffness behaviour of the flexure pattern. Effects like strength, fracture mechanics and fatigue probably play a significant role for the durability of the flexure pattern in applications, but is not within the scope of this study.
2. *Numerical approach*: the nature of solving a problems numerically instead of analytically, implies there is a correlation between input parameters and output parameters. The results are not derived or proved, but a discussion on the reliability of the results are done. Some validation of the numerical models was done in the Project work of fall 2017, but physical testing is not within the scope of this study.
3. *Geometry*: there are numerous ways flexures can be combined in the plane. Here only a few geometries are investigated.

4. *Implementation*: there is a limit in how far the code is being implemented into a finished product. The work that has been preliminary for making a program for generating flexure patterns.

Acknowledgements

I will first give a huge thanks to my excellent supervisor Nils Petter Vedvik for a sincerely dedication in this work. The feedback, guidance and theoretic input has been invaluable for the result presented here.

This work is also based on the preliminary study on flexure patterns by Stian Waagner Birkeland, Eivind Lystad Grimstad and myself from the fall of 2017. The cooperation during the project has been a flying start for this thesis and deserves its acknowledgement.

For help of making this thesis easier to read and for spotting some of my crooked formulations, recognition is given Nora Arnøy and Olav-Kjetil Myrvang.

It is worth to mention the motivation given by my family, the support from Tale Buan Dahlen and all friends that have encouraged me and made jokes about my new hobby of "finding new patterns everywhere". I am grateful to all of you.

Homage is also due to the people whom have helped me in this endeavor that have not been mentioned specifically. Thank you.

Oddvin Agnalt Østmo

Department of Mechanical and Industrial Engineering
NTNU, the Norwegian University of Science and Technology
Trondheim

Acronyms and symbols

Acronyms

ASI	abaqus scripting interface
CA	compliant array
CAD	computer aided design
CAE	computer aided engineering
CAM	computer aided manufacturing
DOF	degree of freedom
FEM	finite element method
FEA	finite element analysis
LEM	lamina emergent mechanism
LET	lamina emergent torsional hinge
MTP	Department of Mechanical and Industrial Engineering
MDF	Medium-density fiberboard
NTNU	Norwegian University of Science and Technology
PMMA	Poly methyl methacrylate
RVE	Representative volume element

Symbols

A	area
C_{ij}	stiffness coefficients
E	Young's modulus
F	force
G	shear modulus
I	moment of inertia
J	moment of torsional inertia
k	general stiffness component
K	general geometric stiffness
L	length of beam
M	bending moment
N	normal force
R	radius
T	torsion moment
U	energy
V	volume
u, v, w	displacements components
x, y, z	Cartesian coordinates
α	angle of principal axes
γ	shear strain
δ	partial
Δ	distance between points
ε	normal strain
ϵ	macroscopic strain
θ	angle of rotation, counter clockwise
κ	curvature
ν	Poisson's ratio
σ	stress
Σ	macroscopic stress
τ	shear stress

Matrices and vectors

Matrices and vectors are denoted with square brackets $[\bullet]$.

A laminate in plane stiffness

B laminate coupling stiffness matrix

C stiffness matrix

D laminate bending matrix

Q plane stress stiffness matrix

S laminate compliance matrix

ε strain vector

κ curvature vector

Chapter 1

Introduction

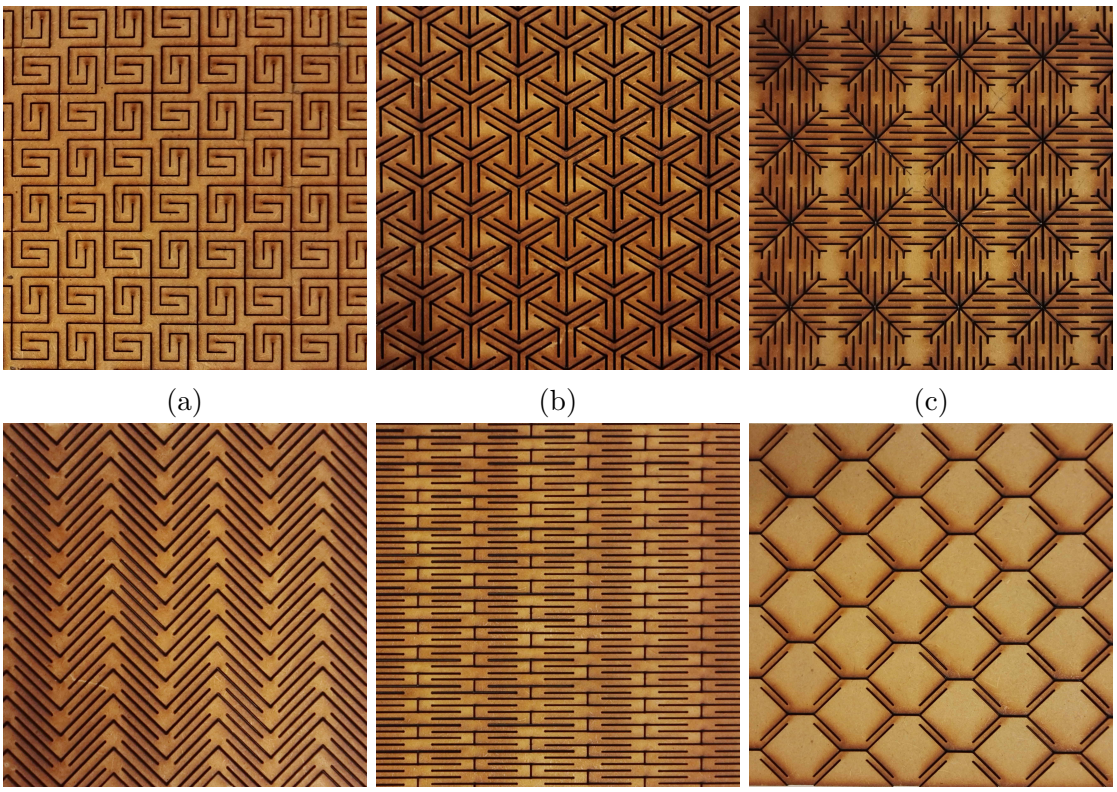

(a) (b) (c)

(d) (e) (f)

Figure 1.1: Examples of different flexure patterns.

1.1 What is a flexure pattern?

The term *flexure pattern* is used in this thesis for the concept of introducing specific cuts in a plate in order to reduce the resistance to bending and stretching. The most characteristic property of a flexure pattern is the ability to make a superelastic and flexible surfaces from a hard material. The concept appeared first in various *Maker Spaces* and home at hobbyists with access to a laser cutter and has been around for a decade ago.

It is emphasized that this thesis *introduces the definition* of flexure patterns as it is a term invented by the author and his co-authors from the project thesis in the autumn of 2017. Other terms like *living hinge, lattice hinge, kerf bend* and *compliant array* is also used for the same concept. A discussion on the terminology is found in section 5.1.

In order to develop a language to describe the different elements of a flexure pattern precise, a definition is needed:

A flexure pattern is characterized as a 2D mechanical metamaterial that consist of flexures configured in a pattern that increase the compliance compared to the bulk material of which it has been made. The flexures are patterned onto the plane according to a set of rules.

Flexure patterns have a bending dominated structure. This is in opposition to *lattice truss materials* where optimal design lead to a stretching dominated structure [2]. A building block to achieve large deformation is the *flexure* which is a flexible member that is engineered to be compliant in some DOFs. It rely on elastic deformation in various modes like bending and torsion to achieve larger travel distances than what is achieved through tensile or compression Th term flexibility is also used to describe the ability to bend. A *flexure region* is the part of a flexure pattern that consists of a flexure or a configuration of flexures. The flexure region is engineered to be compliant and is responsible for most of the increased travel distances found in a flexure pattern. A flexure region can be a flexure mechanism which is used synonymously to compliant mechanisms, or more generally as a flexure configuration. A *rigid region* is the rigid part of a flexure pattern where flexures meet to form a joint or a larger area of the flexure pattern where no flexures are present. More background on flexure elements, configurations and compound flexure mechanisms is given in section 2.3.

The term *pattern* is defined as a combination of qualities, acts, tendencies, etc., forming a consistent or characteristic arrangement(...)[4]. When speaking of a *periodic flexure pattern* one can define the elements for patterning the plane through two non-parallel vectors: the unit of the pattern. The *unit of the pattern* corresponds to the smallest region that preserves all symmetries of the pattern when translated under two non-parallel vectors. The unit of the pattern is defined independently of the flexure configuration and can sometimes seem a bit odd when describing the flexure pattern as we observe it. A better method for describing a repeating region of a pattern is by the *prototile*. This correspond to the tile or set of tiles that capture the whole flexure configuration as a continuous piece and can be used to tile the plane though a translation in two directions. More background on the terms of periodicity, unit and prototile is found in sections 2.1.3 and 2.1.1.

As a flexure pattern is defined as a mechanical metamaterial, it is interesting to look at the bottom up approach for creating metamaterials. This includes constructing patterns that can repeat with other rules than periodicity like a non-periodic manner like Voronoi tilings or an aperiodic manner. The aim can be a structure that create equal curvature for an uneven loaded plate. More information on meta materials is given in section 2.2.

1.1.1 Classification

By breaking a complex structure into its less complex constituents, it is possible analyze and understand the governing principles. A flexure pattern is classified according to the

flexure configuration and the *plane symmetry groups*. The plane symmetry groups are used to classify the general symmetries present in the pattern and include periodicity, reflections, rotations, and glide reflections. The flexure configurations are different ways to combine flexures in arrays, or in compound mechanisms that involves multiple flexures.

An example of a classification is *LET p4m*. This refers to the flexure configuration of a *LET* or *lamina emergent torsion hinge* and the plane symmetry group *p4m*. A schematic representation of the different elements of a flexure pattern can be seen in figure 1.2.

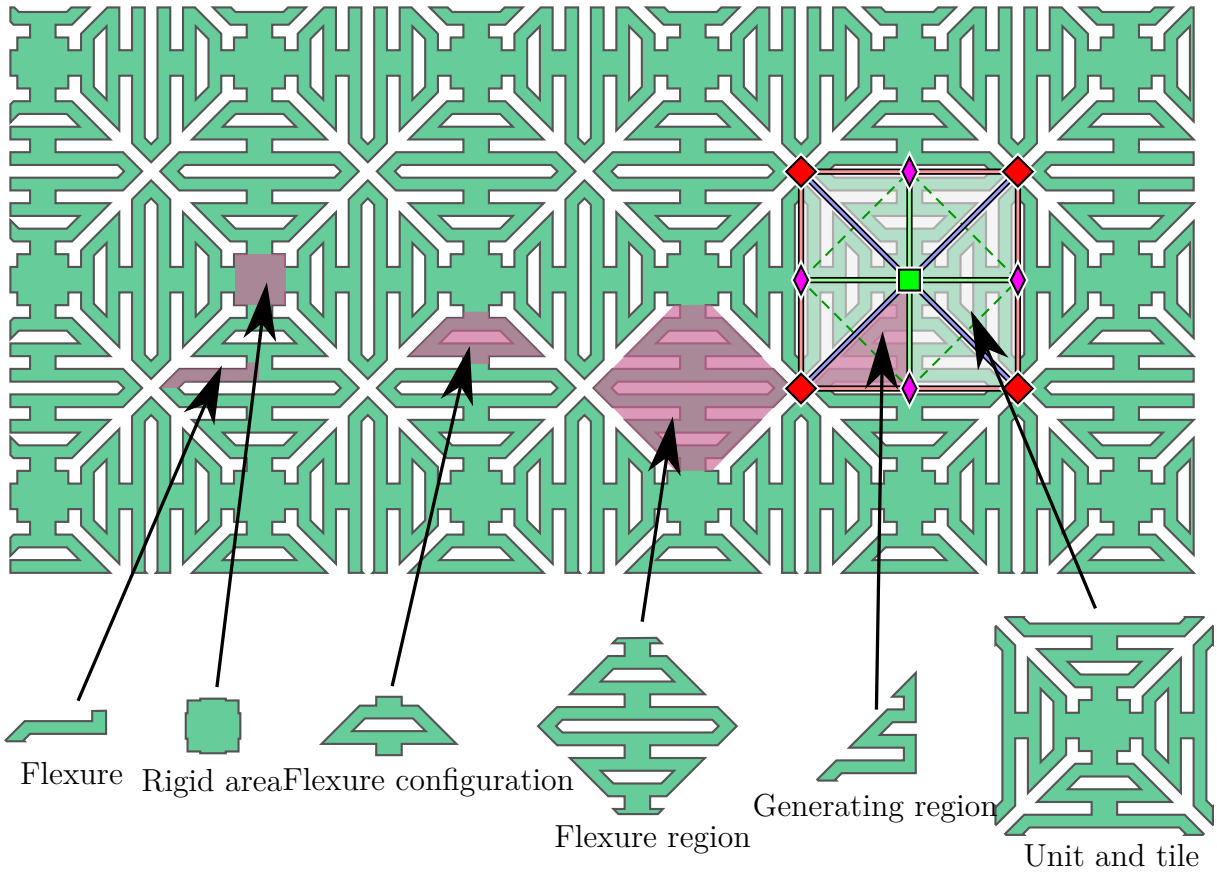

Figure 1.2: Differents parts of a flexure pattern. Here presented for a *LET p4m* pattern.

1.1.2 Behaviour

When deformed, a complex system of flexible members work together to achieve a larger deformation than would be impossible if it was not any cuts in the material.

The behaviour of flexure patterns are diverse and rely on the symmetry of the pattern and the flexure configuration. The qualitative modes to bending and stretching are obviously different, as well for the different response when deformed in a direction. Some flexure patterns show equal behaviour in 2, 3, 4 or 6 directions while other show almost no difference when bent or stretched in different directions. This *anisotropy*, the unequal stiffness[1] properties along different axes is discussed in section 5.2.2.

[1]The term stiffness is used in this thesis to describe the elastic resistance to a force or a moment.

(a) A flexure pattern bent along one axis and with a smooth surface.

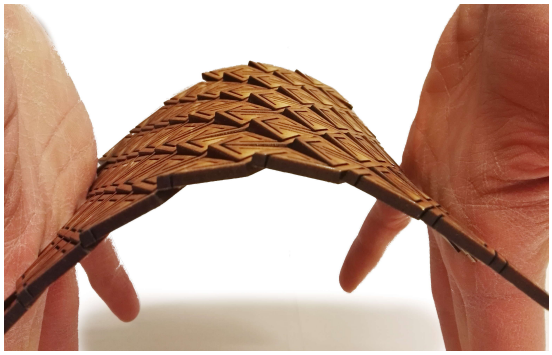

(b) A flexure pattern bent along one axis, but with parts sticking up.

(c) A flexure pattern that deforms in a stepwise manner.

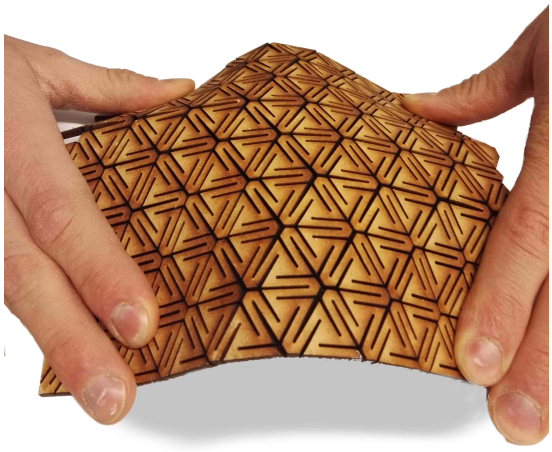

(d) The response of a flexure pattern with double curvature.

Figure 1.3: Examples of responses of flexure patterns.

The behaviour of flexure patterns also vary when parameters that describe the geometry, like length, thickness and width is varied. The trends of the quantitative response is important to understand how to change the stiffness when designed to meet target properties. This is discussed further in section 5.2.1.

In some cases the stretching trigger a rare behaviour where axial motion results in an expansion of the pattern in the opposite direction. This is called an *auxetic* behaviour and is characterized by a negative Poisson's ratio and is discussed in section 5.2.3.

1.2 Manufacturing

A popular method for manufacturing flexure patterns is by CNC laser cutting. Even though any material that can be cut with a laser cutter is suitable as a base for manufacturing flexure patterns, the popular choices are ply wood and medium-density fiberboard (MDF) plates due to its low price and easy accessibility. Another popular material is ploy methyl methacrylate (PMMA) because it is easily cut, but the brittle behaviour results in the flexure pattern being at risk of cracking. The CNC laser cutting and ply wood /

MDF combination takes short time to manufacturing and is relative cheap compared to other techniques and materials.

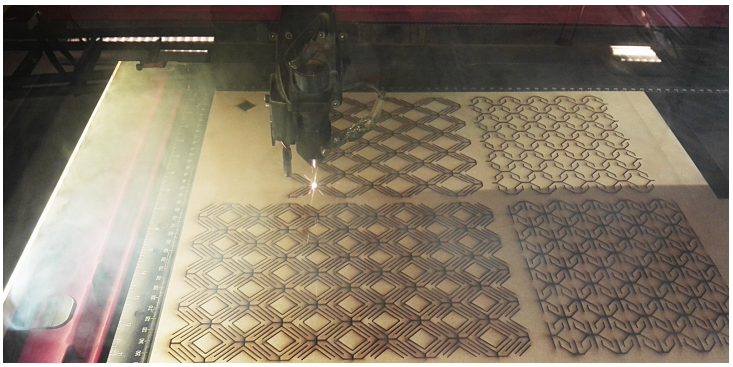

Figure 1.4: The making of flexure patterns out of a MDF plate on a laser cutter.

Other possible subtractive manufacturing methods are: water cutting, milling and plasma arc cutting. The advantages of these are primary the possibilities to cut thicker materials and to cut metals. Within additive manufacturing 3D printing is a promising candidate. As 3D printed products are often designed for a reduced assembly, flexure patterns can be used to integrating functionality into the 3D printed product or to get different material behaviour.

1.3 Applications

Flexure patterns have much potential and have shown its applicability in manufacturing 3 dimensional flexible objects from flat plates. Various blogs and sites from the *maker community* promote several free designs like the ones seen in figure 1.5. Other architecture projects with flexure patterns involve simple shapes and objects like enclosures, book covers, chairs and lamps are some examples.

Figure 1.5: Some examples of free designs on pages for the maker community.

More engineering demanding applications are shape changing structures, surfaces of double curvature and structures where deploy-ability and size is important. Double curvature surfaces has long been a challenge in the boat hull design industry while deployable

structures are of interest of space organizations as deployable solar panels [39] and in research for human shelters [28]. Applications of shape-changing structures have been introduced in wearable electronics where flexible lithium-ion batteries [34] flexible circuit boards [38] are good examples.

1.3.1 Advantages

Flexure patterns can have advantages in product and material design compared to traditional solid plates of a soft material or rigid-body mechanisms. Many of the listed advantages are shared with lamina emergent mechanisms (LEMS)[1]

Reduced assembly Products manufactured from one sheet are often monolithic; being made of one piece. Techniques from origami inspired design can create folding structures that require little assembly.

Planar manufacturing Flexure patterns are fabricated from flat materials which can reduce costs while still remaining good tolerances.

Size and weight saving Products that can be stored flat allow saving costs in regards of storage space or transportation, as the assembly can be done at a later time. This can also be practical in aerospace, outdoor equipment, invasive surgery or space-saving furniture or utilities in apartments. The space saving aspect combined with the in-plane manufacturing also allows for emergency devices that do not take up much space, for example self-assembling structures that activates remotely when needed [12].

Double curvature surfaces Flexure patterns can introduce auxetic material properties to a plate that otherwise do not show this behaviour. Auxetic materials deform such that they easily can make domes, a shape that for solids usually require high stresses. The ability to relieve these stresses allow for even more complex structures like three dimensional objects like faces, helmets and shoes made from flat sheets [19] [11].

Different properties in different directions Moving plates might have desired directions of bending and stretching. Flexure patterns can be manufactured with properties according to the specific application.

Chapter 2

Background

The theory given in this chapter lays the foundation for the objectives with emphasis on: (1) elaborating on the basic understanding by describing the deformation mechanisms and (2) to obtain the properties of different flexure patterns. To accomplish the first, plane geometry and the mechanics of flexible members play an important role. This includes various ways of viewing the geometric patterns: as *tiles*, *periodic patterns* and as flexible beams that undergo deformation. For the latter objective, *plate theory*, *material science* and *computational homogenization* show to be especially useful. We investigate some exciting fields of the new field of metamaterials but also go back to basics when the constitutive equations are carried out.

2.1 Plane geometry

Symmetries and different possible ways to pattern the plane by shapes can be described by logical and mathematical rules. This is the foundation in which the geometry of flexure patterns can be understood and described from a scientific perspective. Here, are an introduction to some concepts relevant to flexure patterns given. The classifications and definitions are of great importance when the rules of the geometry are coded into a computer program as well as it serves as good sources for inspiration when new patterns are to be constructed.

The main sources for the fields of *tiling* and *symmetry groups* in the literature are the works of Garcia [9] and Schattschneider [32] where the concepts are precisely described.

2.1.1 Tiling

Through tiling, one can study the different ways one can arrange the boundary flexure configurations in the plane and study how the boundaries are connected. It is a simplification where the flexures are left out, and only the different ways to combine different shapes are considering. A *plane tiling* [1] is a set of shapes that fits together. More formally it is a countable family of closed shapes that covers the plane with no overlapping or empty spaces [9]. By the plane we mean the *Euclidean plane* of elementary geometry which preserves qualities like straightness, length, angle, area and congruence.

[1] The words tessellation, paving, mosaic and parqueting are used synonymously in other literature.

The closed shapes are also known as *tiles* which generally can be considered a *topological disk* whose boundary is a single simple closed curve. By this we mean a curve with ends that join to form a *loop* with no crossings or branches. The intersections between tiles are the points and arcs. A point laying in the intersection between three or more tiles is called a *vertex* and the arcs between the vertices are called *edges*. The number of edges that meet at a vertex is called the *valence* of the vertex. In general vertices, edges and tiles are called the *elements* of a tiling.

A special type of tilings that is considered here, consists only of polygons. As polygons often are referred to with edges and vertices, it could lead to confusion to use these terms here, so the corresponding terms for a polygon will be *corners* and *sides*.

An overview of the different types of tilings are shown in figure 2.1.

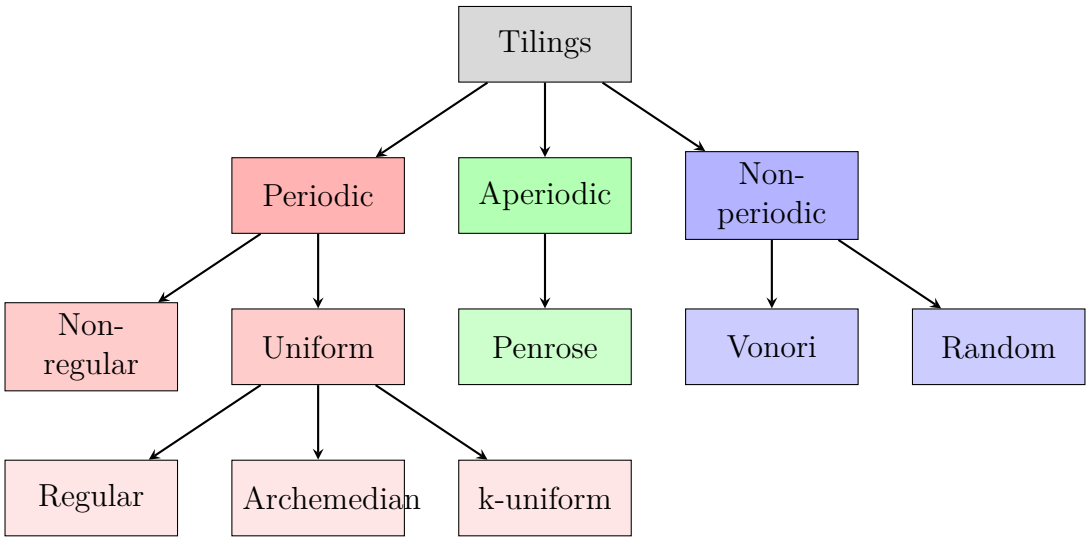

Figure 2.1: An overview of different tilings.

Tiling with tiles of a few shapes

The simplest tiling can be said to be the ones which are made with only one shape. These are called *monohedral* which means that every tile of the tiling is congruent. A familiar example of monohedral tilings are the *regular tilings* as shown in figure 2.2. These are tiles made from regular polygons where all edges, angles and vertices are equal. These polygons are also the only regular polygons that tile the plane monohedrally. A simple proof for this can be seen when inspection the interior angles of the polygons. As a tiling has no gaps or overlaps, the angles at each vertex must add up to 360°, thus the interior angle must be a multiple of 360. The formula for a regular polygon is given in equation 2.1 where $m\angle$ is the interior angle and n_r is is the number of sides. From this, it becomes evident that the triangle, square and hexagon are the only regular polygons to tile the plane.

$$m\angle = \frac{180(n_r - 2)}{n_r} \qquad general formula \qquad (2.1)$$

$$m\angle = \frac{180(3 - 2)}{3} = 60^\circ \qquad triangle \qquad (2.2)$$

$$m\angle = \frac{180(4 - 2)}{4} = 90^\circ \qquad square \qquad (2.3)$$

$$m\angle = \frac{180(5 - 2)}{5} = 108^\circ \qquad pentagon \qquad (2.4)$$

$$m\angle = \frac{180(6 - 2)}{6} = 120^\circ \qquad hexagon \qquad (2.5)$$

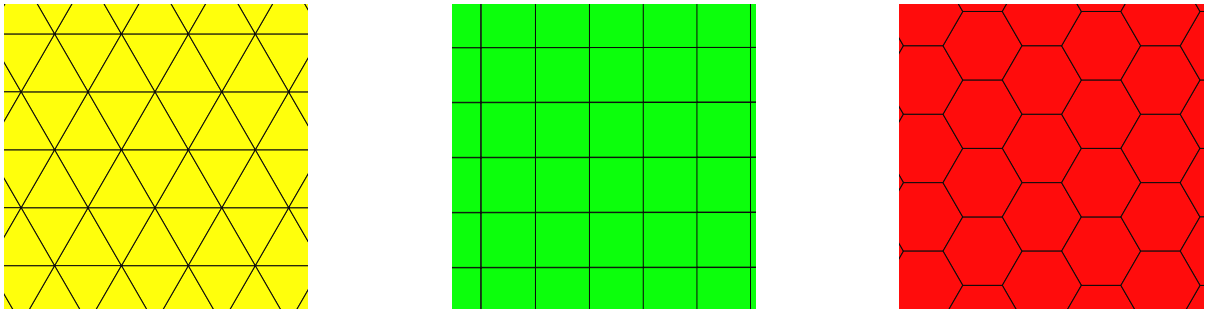

Figure 2.2: The 3 regular tilings of the plane.

The regular tilings have all the same vertices. When cycled around the vertices, the sides of the polygons that come together are listed. We say that the regular tilings are of types 3.3.3.3.3.3, 4.4.4.4 and 6.6.6. A shorter notation often used is $(3^6), (4^4)$ and (6^3). Similar notation is used for for the uniform tilings. Figure 2.3 shows this for an Archimedian tiling.

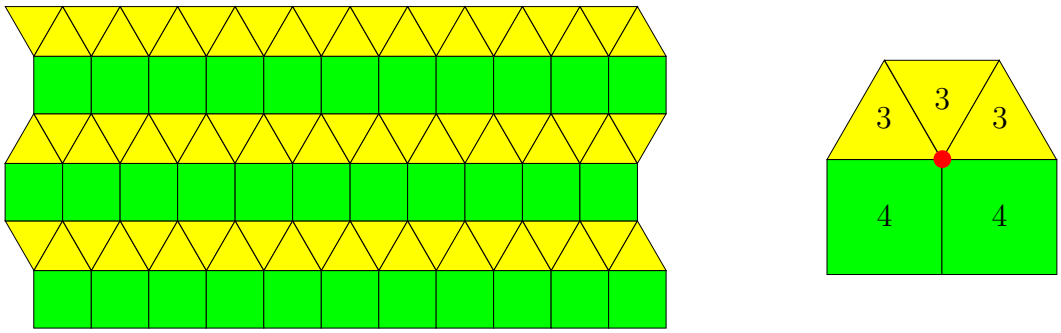

Figure 2.3: A tiling notated as 3.3.3.4.4 or $3^3.4^2$.

The problem of monohedral tilings becomes more complex when other polygons are considered. An illustration of this is represented by the fact that we don't know all the different convex pentagons that tiles tile the plane monohedrally. The last tiling in figure 2.4 was discovered in 2015.

Sticking to regular polygons, the case gets much more interesting when multiple regular polygons are considered to tile the plane. The criteria for a tiling with no gaps and overlaps

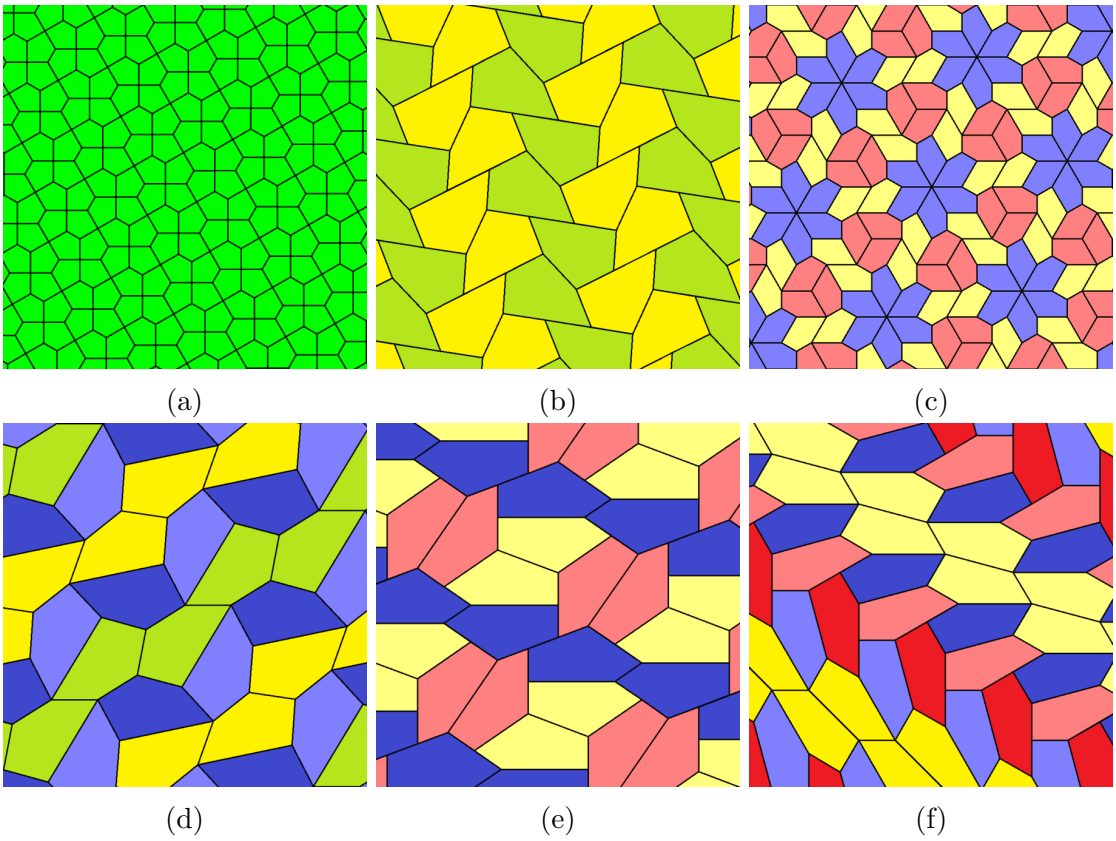

Figure 2.4: Monohedral tilings with convex pentagons.

still remain: the sum of interior angles for each polygon at a vertex should equal 360°. Together with equation 2.1, the sum of these show that there are only 17 combinations that satisfy the equation

$$\frac{n_1 - 2}{n_1} + ... + \frac{n_r - 2}{n_r} = 2 \tag{2.6}$$

Among these 17, four of the cases has two distinct ways in which the polygons can be arranged, resulting in 21 possible types. In addition there are needed a few assertions to not end up with infinite possibilities of possible tiles.

With the restrictions, the following result: there are precisely 11 distinct edge-to-edge tilings by regular polygons such that all vertices are of the same type. These are (3^6), $(3^4.6)$, $(3^3.4^2)$, $(3^2.4.3.4)$, $(3.4.6.4)$, $(3.6.3.6)$, (3.12^2), (4^4), $(4.6.12)$, $(4, 8^2)$ and (6^3). These are usually called the *Archemedian* tilings [2]. A figure of the Archimedian tilings where the regular tilings are left out is seen in figure 2.5.

All these tilings are isogonal which means that all its vertices are equivalent under the symmetries of the figure [3]. For this reason the tilings is also called *uniform*. This distinction from means that not only does the vertices of the neighbouring vertices look the same, but is also equivalent under the symmetry of the figure.

[2]some literature call these homogeneous or semi regular, even though they include the three regular tilings.

[3]This implies that each vertex is surrounded by the same kinds of face in the same or reverse order, and with the same angles between corresponding faces.

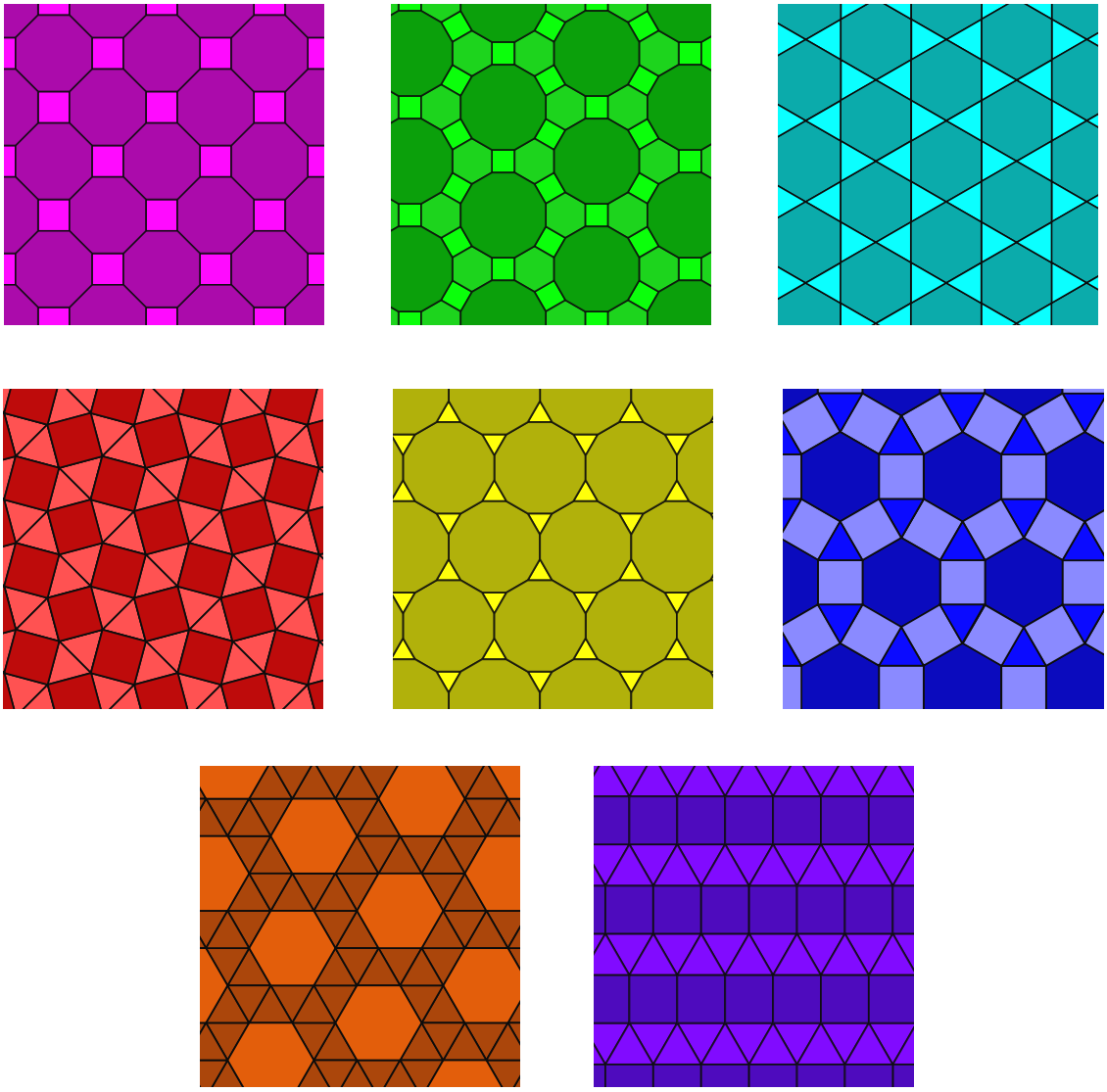

Figure 2.5: The Archimedian tilings.

The observation that the Archemedian tilings are isogonal and therefore uniform, point in the way of a generalization. An edge-to-edge tiling by regular polygons is called k-uniform if its vertices form precisely k transitivity classes with respect to the group of symmetries of the tiling. In other words: the arrangement of polygons are the same at each k-vertex. It is interesting to know that there exists up to 7-uniform tilings and that all possibilities are known, see table 2.1. There is however no point on elaborating the concept more as only some of the Archemedian tilings are used later in this thesis to form new flexure patterns, even though the possibilities are great.

k-uniform	number of tilings
k = 1	11 tilings
k = 2	20 tilings
k = 3	39 tilings
k = 4	33 tilings
k = 5	15 tilings
k = 6	10 tilings
k = 7	7 tilings
k = 8	no tilings

Table 2.1: Number of tilings for each k-uniform [9]. Regular tiling are k-uniform when there are precisely k different kinds of tiling. k is the different kinds of vertices that shows up in the tessellation.

Non-regular tiling

Non-regular polygons don't follow the same strict rules, resulting in an infinite number of different tiling possibilities. An example of a non-regular and non-uniform tiling is shown in figure 2.6.

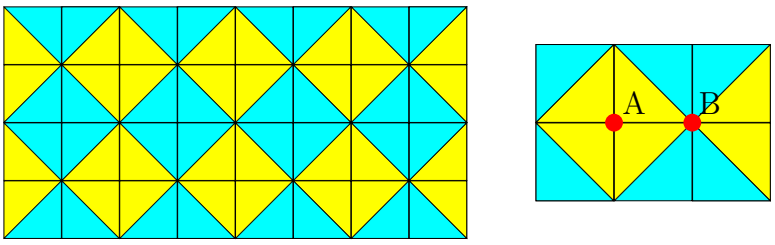

Figure 2.6: A tiling consisting of non-regular triangles. Point A has four meeting polygons while point B has eight.

2.1.2 Symmetry and regularity

Many important mechanical properties of flexure patterns depend upon the idea of symmetry. In this section we explain what is meant by the term and give examples of flexure patterns with various kind of symmetry.

An *isometry* or *congruence transformation* is any mapping of the Euclidean plane E^2 onto itself which preserves all distances. A mapping is denoted as $\sigma : E^2 \to E^2$ and A and B are two points. Then the distance between A and B is equal to the distance between the images $\sigma(A)$ and $\sigma(B)$. Less, formally it can be stated that an isometry is a transformation of the pattern so it looks the same after the transformation.

It can be shown, but is never the less, intuitive that every isometry is of one of four types, also seen in figure 2.7:

1. *Rotation* about a point O through an angle θ. The point O is the center of rotation. In the case when $\theta = \pi$ the line joining A to $\sigma(A)$ will be bisected by O, and in case the mapping is called a *2-fold rotation*, half turn, central reflection or reflection in the point O.

2. *Translation* in a given direction through a distance d.

3. *Reflection* in a given line L, is called the *mirror* or *line of reflection*

4. *Glide reflection* where a reflection in a line is combined with a translation through a given distance d parallel to the line.

The rotation and translation isometries are usually called *direct* because if point ABC form the vertices of a triangle named clockwise, then the same is true for the transformed image. The reflection and glide reflection will, however for the ABC triangle create a new triangle with vertices named counterclockwise. They are therefore called *indirect* or *reflective* isometries.

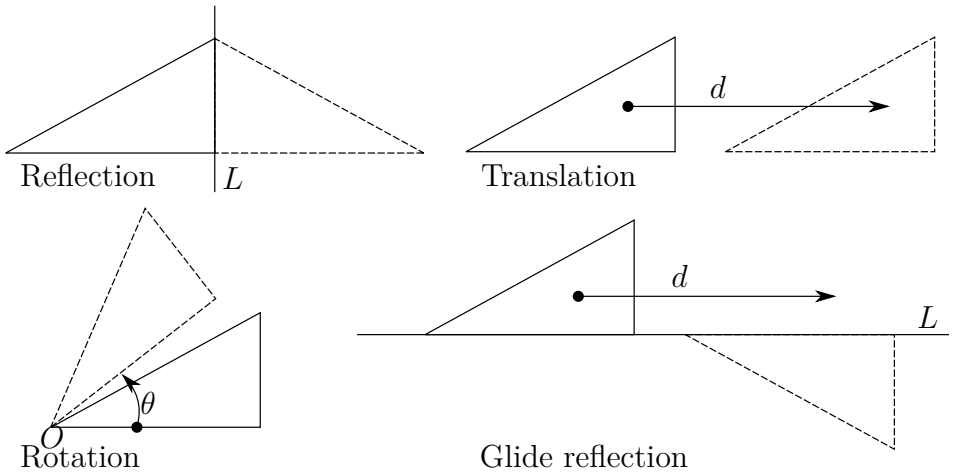

Figure 2.7: The four shape preserving transformations.

By a symmetry of a set S we mean an isometry σ that maps S onto itself. As an example, any rotation about the center of a circular disk is a symmetry of the disk. In the case of a square, as seen in figure 2.8, the reflections in the lines L_1, L_2, L_3 and L_4 are symmetries. The rotations of angle $\pi/2, \pi,$ and $3\pi/2$ about the center are also symmetries. The center is then called a *center of 4-fold rotational symmetry.* More generally a symmetry by rotation of $2\pi/n$ about a point is a *center of n-fold rotational symmetry.* Since centers of rotation of a pattern are mapped by translation to new centers of rotation, only rotations of order 2, 3, 4, and 6 can occurs as isometries of a periodic pattern[4].

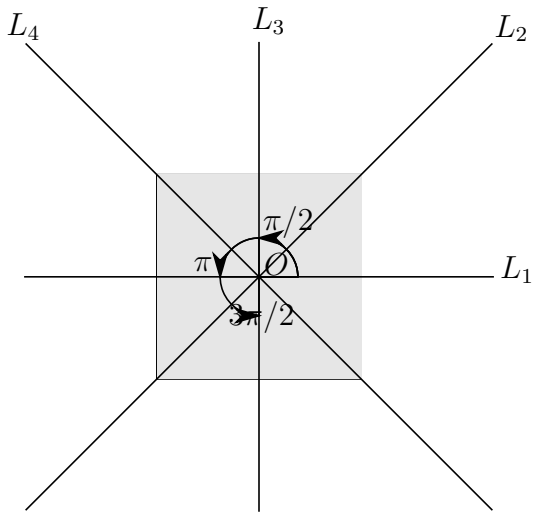

Figure 2.8: Example of the symmetries of a square. L_1, L_2, L_3 and L_4 are reflective lines, while $\pi/2, \pi, 3\pi/2$ are rotational symmetries. Rotation of 2π is the identity symmetry.

The isometry that maps every point onto itself is known as the *identity isometry.* It is a symmetry of every set. In the case of the square, it contains eight symmetries: four reflections, three rotations and the identity isometry.

A *motif* of the pattern is a distinctive and reoccurring form. If a motif has any symmetry in addition to the identity symmetry then it is called *symmetric.* If its symmetry group contains at leas two translations in non-parallel directions, then the motif is called *periodic.* By representing the two non-parallel translations by the vectors a and b. Then the pattern contains all translations $na + mb$ where n and m are integers. Starting from any fixed point, the set of images under the set of translations $na + mb$ forms the *lattice.* It can then be stated that with every periodic pattern, there is associated a lattice, and the point of the lattice can be regarded as the vertices of a parallelogram with the five shapes shown in figure 2.9 where the two non-parallel sides represents the vectors a and b.

[4]This is often referred to as the crystallographic restriction theorem

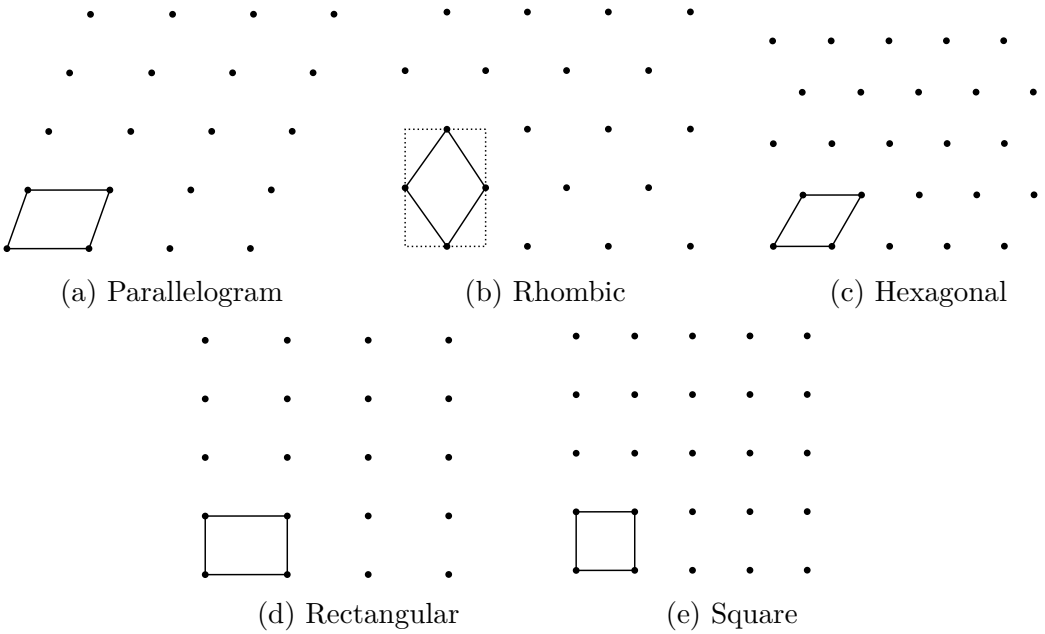

(a) Parallelogram (b) Rhombic (c) Hexagonal

(d) Rectangular (e) Square

Figure 2.9: The five different lattice units. The rhombic lattice is given for both the centered cell and the primitive cell being twice the area but with square corners.

2.1.3 Plane symmetry groups

A plane symmetry group, also termed *wallpaper group* or *plane crystallographic group* is a mathematical classification of a two dimensional repetitive pattern based on the symmetries of the pattern. We define that a pattern which are invariant under linear combinations of two linearly independent translations repeat at regular intervals in two directions are the plane symmetry groups.

It is a type of topologically discrete group of isometries of the Euclidean plane. By arguing the possible isometries for each of the five lattice types, it can be shown that there are 17 distinct plane symmetry groups [32]. These are classified in terms of a unit, as well as their internal symmetries, lattice and generating region.

The commonly used notation is the symbolism used in the International Tables for X-ray Crystallography [12] and is shown in table 2.3. A complete list of these are given in table 2.2. The symbols used for the names of the wallpaper groups are structured as following:

- Letter p or c denotes primitive or centered cell.
- Integer n denotes highest order of rotation
- Symbol denotes a symmetry axis normal to the x-axis, where m denotes reflection, g denotes a glide reflection and *1* denotes no symmetry
- Symbol denotes a symmetry axis at angle dependent on n the highest order of rotation

Type	Lattice	Highest order of rotation	Reflections	Non trivial glide reflection	Generating region
p1	parallelogram	1	no	no	1 unit
p2	parallelogram	2	no	no	1/2 unit
pm	rectangular	1	yes	no	1/2 unit
pg	rectangular	1	no	yes	1/2 unit
cm	rhombic	1	yes	yes	1/2 unit
pmm	rectangular	2	yes	no	1/4 unit
pmg	rectangular	2	yes	yes	1/4 unit
pgg	rectangular	2	no	yes	1/4 unit
cmm	rhombic	2	yes	yes	1/4 unit
p4	square	4	no	no	1/4 unit
p4m	square	4	yes	yes	1/8 unit
p4g	square	4	yes	yes	1/8 unit
p3	hexagonal	3	no	no	1/3 unit
p3m1	hexagonal	3	yes	yes	1/6 unit
p31m	hexagonal	3	yes	yes	1/6 unit
p6	hexagonal	6	no	no	1/6 unit
p6m	hexagonal	6	yes	yes	1/12 unit

Table 2.2: Recognition chart for wallpaper groups [32].

Symbol	Meaning
========	Line of reflection
− − −	Line of glide reflection
◊	Center of 2-fold rotation
△	Center of 3-fold rotation
□	Center of 4-fold rotation
⬡	Center of 6-fold rotation

Table 2.3: The symbols used to represent the symmetry elements in diagrams. Colors of the symbols are also used to distinguish between different centers of rotation of the same order.

Unit of the pattern

The smallest region of the pattern having the properties of all images under the translation group covers the plane is called the *unit* of the pattern. This unit correspond to the lattice unit of the same pattern. All units have its distinct symmetries, but their motifs can have infinite variations. They are like tiles; laid in parallel rows and fill the plane without gaps or overlaps. A diagram of the 17 units of a periodic pattern is given in figure 2.11. Some examples of categorization of some flexure patterns by its plane symmetry groups are found in figure 2.10. As one can see from this, not all units corresponds to the flexure region as for the p4 and cmm pattern.

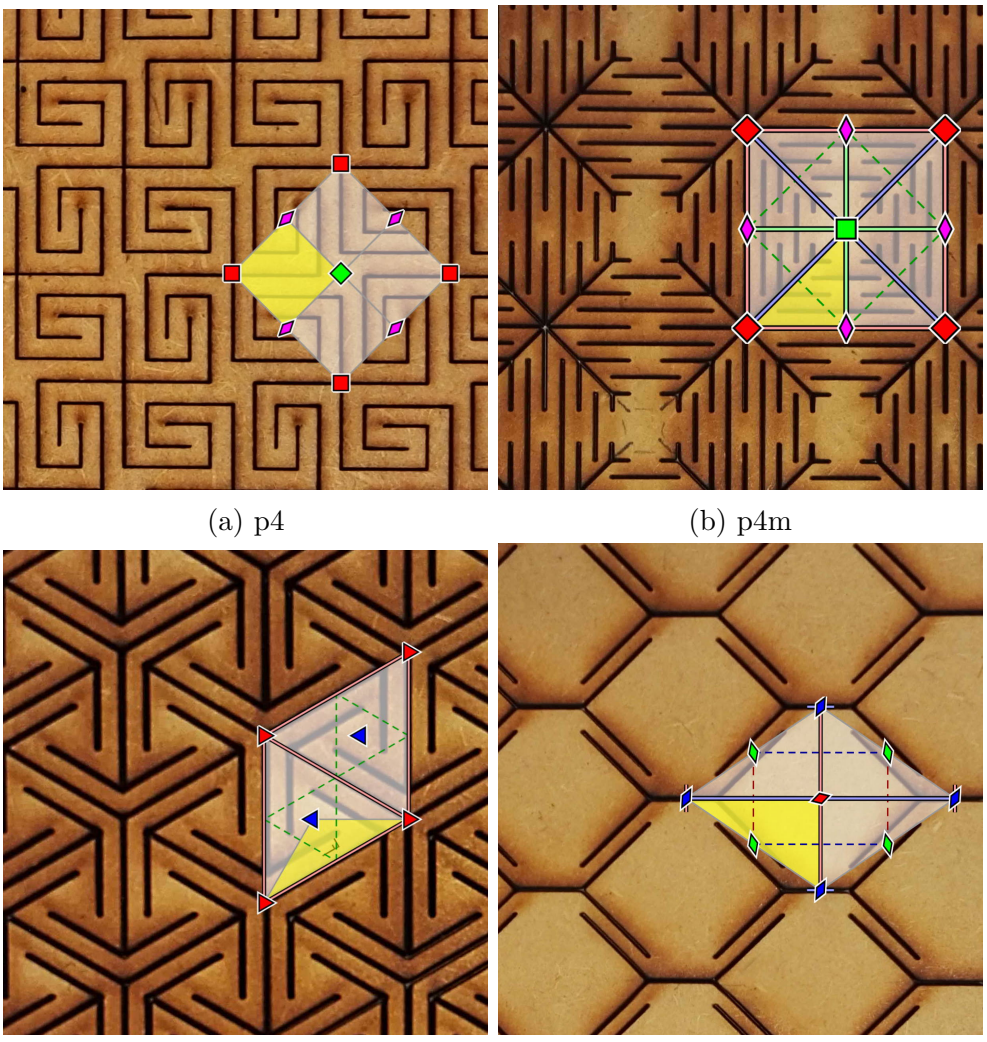

(a) p4 (b) p4m

(c) p31m (d) cmm

Figure 2.10: Example of classification of some flexure patterns with the unit of the pattern marked. The yellow region correspond with the generating region.

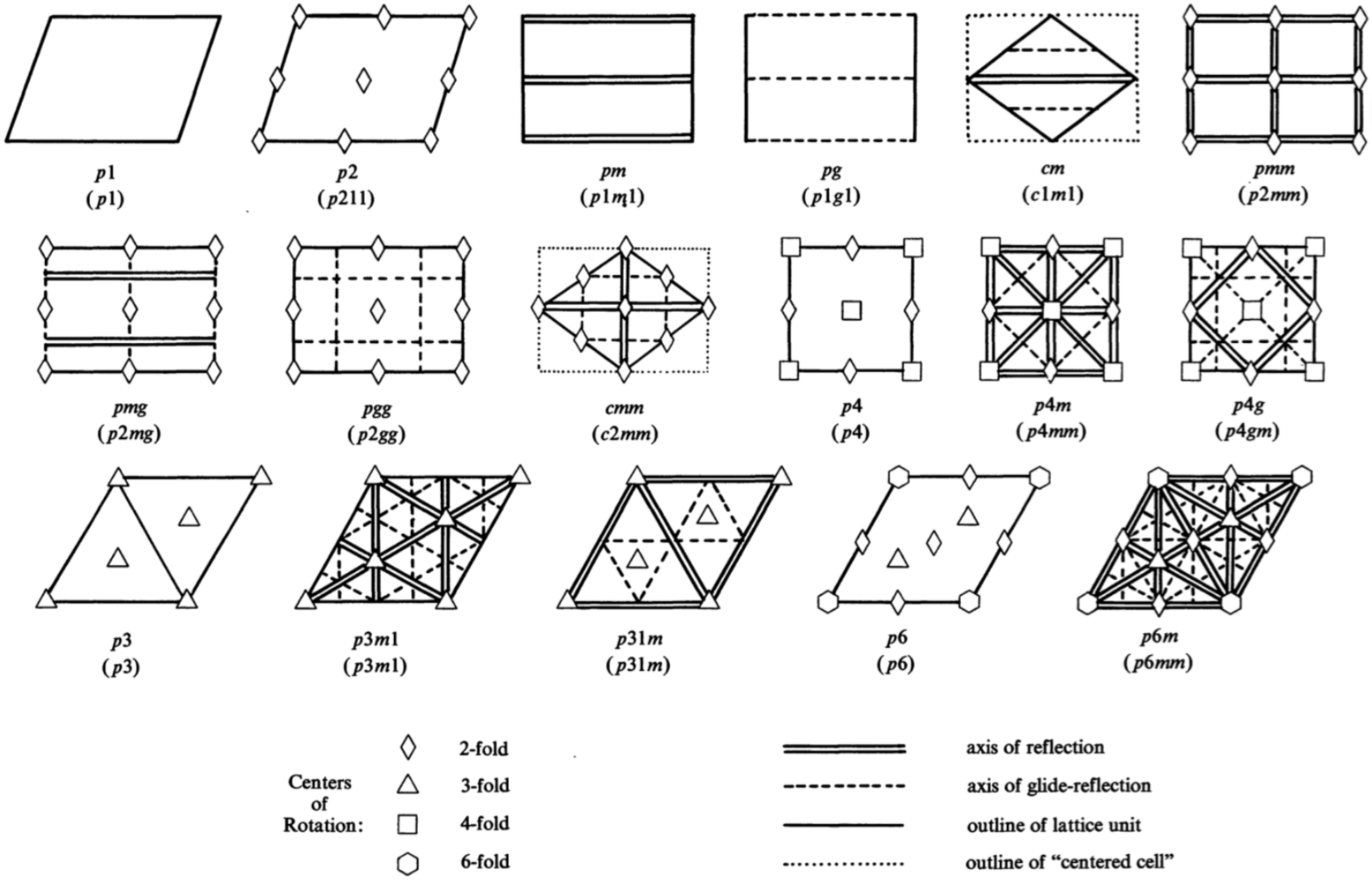

Figure 2.11: The unit of the pattern for the 17 different plane symmetry groups. Diagram adapted from D. Schattchneider[32].

Group generators

We call a generating region of a pattern the smallest region of the plane whose images under the full symmetry group covers the plane[5].

For geometric analysis these groups serve as the minimal set of generators that will generate the unit or that will map the plane and is therefore preferred for creating a unit with the least effort.

Chart 2.12, adapted from D. Schattchneider[32] shows two generators for each group. The second set of generators given includes the translation vectors which form the sides of the lattice unit.

[5]Crystallographers use the term *asymmetric unit*. Other terms are *fundamental region or fundamental domain*

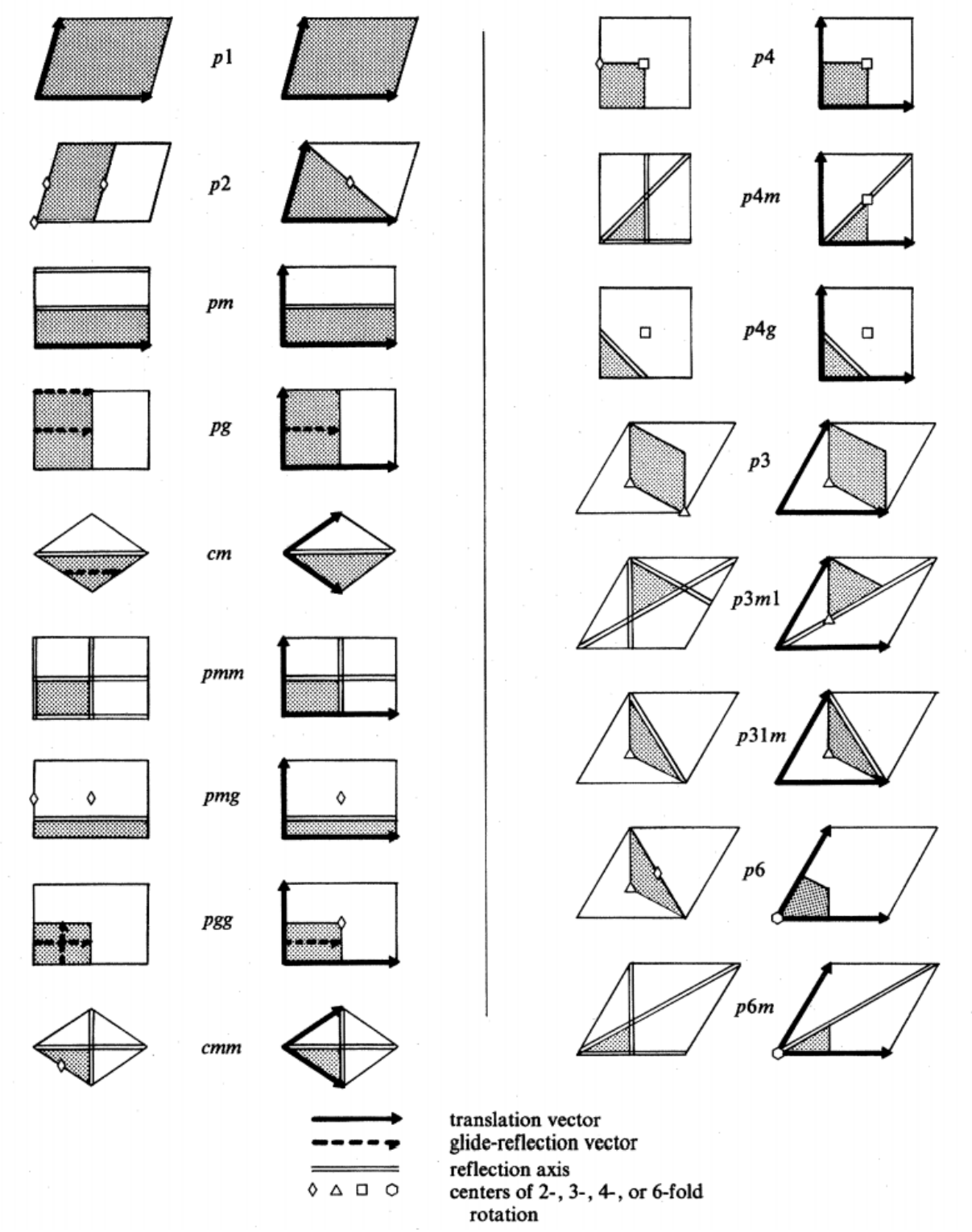

Figure 2.12: The generators for the plane symmetry groups.

2.1.4 Curvature

Curvature correspond to our intuitive understanding of what it means for something to be curved: spheres, cylinders and spiraling cables have curvature. Curvature is often described in terms of curves travelling along a surface' tangent at a point where the

corresponding normal to the tangent is the curvature. This is a signed quality, meaning the surface can be bent towards the normal or away from it, leaving a positive or negative sign. An example of this is the difference of the curvature inside and outside of a torus. The inside curvature is negative because it is pointing inwards, while the outside is positive because it points outwards.

The maximum and minimum curvatures at a point is called the principal curvatures κ_1, κ_2. A property derived from the maximum and minimum curvatures is the Gaussian curvature given as $\kappa_g = \kappa_1 \kappa_2$.

Zero-curvature surfaces has no curvature along one direction, meaning κ_1 or κ_2 is zero, and are well studied in mathematics. They are called *developable surfaces* because they can be developed into simple shapes and flattend out without stretching and tearing. For instance, any piece of a cylinder is developable since the principal curvature is zero. Different curvatures are seen in figure 2.13.

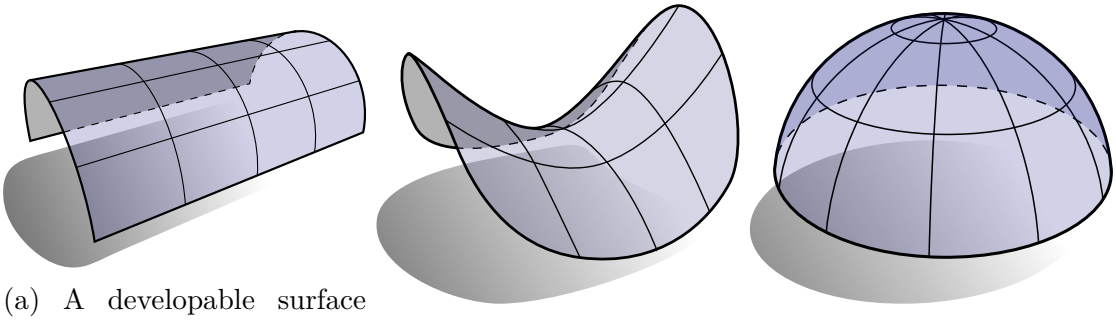

(a) A developable surface with zero Gaussian curvature.

(b) A saddle with negative Gaussian curvature.

(c) A dome with positive Gaussian curvature.

Figure 2.13: Three shapes with different curvature.

2.2 Material

There are many similarities of how crystallography unifies the theoretical mathematics of spacial symmetry groups with material science and how tilings and the plane symmetry groups together describe the behaviour of different plane arrangements of elements. Different atoms arranges to form lattices that repeats through translation in 3-dimensional space in crystallography. In the same way the 2-dimensional lattices are used to describe repeating arrangements in 2 dimensions.

Material is a broad term for the chemical substance of which a thing is made of. By describing a flexure pattern in terms of a material, one can make use of the developed theories and models in order to classify and describe it. Some material classifications that are good candidates for describing a flexure pattern are: *mechanical metamaterials* and *meso materials*.

Mechanical metamaterials Material properties are governed by the chemical composition and the spatial arrangement of constituent elements at multiple length-scales. This fundamentally limits material properties and generates certain trade-offs. An example of this is how density and strength are inherently linked where the more dense the material, the stronger it is in its bulk form.

A mechanical metamaterial is characterized as a material that inhibit effective properties determined from the internal structure, and not from the properties of the bulk material [21]. This has lead to a shift of focus where internal degrees of freedom are engineered to create materials with a wide range of remarkable mechanical properties such as high strength to weight ratio or auxetic behaviour. Due to the design of the internal structure, a metamaterial is in a category between the classical definition of a material and a device made from that material.

As mechanical metamaterials are highly ordered architectures in cellular solids, crystallographic systems are often used to evaluate and categorize the unique geometrical symmetries in three dimensions. For the simpler two dimensional case the plane symmetry groups are sometimes used [18].

Meso materials originate from the word *meso* which means *middle*. It refers to the length scale in which material properties can be observed. The term has been used for describing material structures fabricated with additive manufacturing [33] and in composite engineering where it has been proven to be a useful tool for predicting the effective mechanical properties of woven fabrics [27].

Most models for predicting the stress-strain response in a material build on the *constitutive equations*. The matices we arrive at in this section the *laminate stiffness matrix* builds on *plate theory*.

2.2.1 Constitutive equations

Three dimensional constitutive equations

In this section we consider ways to write the linear elastic constitutive equations for the effective (or average) response of compliant plates. The goal is to develop equations for predicting the elastic constants required for the average stress-strain relationship, often

referred to as Hooke's law in addition to show the different notations and theories that will later be used. The main source for this section is the book by Herakovich [13].

The generalized Hooke's law, written with Einstein summation notation is

$$\sigma_{ij} = C_{ijkl}\varepsilon_{kl}, \quad i,j,k,l = 1,2,3 \tag{2.7}$$

C_{ijkl} a fourth-order tensor[6] with 81 (3^4) elastic constants. Symmetries of the stress and strain tensors reduces the constants to 36 where 21 are independent in the anisotropic state. With this reduced number of constants, Hooke's law can be written in contracted notation as

$$\sigma_i = C_{ij}\varepsilon_j, \quad i,j = 1,2,...,6 \tag{2.8}$$

The symmetric stiffness C_{ij} can be written with matrix notation as

$$\begin{bmatrix} C_{11} & C_{12} & C_{13} & C_{14} & C_{15} & C_{16} \\ C_{21} & C_{22} & C_{23} & C_{24} & C_{25} & C_{26} \\ C_{31} & C_{32} & C_{33} & C_{34} & C_{35} & C_{36} \\ C_{41} & C_{42} & C_{43} & C_{44} & C_{45} & C_{46} \\ C_{51} & C_{52} & C_{53} & C_{54} & C_{55} & C_{56} \\ C_{61} & C_{62} & C_{63} & C_{64} & C_{65} & C_{66} \end{bmatrix} \tag{2.9}$$

The inverted Hooke's law can be written

$$\varepsilon_i = S_{ij}\sigma_j, \quad i,j = 1,2,...,6 \tag{2.10}$$

The coefficients in S_{ij} is called the compliance coefficients. By this, it is evident that the compliance matrix is the inverse of the stiffness matrix $S_{ij} = C_{ij}^{-1}$.

Plane stress

Plane stress corresponds to a condition in which all three out-of-plane components of stress are zero throughout the region and is a good approximation for thin plates. When plane stress conditions in the 1-2 plane are used in this thesis, it is assumed that the components σ_{33}, σ_{13} and σ_{23} are zero. It can be noted that the z-components of strain are not necessarily zero in the plane stress condition.

When the plane stress conditions are applied to the stiffness matrix given in equation 2.9, Hooke's law can be reduced to

$$\begin{bmatrix} \sigma_1 \\ \sigma_2 \\ \tau_{12} \end{bmatrix} = \begin{bmatrix} Q_{11} & Q_{12} & Q_{13} \\ Q_{12} & Q_{22} & Q_{23} \\ Q_{13} & Q_{23} & Q_{66} \end{bmatrix} \begin{bmatrix} \varepsilon_1 \\ \varepsilon_2 \\ \gamma_{12} \end{bmatrix} \tag{2.11}$$

It must be noted that $[Q]$ is the reduced stiffness matrix and is therefore distinguished from $[C]$.

[6]Tensors are mathematical representations of physical quantities and have components that change from one coordinate system to another.

Effective properties

Effective properties are engineering constants that determine the strain response to a plane stress situation. These properties can be found for a plate by considering the equations for plane stress

$$\begin{bmatrix} \varepsilon_1 \\ \varepsilon_2 \\ \gamma_{12} \end{bmatrix} = \begin{bmatrix} S_{11} & S_{12} & S_{13} \\ S_{12} & S_{22} & S_{23} \\ S_{13} & S_{23} & S_{66} \end{bmatrix} \begin{bmatrix} \sigma_1 \\ \sigma_2 \\ \tau_{12} \end{bmatrix} \tag{2.12}$$

The Young's modulii E_1 for a unidirectional loading is defined for a plane stress situation with $\sigma_1 \neq 0$ and $\sigma_2 = \tau_{12} = 0$ through the strain of the material with

$$\varepsilon_1 = \frac{1}{E_1}\sigma_1 \tag{2.13}$$

Which is equivalent to

$$\varepsilon_1 = S_{11}\sigma_1 \tag{2.14}$$

Similar arguments can be made for transverse modulus E_2 and shear modulus G_{12}.

Poisson's ratio v_{12} is defined as the negative ratio of the lateral strain to the axial strain associated with an applied stress. With the same considerations as for Effective moudlii we get the expression

$$v_{12} = \frac{-\varepsilon_2}{\varepsilon_1} = \frac{-S_{12}}{S_{11}} \tag{2.15}$$

The effective engineering constants are then

$$E_1 = \frac{1}{S_{11}} \qquad E_2 = \frac{1}{S_{22}} \qquad G_{12} = \frac{1}{S_{33}} \qquad = \nu_{12} = \frac{-S_{12}}{S_{11}} \tag{2.16}$$

Rotation about the 3 axis

Transformation matrices are used to transform tensors from one coordinate system to another and is illustrated in figure 2.14. The construction of these matrices done through direction cosines, but ant derivation is not carried out here.

The 2-D transformation equations for plane stress are simplifications of the 3-D transformation equations used in solid mechanics. The $[T_\sigma]$ matrix is used as the transformation matrix for stress $[\sigma] = [T_\sigma][\sigma]'$ and $[T_\varepsilon]$ matrix is used for transformation of strain $[\varepsilon] = [T_\varepsilon][Q][\varepsilon]'$ from a coordinate system x, y, z to coordinate system x', y', z.

$$[T_\sigma] = \begin{bmatrix} c^2 & s^2 & 2cs \\ s^2 & c^2 & -2cs \\ -cs & cs & c^2 - s^2 \end{bmatrix} \quad [T_\varepsilon] = \begin{bmatrix} c^2 & s^2 & cs \\ s^2 & c^2 & -cs \\ -2cs & 2cs & c^2 - s^2 \end{bmatrix} \tag{2.17}$$

where $c = cos(\theta)$ and $s = sin(\theta)$ are given for the angle θ in a counter clockwise direction. For transforming the constitutive equation we combine the two transformation matrices $[T_\sigma]$ and $[T_\varepsilon]$

$$[\sigma]' = [T_\sigma^{-1}][Q][T_\varepsilon][\varepsilon]' \tag{2.18}$$

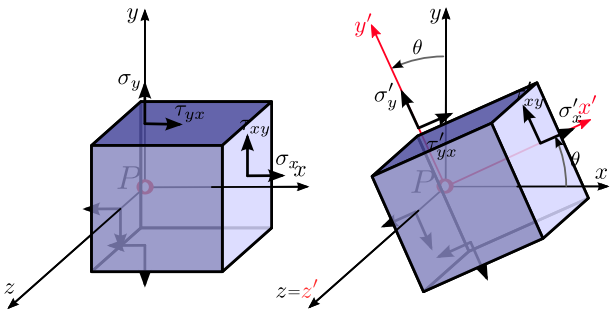

Figure 2.14: Material properties when rotated about the 3 axis

The stiffness matrix $[Q_\theta]$ in the rotated coordinate system related to the stiffness $[Q]$ in the initial coordinate system is denoted by:

$$[Q]' = [T_\sigma][Q][T_\varepsilon] \tag{2.19}$$

Which can be written as

$$[Q]' = \begin{bmatrix} c^4 & c^2s^2 & c^3s \\ & s^4 & cs^3 \\ Sym. & & c^2s^2 \end{bmatrix} [Q] \tag{2.20}$$

The transformation is a tensor transformation of stiffness components from one coordinate system to another and is independent from any scalars coupled with the stiffness components. For this reason, $[T]$ is the same for transforming the both $[A]$ and $[D]$ matrices.

2.2.2 Plate theory

In this subsection we want to describe the linear elastic response of a plate subjected to in-plane loads and out-of-plane bending moments as seen in figure 2.15. Plate theory is used on flat structural elements with a small thickness compared to the surface dimensions. Assumptions of this theory are as follows:

1. The plate consists of homogeneous material with known effective properties
2. There plane stress
3. The plate deforms according to the following Kirchhoff-Love assumptions:
    - Normals to the midplane remain straight and normal to the deformed midplane after deformation
    - Normals to the midplane do not change length

The total x-displacement of a generic point can be written as the sum of the midplane displacement, u^0 plus the rotation α of the normal to the midplane. Likewise consideration of the y-displacements.

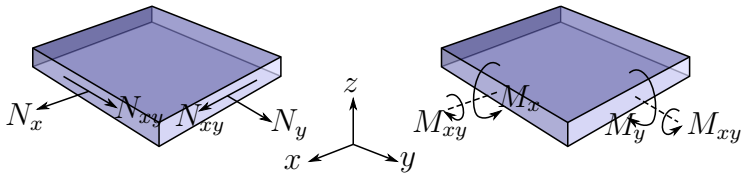

Figure 2.15: Plate element with load components.

$$\begin{aligned}
\varepsilon_x &= \frac{\partial u}{\partial x} = \frac{\partial u^0}{\partial x} - z\frac{\partial^2 w}{\partial x^2} = \varepsilon_x^0 + z\kappa_x \\
\varepsilon_y &= \frac{\partial v}{\partial y} = \frac{\partial v^0}{\partial y} - z\frac{\partial^2 w}{\partial y^2} = \varepsilon_y^0 + z\kappa_y \\
\gamma_{xy} &= \left(\frac{\partial u}{\partial y} + \frac{\partial v}{\partial x}\right) = \frac{\partial u^0}{\partial y} - 2z\frac{\partial^2 w}{\partial x \partial y} + \frac{\partial v^0}{\partial x} = \gamma_{xy}^0 + z\kappa_{xy}
\end{aligned} \tag{2.21}$$

Where κ is the curvature for small slopes and the inverse of the curve radius. Deflection is given by w.

$$\kappa_x = \frac{1}{R_x} = -\frac{\partial^2 w}{\partial x^2}, \quad \kappa_y = \frac{1}{R_y} = -\frac{\partial^2 w}{\partial y^2}, \quad \kappa_{xy} = \frac{1}{T_{xy}} = -\frac{\partial^2 w}{\partial x \partial y} \tag{2.22}$$

Combing the previously equations we arrive at the strain relation in matrix form

$$\begin{bmatrix} \varepsilon_x \\ \varepsilon_y \\ \gamma_{xy} \end{bmatrix} = \begin{bmatrix} \varepsilon_x^0 \\ \varepsilon_y^0 \\ \gamma_{xy}^0 \end{bmatrix} + z \begin{bmatrix} \kappa_x \\ \kappa_y \\ \kappa_{xy} \end{bmatrix} \tag{2.23}$$

or more simply

$$[\varepsilon] = [\varepsilon^0] + z[\kappa] \tag{2.24}$$

Coupling this with the stress we can write the stress state in the material as

$$\sigma = [Q]\varepsilon^0 + [Q]z\kappa \tag{2.25}$$

The in-plane forces per unit length N_x, N_y, N_{xy} are defined as the integral of the planar stresses in the plate over the plate thickness.

$$N_x = \int_{-H}^{H} \sigma_x dz, \qquad N_y = \int_{-H}^{H} \sigma_y dz, \qquad N_{xy} = \int_{-H}^{H} \tau_{xy} dz \tag{2.26}$$

Substituting the stresses from (2.25) into (2.26) gives the expression for forces per unit length.

$$[N] = [A][\varepsilon^0] + [B][\kappa] \tag{2.27}$$

where $[A]$ and $[B]$ represents the in-plane stiffness and the bending-stretching coupling matrix defined as

$$\begin{aligned}[A] &= [Q](z_H - z_{-H}) \\ [B] &= \frac{1}{2}[Q](z_H^2 - z_{-H}^2)\end{aligned} \tag{2.28}$$

The moments per unit length M_x, M_y, M_{xy} are defined as the integral of the forces σdz times the moment arm z integrated over the plate thickness.

$$M_x = \int_{-H}^{H} \sigma_x z dz, \qquad M_y = \int_{-H}^{H} \sigma_y z dz, \qquad M_{xy} = \int_{-H}^{H} \tau_{xy} z dz \tag{2.29}$$

Substituting the stresses from (2.25) into (2.29) gives the expression for moments per unit length.

$$[M] = [B][\varepsilon^0] + [D][\kappa] \tag{2.30}$$

where $[D]$ is the bending stiffness matrix defined as

$$[D] = \frac{1}{3}[Q](z_H^3 - z_{-H}^3) \tag{2.31}$$

We now combine equations and arrive at the fundamental equation for describing plate behaviour

$$\begin{bmatrix} N \\ M \end{bmatrix} = \begin{bmatrix} A & B \\ B & D \end{bmatrix} \begin{bmatrix} \varepsilon^0 \\ \kappa \end{bmatrix} \tag{2.32}$$

or in the expanded form

$$\begin{bmatrix} N_x \\ N_y \\ N_{xy} \\ M_x \\ M_y \\ M_{xy} \end{bmatrix} = \begin{bmatrix} A_{xx} & A_{xy} & A_{xs} & B_{xx} & B_{xy} & B_{xs} \\ A_{xy} & A_{yy} & A_{ys} & B_{xy} & B_{yy} & B_{ys} \\ A_{xs} & A_{ys} & A_{ss} & B_{xs} & B_{ys} & B_{ss} \\ B_{xx} & B_{xy} & B_{xs} & D_{xx} & D_{xy} & D_{xs} \\ B_{xy} & B_{yy} & B_{ys} & D_{xy} & D_{yy} & D_{ys} \\ B_{xs} & B_{ys} & B_{ss} & D_{xs} & D_{ys} & D_{ss} \end{bmatrix} \begin{bmatrix} \varepsilon_x^0 \\ \varepsilon_y^0 \\ \gamma_{xy}^0 \\ \kappa_x \\ \kappa_y \\ \kappa_{xy} \end{bmatrix} \tag{2.33}$$

This result is derived only from Kirchhoffs assumptions on displacements and is therefore independent of the material of choice. This means $[Q]$ has a linear relationship to the stiffness components of $[A], [B]$ and $[D]$.

2.3 Mechanical behaviour of compliant elements

This section explores the different mechanical elements that can be used to make compliant structures with specific properties.

Many fields study the behaviour of different compliant elements and structures. The most dominant field is called *compliant mechanisms* and describes a mechanism that "gain at least some of its mobility from the deformation of flexible members rather than from movable joints only"[14]. A subset of compliant mechanisms are *LEMs, lamina emergent mechanisms*. These are mechanisms that focus on out-of-plane motions. The closest field of study to a flexure pattern is the *Compliant Array (CA)* which consist of a single

unit that is patterned in series and parallel, but lack a good description or method for extending the concept to new patterns [25] [20].

The governing principle for a flexure pattern is however only the deformation of flexible members (flexures) and especially the blade flexure. The blade flexure is synonymously with the flexure strip and the mechanical properties of this will therefore be the main focus. Due to the adoptions made from the fields of compliant mechanisms and LEMs, there is given an overview of the important principles and definitions as well as some examples in figure 2.16.

(a) A compliant array.

(b) A compliant mechanism.

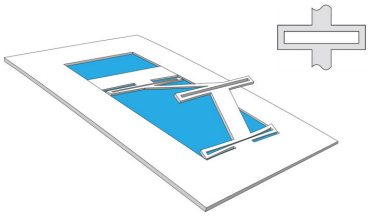

(c) A LEM.

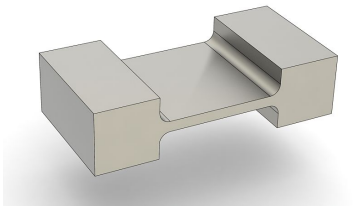

(d) A blade flexure (similar to a flexure strip).

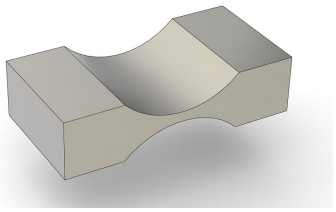

(e) A notch flexure.

Figure 2.16: Example of various types and classification of elements that gain their mobility through the deformation of flexible members.

Compliant mechanisms primarily gain their flexibility from deflection of flexible members rather than a movable joint in order to transfer or transform motion [14].

The benefits of using compliant mechanisms are mainly the lack of backlash for high precision movement, spring behaviour for desired force-deflection relations, in plane manufacturing, part reduction leading to simpler assemblies and compact design. This is described in further details in other papers [16]

Lamina emergent mechanism (LEM) is a subset of compliant mechanisms manufactured form sheet goods with out of plane properties [15]. In-plane properties like compression and tension are important to make non-developable surfaces, also known as surfaces with double curvature.

Compliant arrays (CA) are engineered from an array of subelements, most often a compliant mechanism, that combine to produce a response that is typically not available from a flat panel made of a single material. For this reason it fits the definition of a metamaterial from section 2.2. It is formally defined as panels with geometry consisting of a compliant mechanism that is patterned in parallel and series to achieve target material properties, particularly out-of-plane bending stiffness [25].

The fundamental unit of a CA is the compliant mechanism. In the case of the CA belonging to a rectangular lattice, the centered unit consisting of two units and not the minimal area unit is often used to preserve its parallelism with the translations.

Flexures are flexible members, or compliant joints that gain their motion through the elastic properties of the joint material. Basic flexure elements make up compound compliant mechanisms when combined in different configurations. The basic flexures are the pin flexure, notch flexure and blade flexure, here referred to as a *flexure strip*. Notch flexures are much used in plastic containers as hinges [7] while the flexure strip is the dominant building block of LEMs. The flexure strip rely on bending for a translative motion [16] and torsion for an angular displacement.

The mechanical advantages of such elements are primary the lack of friction, backlash and wear in comparison to other mechanisms that rely on the interaction of multiple rigid moving parts to transfer motion. The primary disadvantages are related to material yielding and fatigue in ares with stress raisers as well as it can give challenges in the design of applications due to its restrictions in geometry. The concept is present in several applications with the typical example being precision instruments where no backlash is crucial. Other mechanisms that use flexures are bi stable mechanisms, compliant parallelogram mechanisms and thermo mechanical in-plane microactuators.

2.3.1 Mechanics of a simple flexure strip

The flexure strip, illustrated in figure 2.17 is a general compliant flexure element [15] and modelled as a rectangular beam. Its compliant degrees of freedom (DOF) are controlled by the complete flexure configuration, but a thin beam is often regarded as compliant in three DOFs: one translative, one bending and one twist. The tension, as also included in figure 2.18 is not regarded as a compliant since the travel distances are much shorter than for bending. Within the fields of complaint mechanism the flexure strip is modelled as a spring with spring constant k_{eq}. Superscript denotes angular (θ) or translative (u) displacement.

The spring constant k_eq for a bending or torsion moment is M, T and force F is given as

$$M = T = k_{eq}^{\theta}\theta \qquad F = k_{eq}^{u}u \tag{2.34}$$

For the different deformation modes is $k_{eq} = K$ where subscript denotes the response force force tension (t), bending (B) or torsion (T).

[7] Notch flexures are often referred to as living hinges.

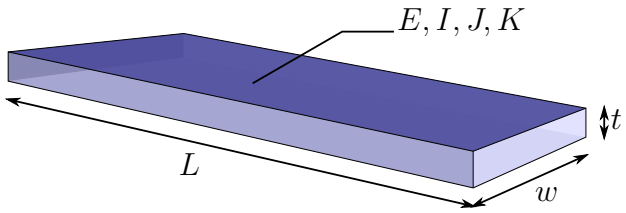

Figure 2.17: A flexure strip with dimensions, material and geometrical properties.

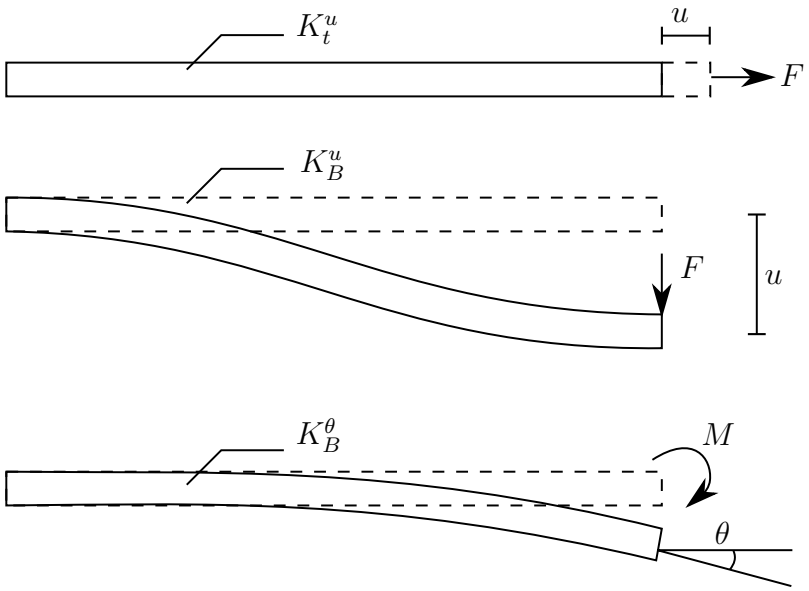

Figure 2.18: A flexure strip with two three deformation modes shown: stretching by tension, translative displacement by bending and angular displacement by bending.

Tension

The tension mode appear when a flexure strip is subjected to an axial force and results in an elongation. The stiffness K_t^u is given by

$$K_t^u = EA = Ewt \tag{2.35}$$

As one can see it is only dependent on the Young's E modulus and the cross section area A.

Bending

In plane and out of plane deflection can be achieved through bending. Two common modes are the fixed-guided and the fixed-free constraints.

The equations for the axial stiffness K_B^u to a force and the angular stiffness K_B^θ to a moment is given by the equations:

$$K_B^u = \frac{cEI}{L^3} \qquad K_B^\theta = \frac{cEI}{L} \tag{2.36}$$

Factor c is the bending mode given by the boundary conditions and can range from 3 for a fixed-free beam to 192 for a fixed-fixed beam, with $c = 12$ being the case for a fixed-guided beam [16]. I is the moment of inertia for a rectangular cross section and is dependent on the axis of bending and is given as $I = \frac{wt^3}{12}$ or $I == \frac{w^3t}{12}$.

The equation shows that the bending stiffness of a member is decreased though: an increasing of L, reduction of moment of inertia I through the variables w and t, or by choosing a less stiff material through E. The parameter c is also an effective way of increasing the compliance, but is given by the compound flexure configuration.

Torsion

Torsion of a flexure strip transfer angular displacement of the flexure strip, as seen in figure 2.19, and can only occur as an out-of-plane motion in a flexure pattern. The stiffness K_T^θ for a member is given by the equation

$$K_T^\theta = \frac{JG}{L} \tag{2.37}$$

where G is the modulus of rigidity and J is a parameter associated with the cross section geometry and is analogous to the the polar moment of inertia for circular cross sections. For an isotropic material G is given as $G = \frac{E}{2(1+\nu)}$. The analytically models for a beam with circular cross-sections are very good, while for rectangular cross-sections, effects like warping come into play. A formula for approximating J where $w > t$ for rectangular cross sections are given as [29]:

$$J = wt^3 \left(\frac{1}{3} - 0.21 \frac{t}{w} \left(1 - \frac{t^4}{12w^4} \right) \right) \tag{2.38}$$

A simplification of the formula can be done by eliminating the higher order terms

$$J = wt^3 \left(\frac{1}{3} - 0.21 \frac{t}{w} \right) = \frac{wt^3}{3} - 0.21w^2t^2 \tag{2.39}$$

By substituting this equation into equation 2.37 we can see that the compliance S_T is linearly dependent on the materials' modulus of rigidity G (or elasticity E) and the length of L, while J gives a relation involving multiple powers. Increased compliance is achieved by reducing G and increasing L.

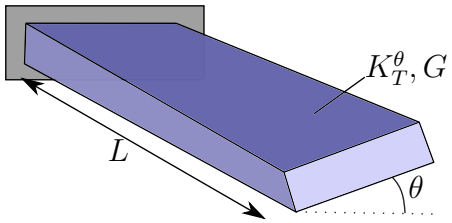

Figure 2.19: Torsion of a flexure strip.

Cross section and resistance to deflection

The cross section with the height to width ratio is an important parameter for the resistance to deflection for different modes. The moment of inertia, or its equivalents can be compared for the different modes: I for bending and J for torsion. This is done in figure 2.20 where one can see that the resistance to bending will increase much more than the resistance to torsion after a $h/w = 3/2$ ratio.

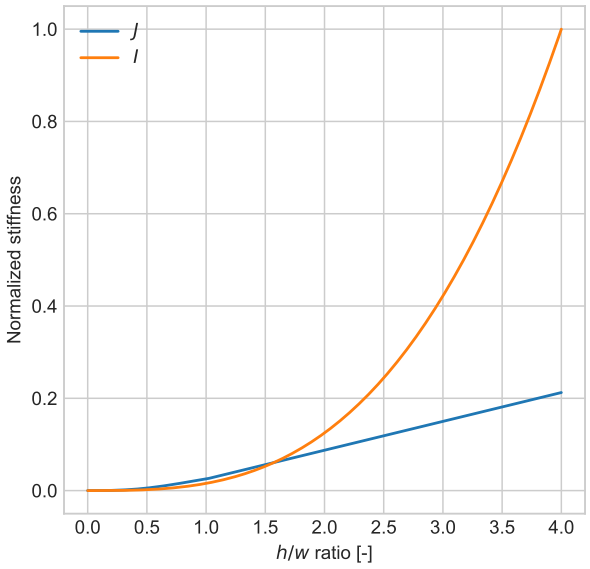

Figure 2.20: Normalized difference of height to width ratio for I and $Kf = J$.

2.3.2 Mechanics of compound flexures

Combinations of the flexure strip implies different boundary conditions and can reduce or increase the DOFs as well as the compliance. We take a look at some common configurations that can be utilized in a flexure pattern. When compliant elements are added in *series*, the total compliance S_{eq} is increased, total deflection u_{eq} and angular deflection θ_{eq} is increased, total force F_{eq} is unchanged and stored energy U_{eq} is increased. On the other hand, compliant elements in *parallel* will result in a less compliant structure and other quantities as one can see from the equations in table 2.4.

Flexures can be combined in symmetric, antisymmetric or asymmetric configurations. The symmetries of the compound flexure and the symmetries of the loading determine the

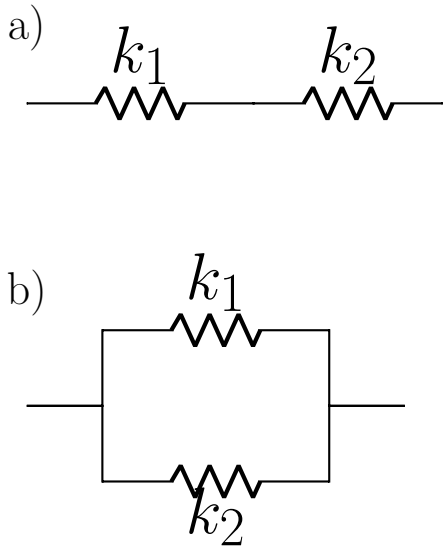

Figure 2.21: a) Springs in series, b) Springs in parallel.

Series	Parallel
$1/k_{eq} = 1/k_1 + 1/k_2 + ... + 1/k_n$	$k_{eq} = k_1 + k_2 + ... + k_n$
$S_{eq} = S_1 + S_2 + ... + S_n$	$1/S_{eq} = 1/S_1 + 1/S_2 + ... + 1/S_n$
$u_{eq} = u_1 + u_2 + ... + u_n$	$u_{eq} = u_1 = u_2 = ... = u_n$
$\theta_{eq} = \theta_1 + \theta_2 + ... + \theta_n$	$\theta_{eq} = \theta_1 = \theta_2 = ... = \theta_n$
$F_{eq} = F_1 = F_2 = ... = F_n$	$F_{eq} = F_1 + F_2 + ... + F_n$
$U_{eq} = U_1 + U_2 + ... + U_n$	$U_{eq} = U_1 + U_2 + ... + U_n$

Table 2.4: The systems of springs coupled in series or parallel.

mechanical response. Symmetric structures with symmetric loading are more stable as the response in the structure will cancel out some forces internally. For an antisymmetric or asymmetric structure this is not the case, resulting in a response that triggers additional moments which creates higher stresses.

Figure 2.22 shows three compound flexure mechanisms that are used in this thesis to make different flexure patterns. A short description of these follows:

Switchback A switchback configuration consists of several flexure elements in series, where the next flexure is a horizontal reflection (or two-fold rotation in a point) of the other. An odd number of flexure elements, results in a antisymmetric configuration, as seen in figure 2.23, while an even number results in a symmetric configuration. By adding more elements, longer travel distance, angular displacement (seen in figure 2.24) and more compliance is achieved.

Lamina emergent torsion joint (LET) The LET joint is a compliant joint for out-of-plane bending and is build from four flexure elements that are combined in a symmetric configuration of two in parallel and two in series. The two possible ways it can be combined are called an outside-LET or inside-LET configuration. The reflective lines ensures symmetric loading when subjected to tensile displacement (seen in figure 2.25) or out of plane bending and is the reason for it being a popular choice in LEMs[16].

Coil A coil configuration of the flexure strip wraps around itself to a central point. This can also be viewed as two switchbacks where a switchback in opposite direction is inserted in the middle. The long flexure along the outer edges results in multiple bending modes being present when deformed. The configuration is antisymmetric with a 2-fold rotation center in the middle and results in an asymmetric responses when a symmetric force is imposed. Since the coil has all parts in a series, the total stiffness is enhanced,

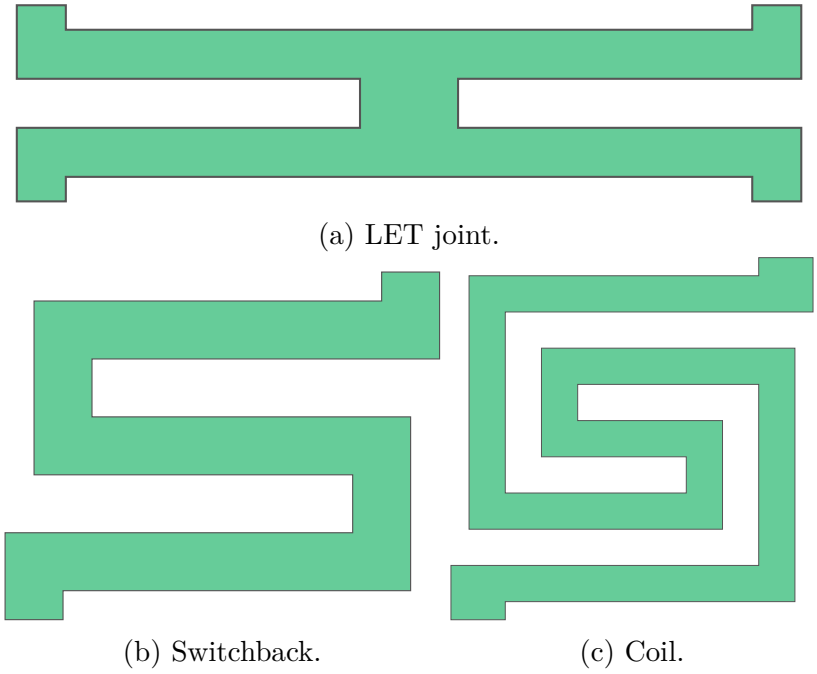

(a) LET joint.

(b) Switchback.

(c) Coil.

Figure 2.22: Three compound flexures.

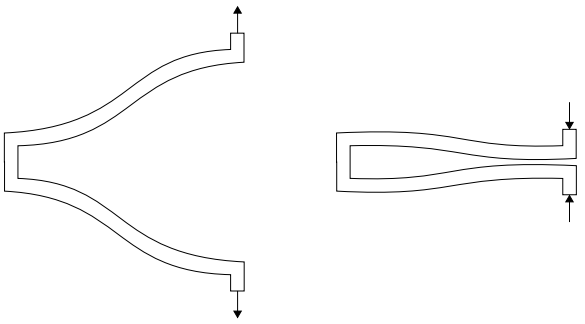

Figure 2.23: The tensile and compression response for a symmetric switchback.

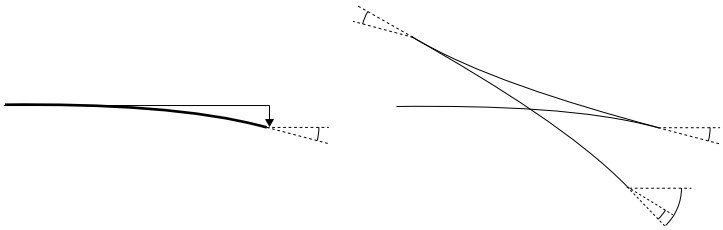

Figure 2.24: The addition of angular displacements when a switchback with three flexure elements in series is twisted

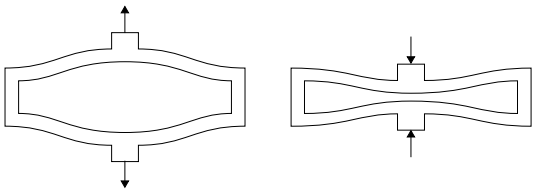

Figure 2.25: The tensile and compression response for a LET.

2.4 Computational geometry

The field of computational geometry forms the basic tools for applications like: robotics, game development, Geospatical Information System, computed aided design (CAD), computer aided manufacturing (CAM), computational fluid dynamics (CFD), finite element analysis (FEA) and many more.

Manipulation of geometrical data sets are most often done with linear algebra. For this reason some transformation matrices are presented in this section to describe parts of the underlying theory that is coded into the programs used or made in this thesis.

2.4.1 Geometrical representation

A spatial data model consists of objects defined in the geometrical space. Most spacial models can represent simple geometric objects like *points*, *curves* and *surfaces* while more complex models handle complex structure like 3 dimensional objects. These types are implemented in classes. The most basic representation of a curve is through *linear splines*. A rounded patch is then represented by regions bounded by linear splines. More advanced curves are the Bezier curve or non-uniform rational B-spline (NURBS). Operations on a spacial data model are important for objects to interact with each other such as calculating the union, intersection and the affine transformations.

In order to describe the 2 dimensional objects a set of features: *interior, boundary* and *exterior* are used.

Points has topological dimension of 0. Its interior consists of exactly one point. It has an interior set of exactly one point, a boundary set of no points and an exterior set of of all other points.

Curves has topological dimension of 1 and consists of infinitely many points along its length (imagine a point dragged in space). The boundary set consists of the two end points and an exterior set of all other points.

Surfaces has topological dimension of 2 and has an interior, exterior and boundary. The interior is the infinitely many points within (imagine a curve dragged in space to cover an area), a boundary consisting of one or more curves, and an exterior set of all other points including those within holes that might exist in the surface.

The Nine-intersection model (9IM) or Egenhofer-Matrix model is a method for computing the spatial relationships between geometries through a 3x3 matrix. The model considers two objects (A and B) with its respective interiors, boundaries and exteriors and analyzes the intersections of these nine objects parts for their relationships of the intersection geometries.

	Interior(B)	Boundary(B)	Exterior(B)
$Interior(A)$	$dim(I(A) \cap I(B))$	$dim(I(A) \cap B(B))$	$dim(I(A) \cap E(B))$
$Boundary(A)$	$dim(B(A) \cap I(B))$	$dim(B(A) \cap B(B))$	$dim(B(A) \cap E(B))$
$Exterior(A)$	$dim(E(A) \cap I(B))$	$dim(E(A) \cap B(B))$	$dim(E(A) \cap E(B))$

Table 2.5: The 3x3 9IM relationship matrix where I is interior, B is boundary and E is exterior.

Topological predicates are spatial relationships described by the 9IM in table 2.5. These Boolean functions test the 8 relationships: *equal, disjoint, intersects, touches, crosses, within, contains* and *overlaps*[36] between the geometries. A furhter explanaiton of these relationships are found in table 2.6. Each relationship is identified with a special characteristic of the 3x3 relationship matrix.

Topological predicate	**Meaning**
Equals	Geometries are topologically equal
Disjoint	Geometries have no point in common
Intersects	Geometries have at least one point in common
Touches	Geometries have at least one boundary point in common, but no interior points
Crosses	Geometries share some but not all interior points, and the dimension of the intersection is less than that of at least one of the geometries.
Overlaps	Geometries share some but not all points in common, and the intersection has the same dimension as the geometries themselves
Within	Geometry A lies in the interior of geometry B
Contains	Geometry B lies in the interior of geometry A (the inverse of within)

Table 2.6: Topological predicates

2.4.2 Affine transformations

The affine space has the generalized properties of the Euclidean space. An affine transformation preserves points, straight lines and planes, and sets of parallel lines, remain

parallel after a transformation. As we will see, an affine transfomation does not necessarily preserve angles between lines or distances between points, but it preserve the ratio of distances between points lying on a straight line. A figure of the most important transformations are seen in figure 2.26.

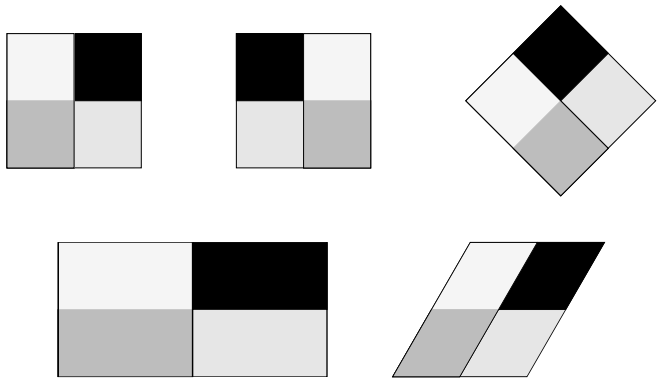

Figure 2.26: Affine transformations of an object. From top left: original motive, reflection along x-axis, rotation by $\theta = 45°$, stretching by a factor 2 in x-direction and shearing by $\theta_x = 30°$.

The general affine transformation can be written as following in equation 2.40

$$\begin{bmatrix} x' \\ y' \\ 1 \end{bmatrix} = \begin{bmatrix} a & b & \Delta x \\ c & d & \Delta y \\ 0 & 0 & 1 \end{bmatrix} \begin{bmatrix} x \\ y \\ 1 \end{bmatrix} \tag{2.40}$$

Where x', y' are the transformed coordinates and x, y are the initial coordinates, a, b, c and d are transforming coefficients and Δx and Δy are the translation coefficients.

Examples of 2D affine transformations

Translation by a distance Δx and Δy is done through the matix T_1

$$T_1 = \begin{bmatrix} 1 & 0 & \Delta x \\ 0 & 1 & \Delta y \\ 0 & 0 & 1 \end{bmatrix} \tag{2.41}$$

Reflecting T_2 about the x- or y axis is done for the case where $a = -1$ or $c = -1$ respectively.

$$T_2 = \begin{bmatrix} -1 & 0 & 0 \\ 0 & -1 & 0 \\ 0 & 0 & 1 \end{bmatrix} \tag{2.42}$$

Rotation a rotation in origo by an angle θ is done through the matrix T_3

$$T_3 = \begin{bmatrix} cos(\theta) & -sin(\theta) & 0 \\ sin(\theta) & cos(\theta) & 0 \\ 0 & 0 & 1 \end{bmatrix} \tag{2.43}$$

Rotation an arbitrary point Since all transformations take basis in a transformation around an origin in origo. A transformations around an arbitrary point is done by combining a translation to origo before and a translation back to the original point after the rotation.

$$T_4 = T_1 T_2 T_1^{-1} \tag{2.44}$$

Glide reflection In order to create a Glide reflection transformation about origo, there is needed the combination of a mirroring and a translation

$$T_5 = T_3 T_1 \tag{2.45}$$

Stretching is achieved when the coefficients $b = c = 0$. An elongation is done for a $a > 1$ while a compression is done for $a < 1$. A matrix associated with a stretch by a factor $a > 0$ along the x-axis is given by:

$$\begin{bmatrix} a & 0 & 0 \\ 0 & 1 & 0 \\ 0 & 0 & 1 \end{bmatrix} \tag{2.46}$$

Similarly, a stretch by a factor b along the y axis is given by $a = 1$ and $c > 0$.

Shearing by a given angle θ is done with $a = d = tan(\theta)$ for a skew deformation along the x- or y-axis respectively. The affine transformation matrix is

$$\begin{bmatrix} 1 & tan(\theta_x) & 0 \\ tan(\theta_y) & 1 & 0 \\ 0 & 0 & 1 \end{bmatrix} \tag{2.47}$$

2.5 Multi-scale computational homogenization

Most materials are used on a macro-scale, while the understanding of its fundamental mechanisms are established on a micro-, nano-, and atomic level. Multi-scale methods tries to predict the general material properties by using models or information on one scale on another. In this sense it plays an important role in connecting the field of mechanics of materials to the field of material science [8].

There are many ways of applying multi-scale methods in a general setting. Some used are the asymptotic homogenization method (AHM), eigenvalue expansion-variational method (EEVM) and the computational homogenization technique, which is presented there. This technique is also the most accurate technique in upscaling the non-linear behaviour of a well-characterized microstructure [10].

The first homogenization dates back to 1985 and is devoted to general considerations on representative volume elements (RVE), statistical volume elements (SVE), averaging micromechanics and linear problems [30]. With increasing computational power, the concept is further developed and transferred to many fields, especially through FE analysis.

[8]The general difference of these fields are that mechanics of materials tries to understand how the materials behave, while material science focuses on understanding how materials are build.

2.5.1 Basic theory

In order to establish the macroscopic properties of a hetrogeous medium, the RVE or SVE has to be defined. The two scales that are involved are called the macroscopic scale where the hetrogeneties are small and the microscopic scale which is the scale of the hetrogeneties. In the homogenization theory of a periodic media, the RVE is the unit cell, which generates by periodicity the entire structure. This unit can be considered a paralellogrammice block and and is similar to the unit of the pattern described for the wallpaper groups in section 2.1.3.

The assumption of separation of scales must be emphasized that the microscopic scale is much smaller than the characteristic length where the macroscopic loading varies. In most cases this implies

$$\mathcal{L}_{discrete} \ll \mathcal{L}_{microscopic} \ll \mathcal{L}_{macroscopic} \tag{2.48}$$

At each scale there are associated different variable types: on the macroscopic scale, the material properties are the variables we are looking for and on the microscopic scale we find the idealized variables. We distinguish

$$\begin{aligned} \Sigma, \epsilon &\quad \text{macroscopic stress and strain tensors} \\ \sigma(y), \varepsilon(y) &\quad \text{microscopic stress and strain tensors} \end{aligned}$$

The homogenization techniques assumes that *linear displacements are applied on the macroscopic scale* as well as there is *a periodic structure*. Then it is only necessary to consider a periodic structure V_{rve}, which forms the RVE. The following *boundary value problem* (BVP) has to be solved:

$$\begin{cases} \frac{\partial}{\partial x_i}\sigma_{ij} = 0, & x \in V_{rve} \\ u_i(x) - \varepsilon^0_{ij} x_j & \text{periodic on } \partial V_{rve} \end{cases} \tag{2.49}$$

Where $\varepsilon^0_{ij} x_j$ are the given macroscopic strain tensor, u the displacement of the structure and ∂V_{rve} is the boundary of the RVE. The first condition in the equation preserves elastic deformation of the RVE while the periodic condition ensures continuity of neighbouring cells. The applied loads on the structure makes it possible to derive the constraint equations

$$u_i^{X_j^a} - u_i^{X_j^b} = \varepsilon^0_{ij} x_j (x_j^{X_j^a} - x_j^{X_j^b}) \tag{2.50}$$

The values $u_i^{X_j^a}$ and $u_i^{X_j^b}$ are the ith displacement components on the boundary surface of the cell. The locations in which the values are calculated, are characterized by an offset in x_j direction as illustrated in figure 2.27.

The effective homogenized coefficients of the stiffness tensor, which represents the macroscopic behaviour of the material, are calculated by:

$$\langle \sigma_{ij} \rangle = C^{eff}_{ijkl} \langle \varepsilon_{kl} \rangle \tag{2.51}$$

where the expressions $\langle \bullet \rangle$ represents the average functions of the stress and strain on macro scale. Since ε^0_{kl} is the given macro strain tensor, the following equation holds.

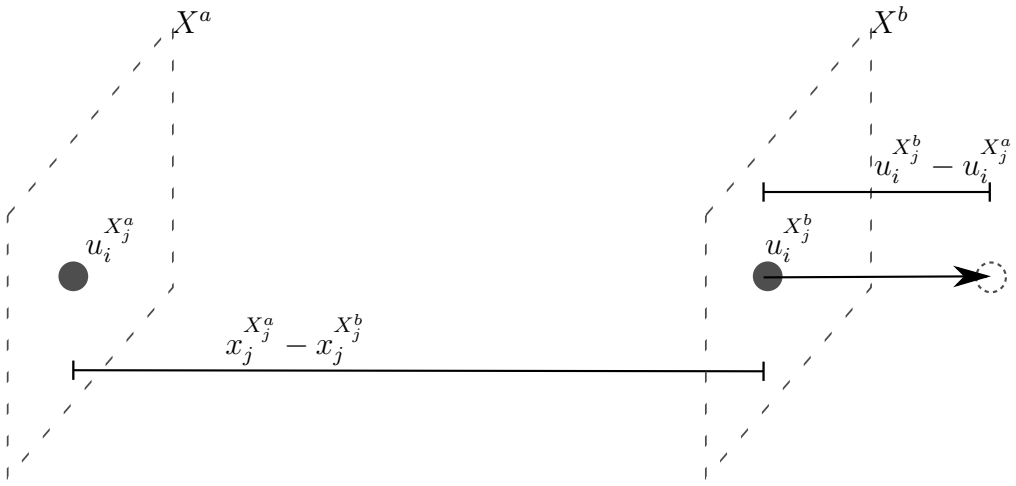

Figure 2.27: Constraint equation componentes and relationships.

$$\begin{aligned} \langle \sigma_{ij} \rangle &= \frac{1}{|V_{rve}|} \int_{V_{rve}} \sigma_{ij} dx \\ \langle \varepsilon_{kl} \rangle &= \frac{1}{|V_{rve}|} \int_{V_{rve}} \varepsilon_{kl} dx = \varepsilon^0_{kl} \end{aligned} \tag{2.52}$$

The stiffness coefficients are calculated from

$$C^{eff}_{ijkl} = \frac{\langle \sigma_{ij} \rangle}{\langle \varepsilon_{kl} \rangle} \tag{2.53}$$

2.5.2 RVE for thin structures

Computational homogenization of shells and plates is useful if complex substructures exists which cannot be captured in a layered-wise composite shell approach. An in-plane periodicity of the substructure is found in flexible elements and electronics, sandwich panels, ship hull core structures etc. Like other computational homogenization problems, microscopical kinematical quantities like in-plane membrane strains ε and out-of-plane curvature κ are passed to the micro-scale to conduct the boundary value problem.

$$[u]^* = f([u], \varepsilon, \kappa) \tag{2.54}$$

The formulation relies on a through-thickness representative volume element where the top and bottom surface of the shell are physically incorporated at the RVE level.

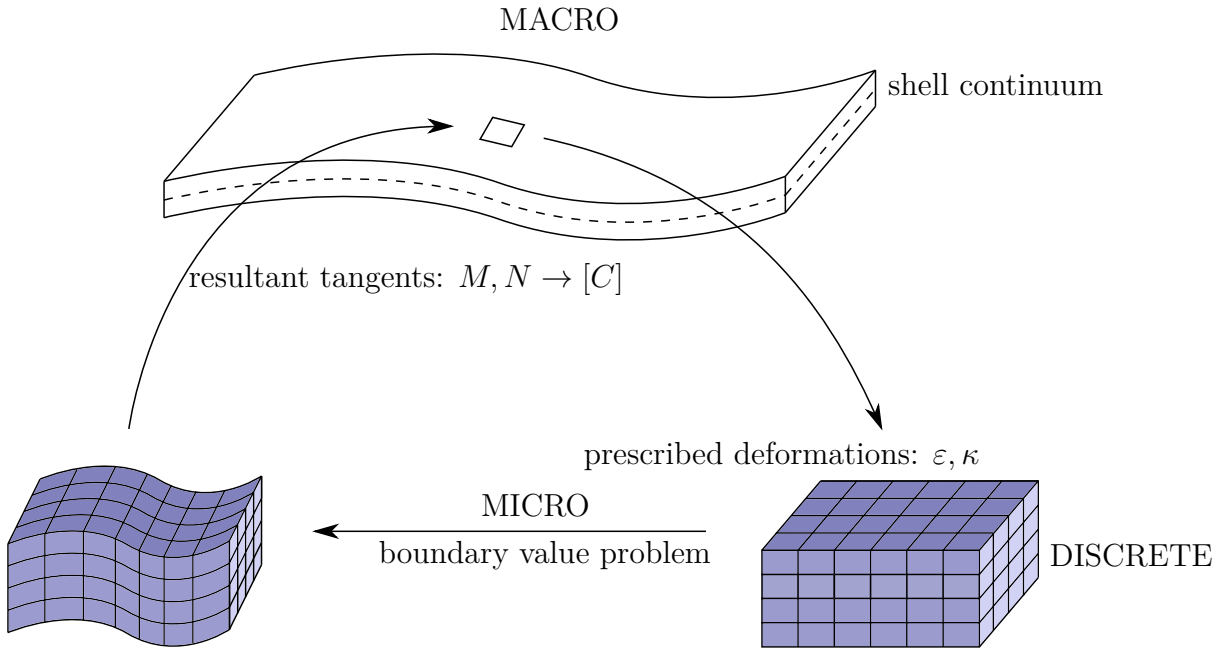

Figure 2.28: Multi scale computational homogenization of shells with a through thickness RVE.

2.5.3 Numerical model and algorithm

Because of finite element discretization, the integrals in equation 2.52 are changed to sums with σ_{ij}^e and ε_{kl}^e are averaged element values for tensor stress and strain and $|V_e|$ is the volume of the finite element.

$$\begin{aligned} \langle \sigma_{ij} \rangle &= \frac{1}{|V_{rve}|} \sum_e \sigma_{ij}^e |V_e| \\ \langle \varepsilon_{kl} \rangle &= \frac{1}{|V_{rve}|} \sum_e \varepsilon_{kl}^e |V_e| \end{aligned} \tag{2.55}$$

When the prescribed unit displacements are set, the calculated stiffness components correspond to the forces and derived quantities that can be measured at the boundary nodes.

$$\begin{aligned} C_{ijkl}^{eff} &= \frac{\langle \sigma_{ij} \rangle}{\langle \varepsilon_{kl} \rangle} \quad \text{for } i,j,k,l = 1,2,3 \quad k = l \\ C_{ijkl}^{eff} &= \frac{\langle \sigma_{ij} \rangle}{2\langle \varepsilon_{kl} \rangle} \quad \text{for } i,j,k,l = 1,2,3 \quad k \neq l \end{aligned} \tag{2.56}$$

2.6 Statistics

2.6.1 Simple linear regression

Simple linear regression is a linear model with one independent and one dependent variable and is used extensively in practical applications. This is because models which depend linearly on their unknown parameters are easier to fit than models which are non-linearly related to their parameters.

Fitting the regression line is done with the model function that describes a line with slope β and y-intercept α

$$y = \alpha + \beta x \tag{2.57}$$

For a set of data pairs (x_i, y_i), the relationship between x_i and y_i together with an error term ε_i can be described by

$$y_i = \alpha + \beta x_i + \varepsilon_i \tag{2.58}$$

The goal is to find estimated values for $\widehat{\alpha}$ and $\widehat{\beta}$ which provides the best fit of the data. The best fit is determined by the least squares approach which is a line that minimizes the sum of the residuals $\widehat{\varepsilon_i}$ that is the difference between the actual and the predicted values of the dependent variable. The values of $\widehat{\alpha}$ and $\widehat{\beta}$ are found by the equations where

- $\hat{x}$ and $\hat{y}$ are the average of x_i and y_i
- r_{xy} is the sample correlation coefficient between x and y
- s_x and s_y is the uncorrelated sample standard deviations of x and y

$$\begin{aligned} \hat{\alpha} &= \bar{y} - \hat{\beta}\,\bar{x}, \\ \hat{\beta} &= \frac{\sum_{i=1}^{n}(x_i - \bar{x})(y_i - \bar{y})}{\sum_{i=1}^{n}(x_i - \bar{x})^2} = r_{xy}\frac{s_y}{s_x} \end{aligned} \tag{2.59}$$

The coefficient of determination *R squared* is equal to r_{xy}^2 and describes the proportion of the variance in the dependent variable that is predictable from the independent variable.

Nonlinear regression

Nonlinear regression is a form of regression analysis where a nonlinear combination of the model parameters are dependent on one or more independent variables.

A nonlinear regression model is on the form where x is the independent variable and y is the dependent variable.

$$y \sim f(x, \beta) \tag{2.60}$$

Linearization Some functions, such as the exponential or logarithmic functions, can be transformed so that they become linear. When transformed, standard linear regression can be performed but must be applied with caution. The influences of the data values will change, as well as the error structure of the model.

The non-linear regression problem with parameters a and b and with multiplicative error term U can be transformed by taking the logarithm of both sides

$$y = a \ln^{bx} U \ln(y) = \ln(a) + bx + \ln U \tag{2.61}$$

The equation can be fitted with the simple linear regression model where $y = \ln y, \alpha = a, \beta = b$ and $\varepsilon = \ln U$.

Chapter 3

Method

This chapter explains how the research has been designed, how the results are obtained and how it is implemented into a program. It is centred around two main objectives: (1) a method for creating new flexure patterns by using tiles as design strategy and (2) a method for calculating the mechanical properties with the use of finite element analysis and repetitive boundary conditions. A discussion of the proposed methods are found in section 5.4. Before diving into the descriptions of the specific methods, some terms and tools used are presented.

Computational tools Making repeating patterns while convenient ways of varying parameters, calculating stiffness and exchange information is done through computational tools. The generation and export of patterns is done in Python though the use of open source software. The simulations are done in Abaqus CAE. The software packages used to build the tools are listed bellow.

Abaqus is a proprietary commercial software suite for finite element analysis and computer-aided engineering. Abaqus CAE is used for both the modeling and analysis of mechanical components and assemblies (pre-processing) and visualizing the finite element analysis result (post-processing). The Python code takes advantage of the Abaqus Scripting interface (ASI) to communicate with Abaqus. ASI is an extension of the Python 2.7 language and provides a convenient interface to the models.

Pyhton is a high-level programming language for general-purpose programming. It is implemented in C as CPython. One of the biggest strengths of the language is the large standard library and provides tools for many tasks. The syntax is simple which makes it fast to rapid prototype solutions. The language is free and open source.

Shapely is a Python package for geometrical manipulations outside the context of a database. It is build on GEOS, a useful object oriented C++ library in order to make and manipulate geometrical figures. This includes capabilities for defining geometries, predicate intersects, touches, overlaps etc., and to do operations like union, difference, buffer and the affine transformations. Shapely is available under the BSD-licence which is a family of permissive free software licenses, imposing minimal restrictions on the use and redistribution of covered software. The credits of this library goes to Sean Gillies, Aron Bierbaum and Kai Lautaportti.

Matplotlib is a plotting library that provides an object-oriented API for embedding plots into applications using general GUI toolkits. It is designed to be as usable as MATLAB, with the ability to use Python, and the advantage of being free and open-source.

Numpy is a library for the Python programming language, adding support for large, multi-dimensional arrays and matrices, along with a large collection of high-level mathematical functions to operate on these arrays. The ancestor of NumPy, Numeric, was originally created by Jim Hugunin.

Pandas is an open source BSD-licensed library for Python, offering data structures and operations for manipulating numerical tables and time series. It is an easy-to-use tool that is good at handling large amounts of data.

3.1 Creating new flexure patterns

This section introduce a design strategy for making new flexure patterns with *compatible compliant tiles*. A need for a method for creating new flexure patterns comes from the fact that the unit of the pattern only considers the symmetries of the pattern and not the flexure regions which is a more intuitive way of looking at a flexure pattern. The method also serve as a systematization where a flexure pattern is build from basic elements and simple principles that ensure good compliant behaviour.

A compatible compliant tile share many properties with ordinary tiles, but has some additional features. For any tilings the rule is simple: the tiles should fit together with no gaps or overlaps. The features of the method are conveniently summarized in three words that starts with a *C*: *compliant, connected* and *continuous* , where each word has its own set of strategies.

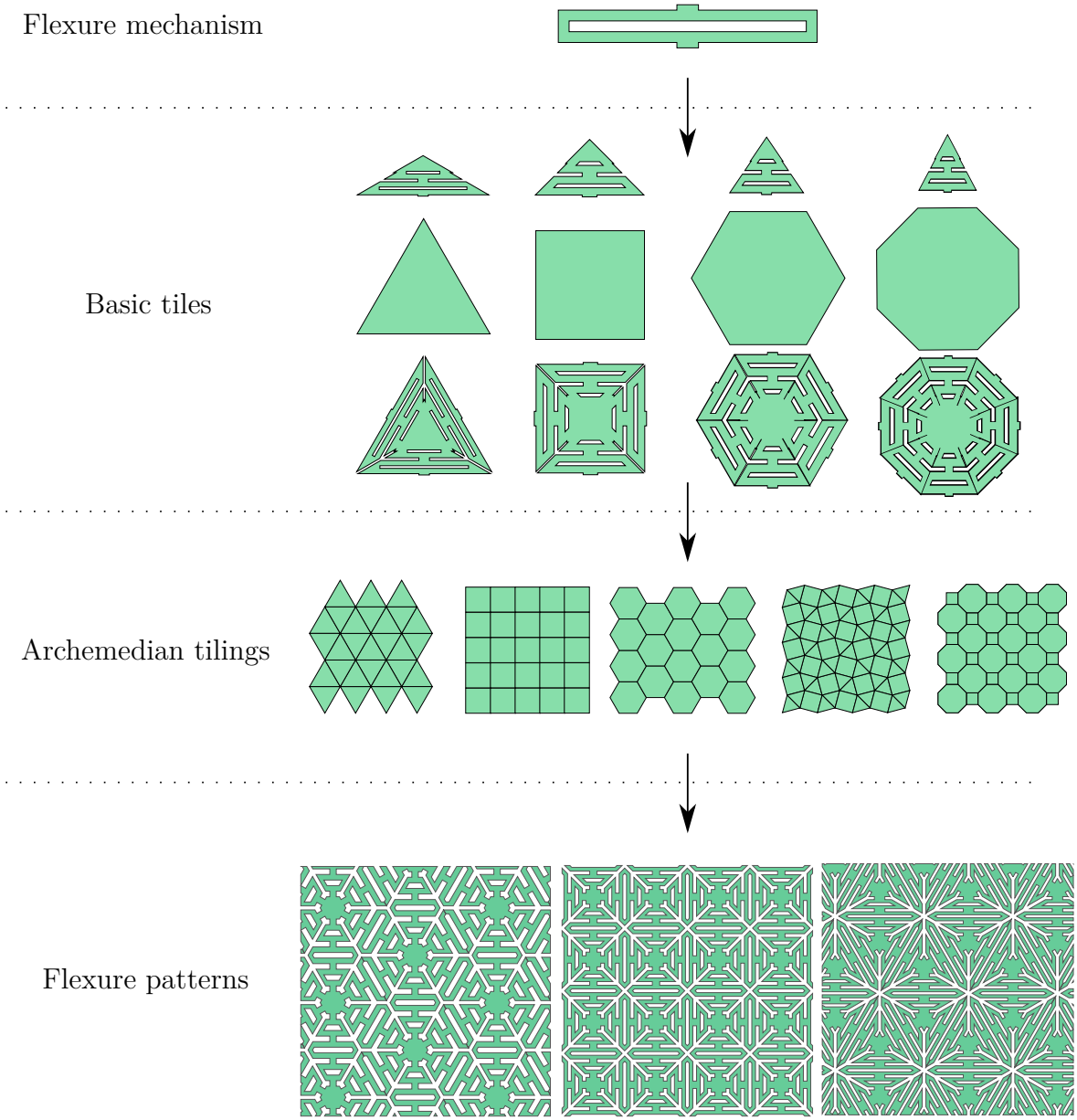

Figure 3.1: Overview of the proposed method for creating new flexure patterns.

3.1.1 Continuous

Choose a tiling

Like tilings, flexure patterns has no gaps or overlaps along the unit boundaries, which makes them continuous. By taking a tiling as a starting point one can ensure that the final flexure pattern tiles the plane. Among the k-uniform tilings there are 135 tilings with regular polygons.

Partition the tile into triangles

As most flexure mechanisms transfer motion from one point to another, it is desired to make a pattern where the points can meet and transfer the motion.

All convex polygons can be represented by a set of triangles. By taking center point inside the boundary to serve as a vertex, triangles can be created inside this point and two neighbouring vertices of the polygon. This triangle can be the region where a flexure mechanism is mapped, either direct or through a natural extension. When representing a regular polygon with triangles, all triangles will be congruent. Non-regular polygons will be represented by multiple different triangles. A figure of the method is shown in figure 3.2.

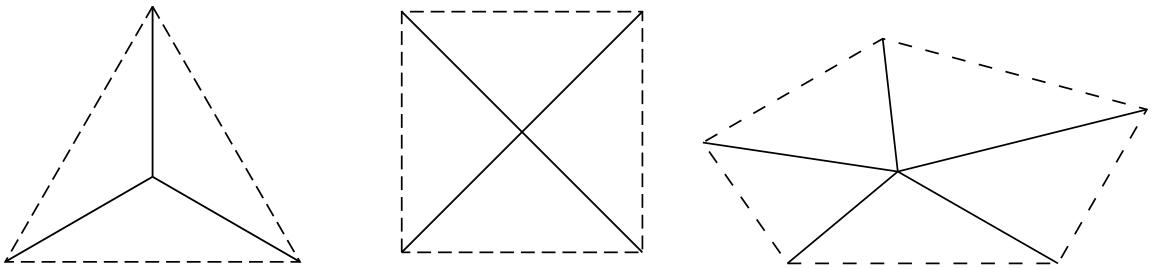

Figure 3.2: Partition a triangle, square and a convex polygon into trangles.

3.1.2 Connected

Matching connection point

The tiles must have a common connection point in order to be a continuous structure. The connection is dependent on which edges that meet and the placement of the connection point. The simplest connection points are symmetric points along the edge. This is illustrated by the arrows in figure 3.3.

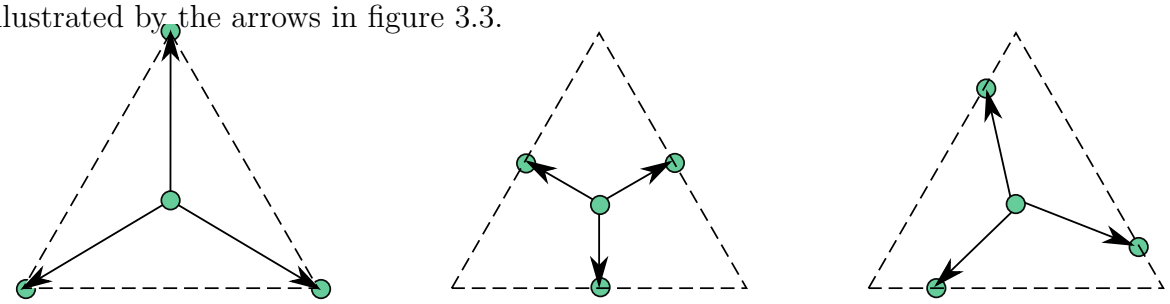

Figure 3.3: Example of two symmetrical and one example of asymmetrical connection points in a triangle.

In the case of a non-symmetric connection point, the corresponding connection must be a mirror. Ensuring that all edges in a tiling is connected, is not a trivial manner and is not carried out for all uniform tilings. For triangles and squares, *mirror tiles* can be used to create a continuous pattern in the case where the edges are not symmetric. These are shown in figure 3.4 for a 3^6 and 4^4 tiling. An example of a symmetric edge is seen for the *LET p4m* tile.

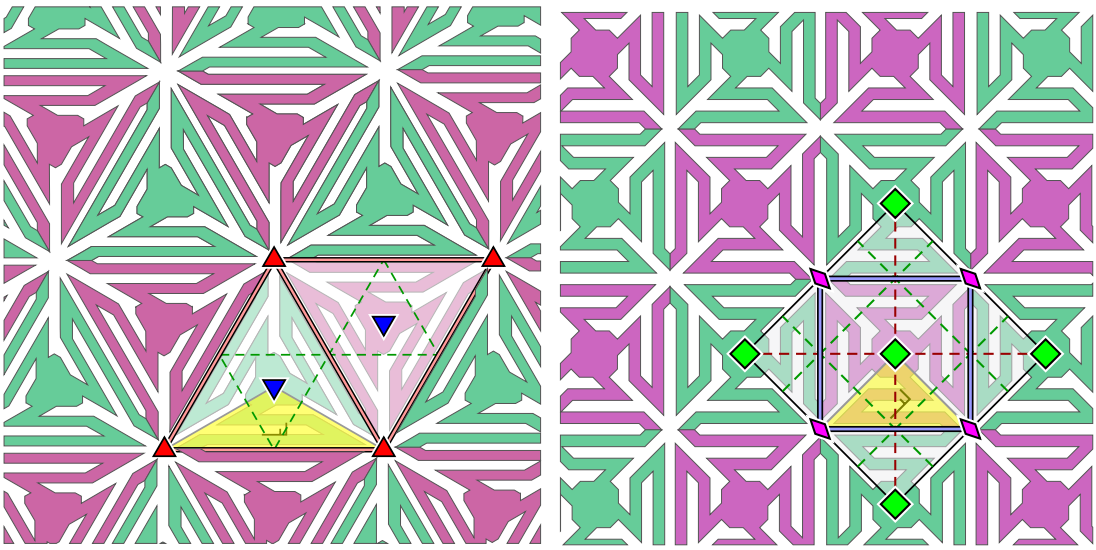

(a) Triangular switchback flexure configuration of a 3^6 tiling. The symmetry group *p31m* is marked.

(b) Square switchback flexure configuration of a 4^4 tiling. The symmetry group *p4g* is marked.

Figure 3.4: Mirror tiles are used to make a connected flexure pattern. The different colors represent the two mirrored tiles.

3.1.3 Compliant

Choose flexure mechanism

All compliant tiles need to have flexible members that increases the compliance and the configuration will determine many of the properties.

The two deformation modes: bending and torsion increase the travel length as seen in section 2.3.2. Bending modes are the only possible deflection modes to increase the compliance in plane. Bending also works out of plane, but will often create a surface where flexures are sticking out, creating a serrated surface. Torsion modes are effective for achieving out of plane deflection.

The flexure configurations LET, Switchback and Coil are the flexure configurations used in this thesis.

Array of flexures and natural extension

The natural extension is when a flexure or flexure mechanism is being repeated in order to fill an area with an other shape. The flexure can repeat in parallel, series and be scaled to fill the space given by the boundary. By patterning flexures in series, the compliance is increased, while flexures in parallel decrease the compliance according to equations 2.4.

When this method is combined with partition the polygon into triangles, compliant tiles can be made as seen in figure 3.5. Different tiles with the same flexure mechanism and the same polygon also share the same symmetries even though it contains more flexures in the array. These tiles belong to the same *family* as seen in figure 3.6.

It is necessary to avoid inactive flexures because it increases the manufacturing time without contributing much to the compliance. When patterned in an array, the flexures

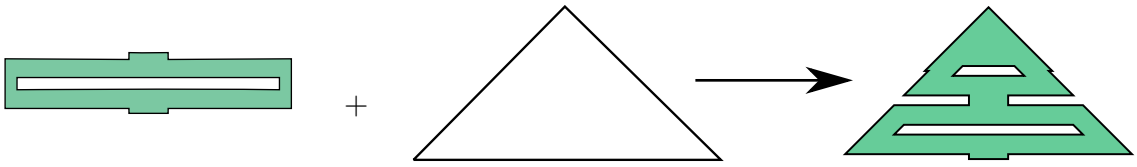

Figure 3.5: A LET extended and patterned in series to fill a new boundary condition.

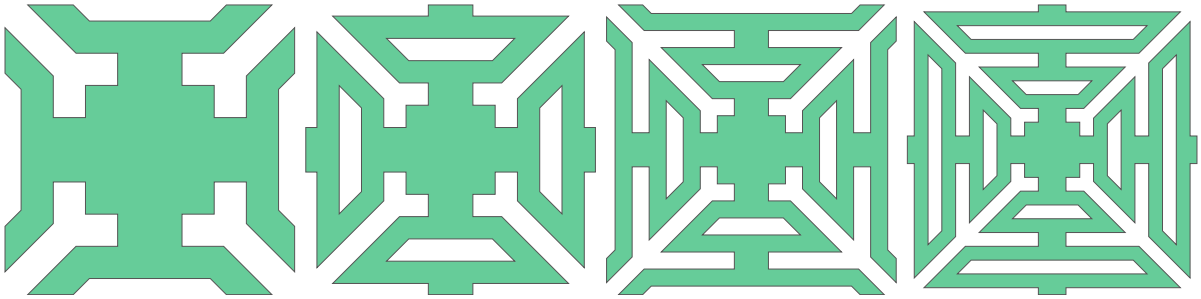

Figure 3.6: A family of tiles with the flexure mechanism patterned in series, forming a natural extension.

should not inhibit other flexures to deform which is the opposite to a truss structure where different members are constructed to inhibit motion.

An example of a flexure pattern found on the internet is the *bastian* pattern that consists of a triangular configuration of LETs. The LETs are connected in a truss triangle that inhibit motion to be transferred to the inner flexures of the triangle. A figure of the pattern with the bend mode is seen in figure 3.7a.

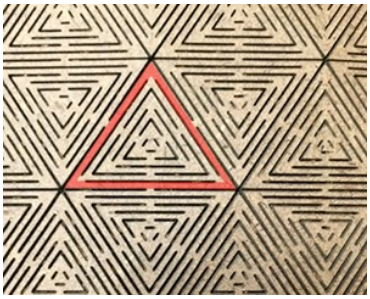

(a) Bastian pattern found on http://fabacademy.org. The flexures inside the red area are concealed and wont increase the compliance.

(b) Bent form of the Bastian pattern.

Figure 3.7: Example of a flexure pattern with inactive flexures.

3.1.4 Summary and example of the method

The method is demonstrated to make a triangle tile. Other new flexure patterns created by this method are found in section 4.1.

Continuous Make a continuous pattern configuration from junction point to junction

point that transfers the deformation mode

- Choose a tiling.
- Make triangles from center of area to the vertices or other polygons from center to the middle of edges.

Connected The corresponding edges must have a common connection point.

- Connections meet at the same place and with the same length; is various for symmetric and asymmetric edge.

Compliant Use a flexure mechanism as deformation mechanism

- Choose deformation modes for out of plane deformation: torsion has no parts sticking up, while bending has.
- Make an array of flexures to increase compliance: consider the natural extension of the flexure mechanism.
- Avoid interlocking regions; either make a flexure region or a rigid region.

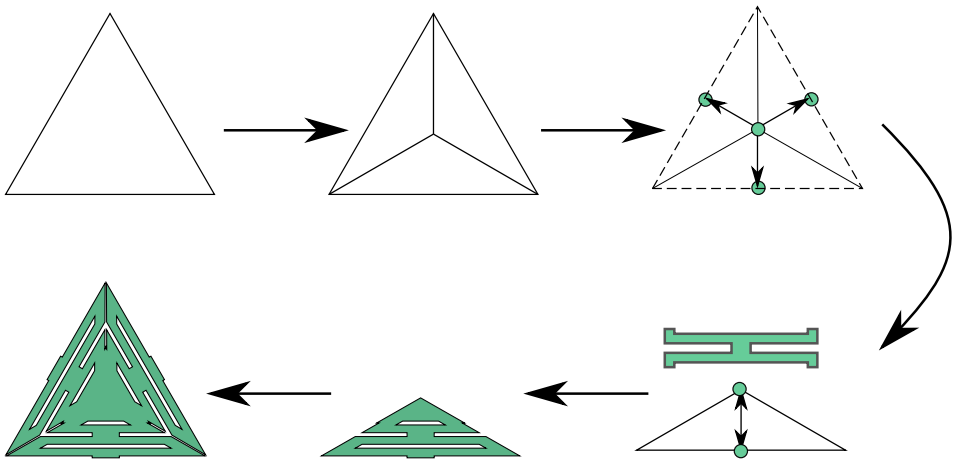

Figure 3.8: The regular polygons can be represented with the natural extension of a compliant mechanisms.

3.1.5 Python implementation

This subsection describes the creation of flexure patterns with Python code. To run this code, Python 2.7 or newer, Numpy, Matplotlib, Pandas and Shapely libraries are required. Particular challenges for making the classes robust are the handling of geometry where

relationships are represented by irrational numbers, as seen in appendix B.1.4. Example code implementations are found in appendix B.

The essential classes are the `Polygon`, `GeneratingRegion` and `Unit`:

Polygon The basic geometrical object is provided by the Shapely library which also contains a set of useful predicates and operations.

GeneratingRegion inherent form the `Polygon` class. It provides the smallest regions of what a unit or a tile is created from. The main attribute is the `generating_region` which holds the geometry of the parameterized generator.

Unit inherent from the `GeneratingRegion` class and is the repeating unit that map the plane through translation. The main attribute is the `unit` which holds the geometry of the generating region. There are methods based on the affine transformations described in 2.4.2 that generates a unit from the generating region according to the right symmetry group. There is also a method that makes a flexure pattern to the requested size. Another method generates an output `.svg` file.

An inheritance ULM diagram of the classes that are created is shown in figure 3.9. The framework is based on the classification of wallpaper groups and tilings.

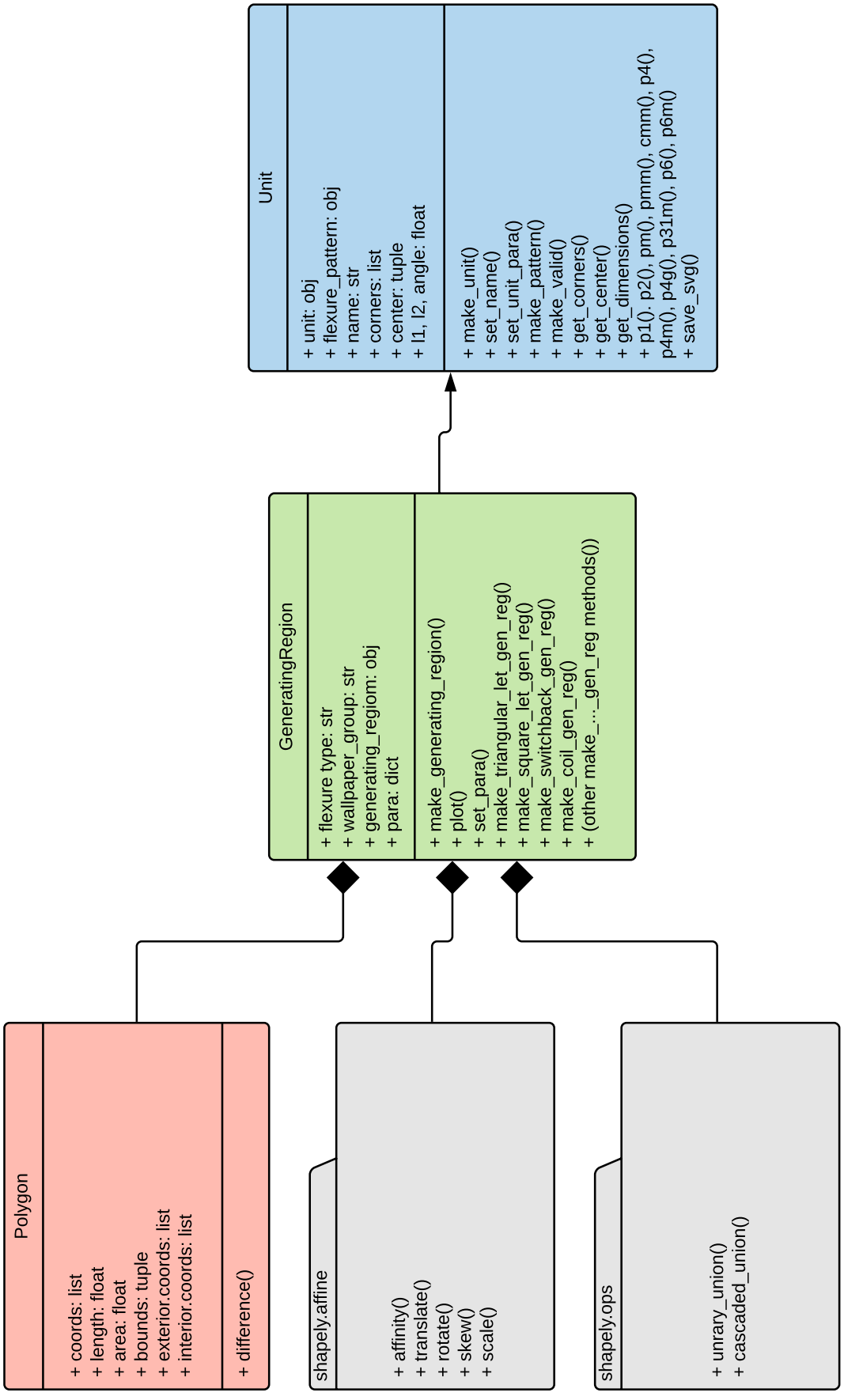

Figure 3.9: ULM diagram describing the class structure.

3.2 Calculating mechanical properties

This section describes the procedure of taking a unit of a pattern or a tile, and calculating the properties using Abaqus CAE with the computational homogenization technique. As Abaqus do not have a built in unit system, the consistent units given in table 3.1 are used:

Mass	1 kilogram (kg)
Length	1 meter (m)
Time	1 second (s)
Force	1 Newton (N)
Moment	1 Nm
Stress	1 Pascal (Pa)
Energy	1 Watt (W)

Table 3.1: Consistent units

Where material data is needed the Young's' modulus E is set to 1000 and Poisson's ratio ν is set to 0.3 for all simulations.

3.2.1 Abaqus implementation of a plate RVE

Constrained equations in Abaqus

The linear *multi point constraint* (MPC) in Abaqus requires that a linear combination of nodal variables is equal to zero. It is defined by the equation

$$A_1 u_i^P + A_2 u_j^Q + ... + A_N u_k^R = 0 \tag{3.1}$$

where u_i^P is the nodal variable at node P, with degree of freedom i and A_N are the coefficients that define the relative motion of the nodes or set of nodes.

The constrained equation for computational homogenization is a nonhomogeneous case where the length between two corresponding nodes are equal to the prescribed elongation $\widehat{u} = \Delta\varepsilon_i$.

$$A_1 u_i^P + A_2 u_j^Q = \widehat{u} \tag{3.2}$$

By rewriting this equation and introducing a node, Z, that is not attached to any element in the model we can control the nonhomogeneous constraint through Z with a suitable degree of freedom m.

$$A_1 u_i^P + A_2 u_j^Q - \widehat{u}_m^Z = 0 \tag{3.3}$$

In the FE model, a reference point (RP) in x, y and z direction (RPX, PRY and RPZ) is created to impose the prescribed unit deformations. The strains and curvatures are set as input variables for each load case, e.g for load case one:

$$(\varepsilon_{xx}, \varepsilon_{yy}, \gamma_{xy}, \kappa_{xx}, \kappa_{yy}, \kappa_{xy}) = (1, 0, 0, 0, 0, 0) \tag{3.4}$$

For a rectangular unit, the nonhomogeneous part of the equation for the nodes on the sides with x-normals can be written as:

$$\begin{aligned}\widehat{u}_1^{RPX} &= (+)\Delta x(\varepsilon_{xx} + z\kappa_{xx}) \\ \widehat{u}_2^{RPY} &= (+)\frac{1}{2}\Delta x(\gamma_{xy} + z\kappa_{xy}) \\ \widehat{u}_3^{RPZ} &= (-)\frac{1}{2}\Delta x(y\kappa_{xy})\end{aligned} \tag{3.5}$$

The nodes with y-normals are written in the same way but with κ_{yy}andΔy as variabels.

Over-constraining the unit

The concept of over-constraining a cell is illustrated in figure 3.10. If we consider the homogeneous case for four constrained equations C_q along the corners of the unit we get

$$\begin{aligned}Cq_{12}: &\quad u_2 - u_1 = 0 \\ Cq_{14}: &\quad u_4 - u_1 = 0 \\ Cq_{43}: &\quad u_3 - u_4 = 0 \\ Cq_{23}: &\quad u_3 - u_2 = 0\end{aligned} \tag{3.6}$$

If the following equations are investigated, one can see that Cq_{23} can be written in terms of the other three equations

$$-Cq_{12} + Cq_{14} + Cq_{43} = -(u_2 - u_1) + u_4 - u_1 + u_3 - u_4 = u_3 - u_2 = 0 \tag{3.7}$$

This is an important aspect, as over-constraining a system will cause the simulation to abort.

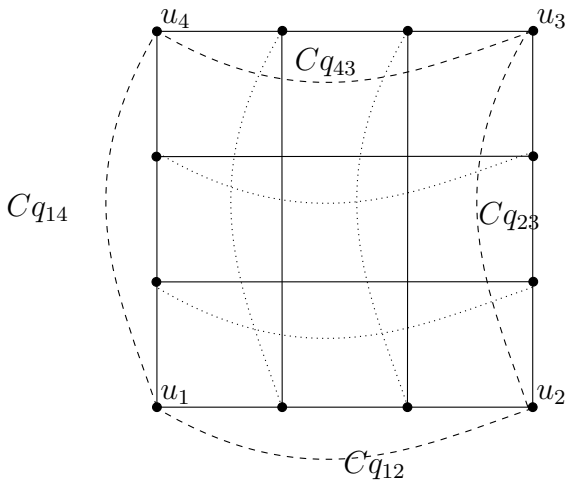

Figure 3.10: Dependent constrained equations. Dotted lines are constrained equations not represented by symbols, while the dashed lines are represented through the $Cq_{..}$ notation.

Obtaining results

By prescribing a strain, or curvature, the sum of the resultant forces or moments along the edges is equal to the stiffness component. Figure 3.11 show the forces and along the different sides.

$$\begin{bmatrix} N_x \\ N_y \\ N_{xy} \\ M_x \\ M_y \\ M_{xy} \end{bmatrix} = \begin{bmatrix} A_{xx} & 0 & 0 & 0 & 0 & 0 \\ A_{xy} & 0 & 0 & 0 & 0 & 0 \\ A_{xs} & 0 & 0 & 0 & 0 & 0 \\ B_{xx} & 0 & 0 & 0 & 0 & 0 \\ B_{xy} & 0 & 0 & 0 & 0 & 0 \\ B_{xs} & 0 & 0 & 0 & 0 & 0 \end{bmatrix} \begin{bmatrix} 1 \\ 0 \\ 0 \\ 0 \\ 0 \\ 0 \end{bmatrix} \tag{3.8}$$

For nods found on side X and Y. B components will equal zero for plane strain and for plain curvature.

$$\begin{aligned} A_{xx} &= \frac{\sum F_x^X}{\Delta_Y}, \quad A_{xy} = \frac{\sum F_y^Y}{\Delta_X} \\ A_{xs} &= \frac{\sum F_y^Y/\Delta_x + \sum F_x^X/\Delta_y}{2} \\ B_{xx} &= \frac{\sum M_x^X}{\Delta_y}, \quad B_{xy} = \frac{\sum M_y^Y}{\Delta_x} \\ B_{xs} &= \frac{\sum M_{xy}^X/\Delta_y + \sum M_{xy}^Y/\Delta_x}{2} \end{aligned} \tag{3.9}$$

Where moments are given as:

$$M_x^X = \sum F_x^X z, \qquad M_y^Y = \sum F_y^Y z, \qquad \begin{aligned} M_{xy}^X &= \sum (F_y^X z - F_z^X y) \\ M_{xy}^Y &= \sum (F_x^Y z - F_z^Y x) \end{aligned} \tag{3.10}$$

For a prescribed curvature κ_x, the components are calculated the same but the components are ordered differently.

$$\begin{aligned} B_{xx} &= \frac{\sum F_x^X}{\Delta_y}, \quad B_{xy} = \frac{\sum F_y^Y}{\Delta_x} \\ B_{xs} &= \frac{\sum F_y^Y/\Delta_x + \sum F_x^X/\Delta_y}{2} \\ D_{xx} &= \frac{\sum M_x^X}{\Delta_y}, \quad D_{xy} = \frac{\sum M_y^Y}{\Delta_x} \\ D_{xs} &= \frac{\sum M_{xy}^Y/\Delta_x + \sum M_{xy}^X/\Delta_y}{2} \end{aligned} \tag{3.11}$$

By repeating this process each load case, the full stiffness matrix can be found.

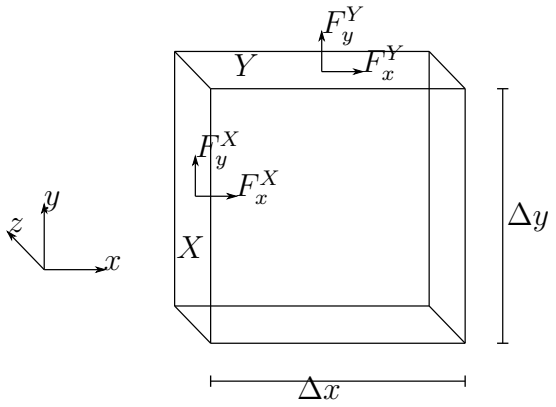

Figure 3.11: The directions of of the nodal forces.

Simulation program

This section explains the basic form of the Python code that controls the Abaqus simulation. The code can be accessed through the menu in Abaqus/CAE: *File* → *Run Script*, or in the terminal with the command `abaqus cae script.py`

A flowchart of the implementation is shown in figure 3.12. The different steps are also visualized in the Abaqus GUI in figure 3.13. The full code is carefully documented and can be found in appendix B.2.The load cases with prescribed strains on a simulated unit can be seen in in figure 3.14.

Part module Creates a part from the coordinates of a Unit object. It partitions it so that there is a node in the middle.

Material and Section module Sets the material properties of the part. In this simulation the material is set to a linear elastic material.

Mesh and assembly module Seeds and creates a mesh on the part. Makes and assembly instance and creates assembly sets that are used to reference the nodes later in the post processing module.

Step module Creates a static step and sets the prescribed displacements to the reference points.

Job module Prepares a job for the specific load case.

Post processing module Reads the output database and takes the sum of the nodal forces and calculates the stiffness components. Writes all data to a text file.

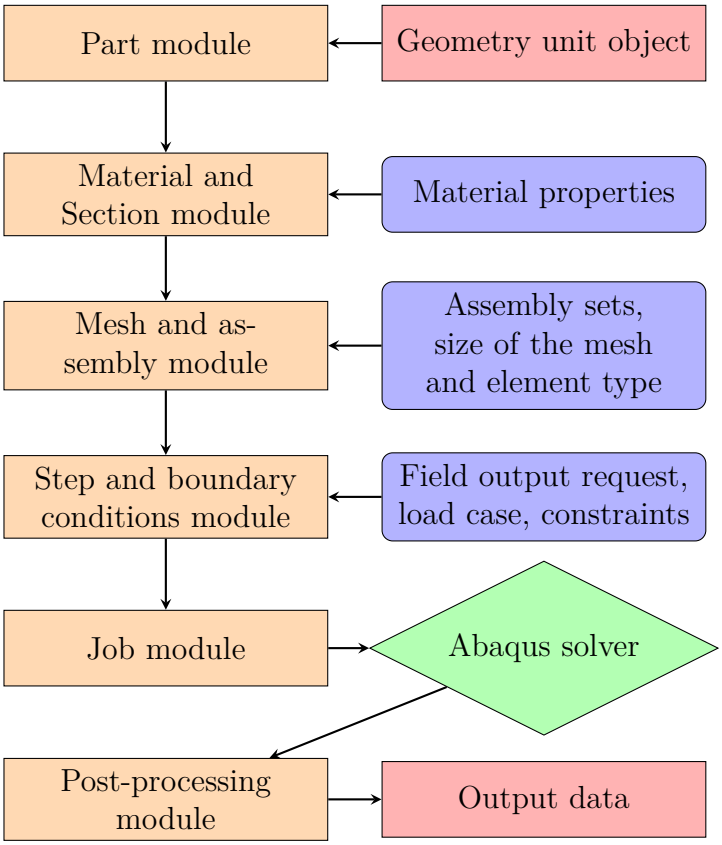

Figure 3.12: Representation of the Python code for computing the stiffness components of the RVE.

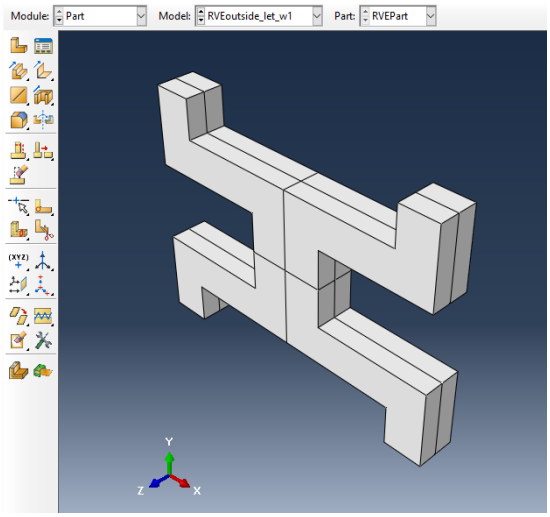

(a) Part module

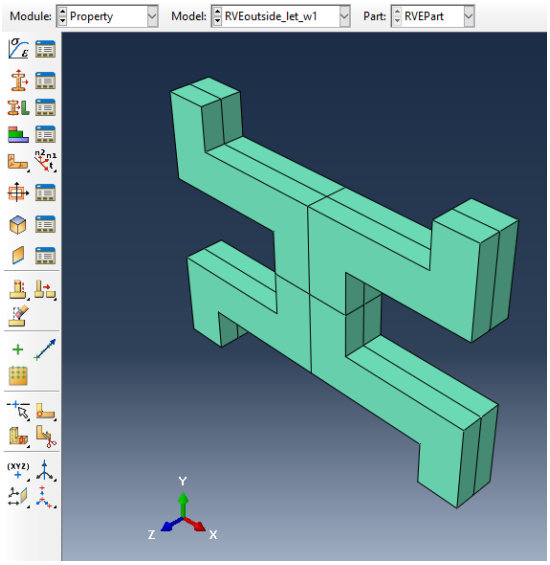

(b) Material and Section module

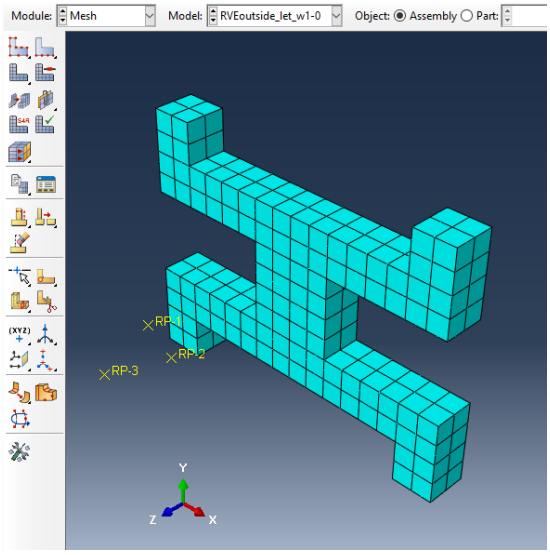

(c) Mesh and assembly module

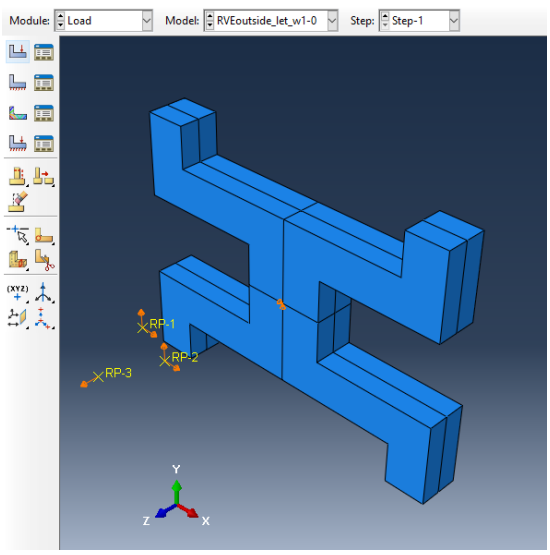

(d) Step and boundary conditions module

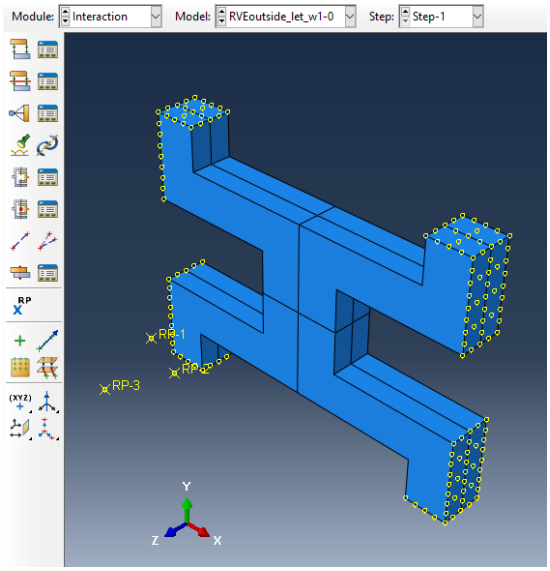

(e) Step and boundary conditions module: constrained equations

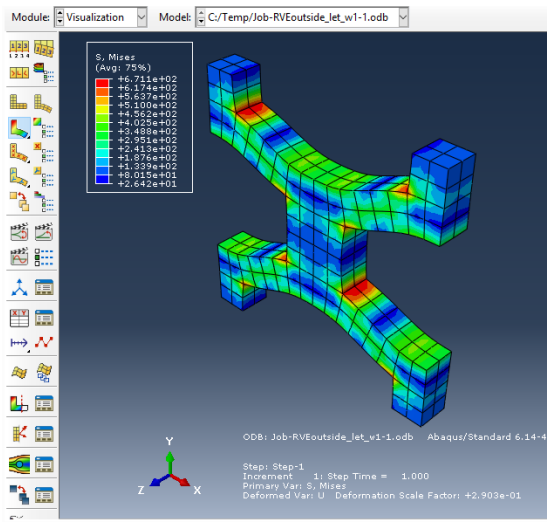

(f) Post processing module after ended Job simulation

Figure 3.13: The different Abaqus modules necessary for obtaining numerical results. The Job module from the flowchart is not visualized.

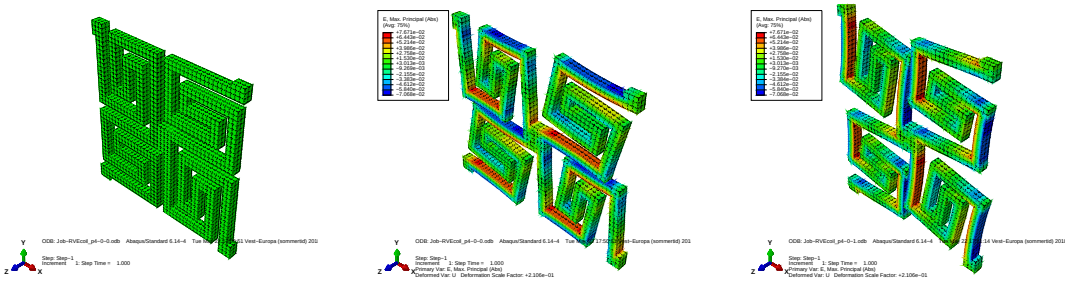

(a) Undeformed model (b) Strain, x-direction (c) Strain, y-direction

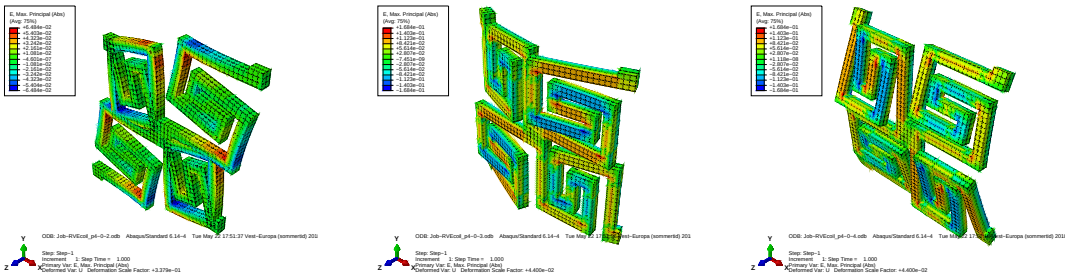

(d) Shear (e) Bending, x-direction (f) Bending, y-direction

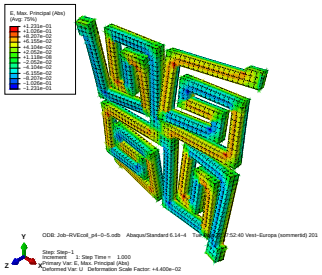

(g) Twist

Figure 3.14: Strain state of a RVE of a flexure pattern.

3.2.2 Evaluation of numerical model

The model can be checked against a solid plate where the stiffness is known beforehand. From figure 3.15 we can observe that the model experiences uniform strain in all cases with the same magnitude as the prescribed strains. The stiffness components of a plate with $E_1 = 1000$ and $v_{12} = v_{21} = 0.3$ is given by the equations:

$$\begin{aligned} A_{11} = A_{22} = h\frac{E_1}{1 - v_{12}v_{21}} \quad A_{12} = h\frac{v_{12}E_1}{1 - v_{12}v_{21}} \quad A_{66} = hG_{12} = h\frac{E_1}{2(1+v)} \\ D_{11} = D_{22} = \frac{h^3}{12}\frac{E_1}{1 - v_{12}v_{21}} \quad D_{12} = \frac{h^3}{12}\frac{E_1}{1 - v_{12}v_{21}} \quad D_{66} = \frac{h^3}{12}G_{12} = \frac{h}{12}\frac{E_1}{2(1+v)} \end{aligned} \tag{3.12}$$

A comparison between results from the simulated and the analytically calculated equations are shown in table 3.2. This show that the results has a small error of ± 0.05 when a solid plate is considered.

Stiffness component	Analytic calculation	Simulated result
A_{11}	1098.90	1098.90
A_{12}	329.67	329.67
A_{66}	384.62	384.62
D_{11}	91.58	91.58
D_{12}	27.47	27.47
D_{66}	32.05	32.05

Table 3.2: Comparison between analytically calculated and simulated stiffness components.

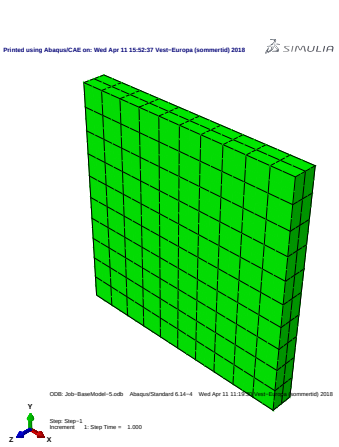

(a) Undeformed model

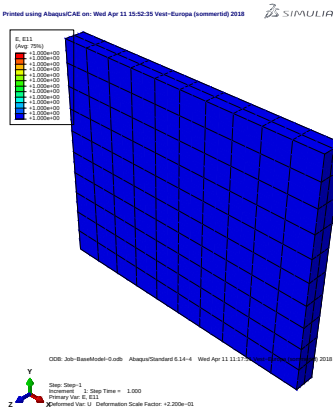

(b) Uniform strain, x-direction

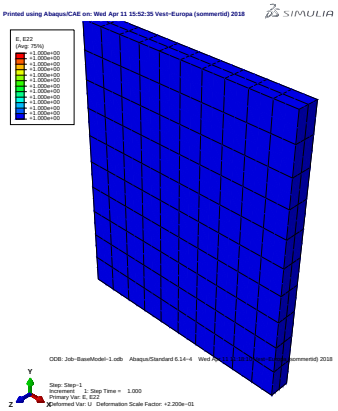

(c) Uniform strain, y-direction

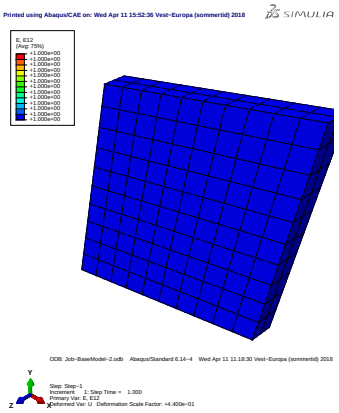

(d) Uniform shear

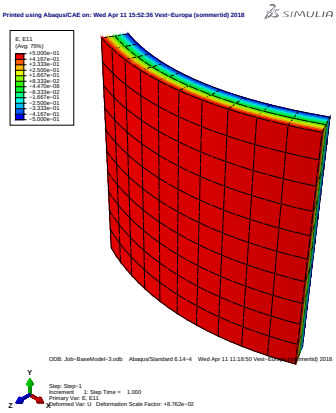

(e) Uniform curvarure, x-direction

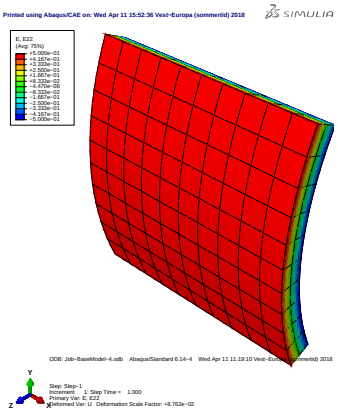

(f) Uniform curvarure, y-direction

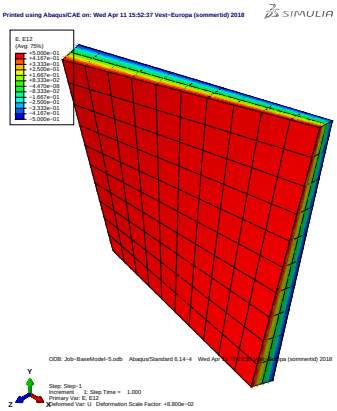

(g) Uniform twist

Figure 3.15: Stain states of a plain plate.

Element convergence test

There are two independent parameters to study when generating a mesh: *element type* and *element size*.

Different element types capture the different deformation modes at different accuracy and is chosen for different models. In this model, solid elements are chosen to capture the resultant moments which distribute along the thickness of the edges.

The convergence test is needed to determine the size of elements. It is carried out by refining the element size until there is no difference in FEA results. The number of element is relevant for time used to conduct an analysis. For this reason the combination of element type and element size is relevant when choosing the mesh size. Stress analyses need finer mesh for capturing correct stress while resultant forces are being captured more correctly by a courser mesh.

The solid elements tested are:

C3D8 linear brick element with 8 nodes

C3D20 quadratic brick element with 20 nodes

C3D20R quadratic brick element with 20 nodes with reduced integration

The expression *full integration* refers to the number of Gauss points required to integrate the polynomial terms in an element stiffness matrix exactly when the element has a regular shape.

Reduced-integration elements use one fewer integration point in each direction than the fully integrated elements. Linear reduced-integration elements tend to be too flexible because they suffer from their own numerical problem called hourglassing.

Linear elements with full-integration tend to be stiffer for bending since they capture bending with a shear like distortion. When bending deformation is present these are recommended to be avoided.

The model geometry and loading determine the different deformations: tension, compression, shear, uniaxial, plane strain etc. and are relevant for the result. The best is to use the actual model for determination of mesh size because small details in the model can render the mesh dependent. Due to the large number of different models, the LET cmm that captures all deformation modes is used. Here A_{11} capture tension, A_{22} capture bending, A_{66} capture shear, D_{11} capture bending, D_{22} capture torsion, D_{66} capture twist.

The best result is obtained by choosing the right element type and to reduce the element size. Some of the meshes used, can be seen in figure 3.17 and the results can be seen in figure 3.16. From this we observe that C3D8 elements show a stiffer behaviour than C3D20 and C3D20R and C3D20R is less stiff than C3D20. 2 elements across the cross section results in C3D20 and C3D20R being 0.02 from the result with 5 elements for all components except for twist of D_{66} where the error is 0.12. Sufficient results for D_{66} is obtained with 4 elements across the cross-section.

Computation time is also a relevant factor when many simulations are ran. A minimum of 2 elements across the cross-section, can be good enough for most results if the errors for D_{66} is acceptable.

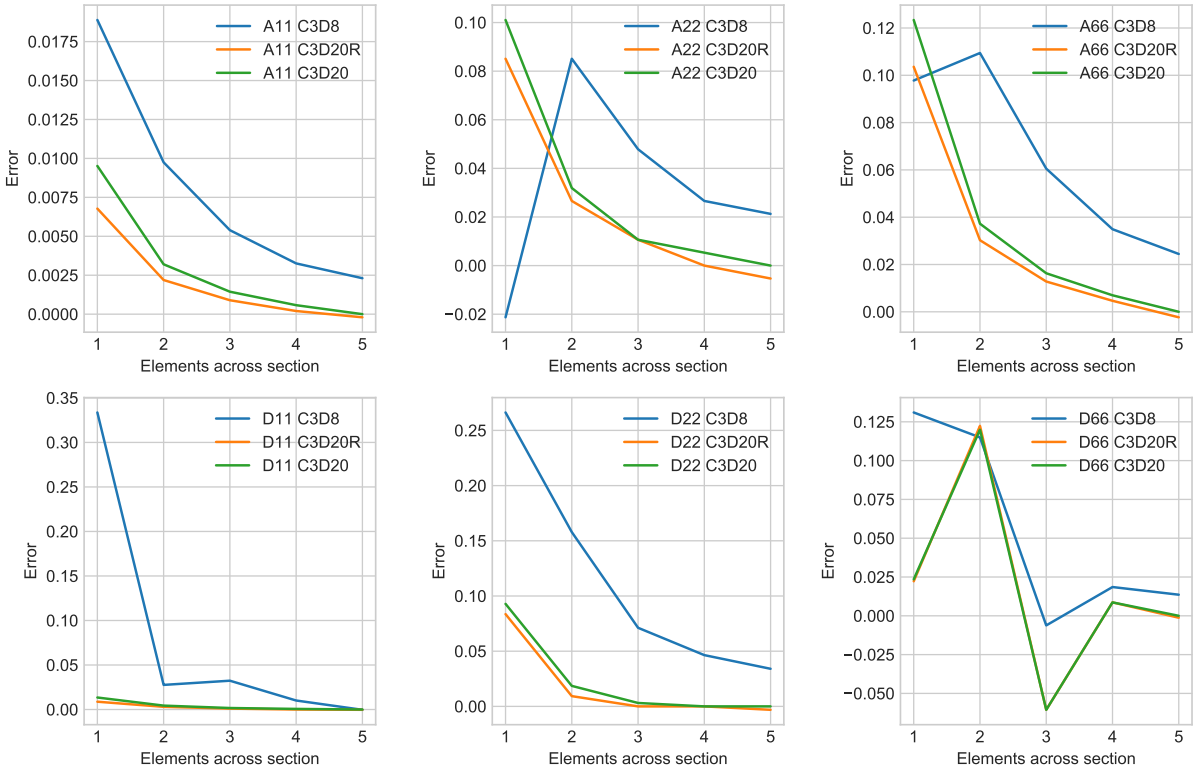

Figure 3.16: Convergence of results for different components with different elements and sizes. X-axis is number of elements across cross-section of the LET, y-axis is error calculated relative from the last result of a C3D20 element.

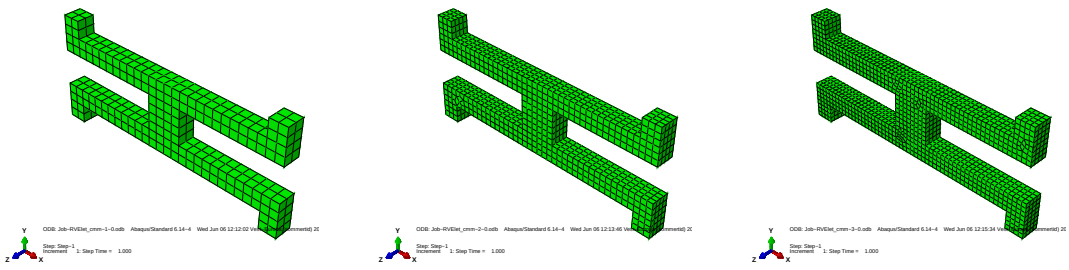

Figure 3.17: Mesh size of LET during convergence test.

3.2.3 Multi-variable simulations

The described computational models are used to simulate a variety of different flexure patterns. The steps to obtain data are briefly summarized:

1. Geometrical variations of flexure patterns are generated through the Python Unit class.

2. The stiffness matrix is calculated with the computational homogenization method and saved to a *.csv* file.

3. The results are analyzed and plotted with the use of Pandas, Matplotlib and statistic regression models.

Relating numerical and analytically stiffness

For comparing the numerical results from the simulations with the expressions for the flexure strip, we want to describe the spring stiffness K given in section 2.3.1 as plate stiffness components in the principal directions. We note that the coupling terms are not taken into the results, but will play a significant role for some patterns. The form the stiffness components with no coupling can be written as

$$N_i = A_{ii}\varepsilon_i \qquad M_i = D_{ii}\kappa_i \tag{3.13}$$

where N_i and M_i are given as force and moment per unit length l_i (as seen in figure 4.3) and $i = 1, 2$. ε is related to the axial displacement u and the length of the unit length l_i. κ is related to the angular displacement θ and the curvature of the simulated unit l_i.

$$u = \varepsilon l_i \qquad \theta = \kappa l_i \tag{3.14}$$

By inserting these into the equation 2.34 for F and M we obtain.

$$N_i = K^u l_i \varepsilon_i = A_{ii}\varepsilon_i \qquad M_i = K^\theta l_i \kappa_i = D_{ii}\kappa_i \tag{3.15}$$

The LET cmm flexure pattern is a good candidate to investigate how the change of geometrical parameters effect the stiffness. This because the deformation modes are closely related to the bending of a flexure strip and occur separated for the different stiffness components. When comparing analytically results with the simulated results, one have to be careful on the axes for I and J as these are different for the various bending modes. From this we expect:

- A_{11} to be a governed by axial tension stiffness K_t^u.
- A_{22} to be governed by bending mode with stiffness K_B^u. that is dependent on both thickness and length for the cross-section
- D_{11} to be governed by a bending mode of a beam K_B^θ.
- D_{22} to be governed by the torsion of a beam K_T^θ.

With the assumption of the flexure length being approximately the length of the simulated units, $L \sim l_i$ for D_{11} the proportions between the stiffness components and the parameters are:

$$\begin{aligned} A_{11} &\propto (E, w, t) \\ A_{22} &\propto (E, w^3, t, L^{-3}) \\ D_{11} &\propto (E, w, t^3) \\ D_{22} &\propto (E, J(w, t), L^{-1}) \end{aligned} \tag{3.16}$$

The full expressions contains more dependencies between the variables like like l_i which is influenced by the width or length of the flexure as well as the rigid regions. These are not considered and will cause some error.

Chapter 4

Results

4.1 New flexure patterns

This section presents the geometry of some new flexure patterns found using the design strategies described in 3.1. Table 4.1 show these flexure patterns with interesting characteristics and describes the patterns by flexure type, symmetry group and regular tiling. All flexure patterns belongs to a family (as described in 3.1.3) and can be extended with more flexures.[1]. Illustrations of the flexure patterns are found in figures 4.1 and 4.2.

Flexure type	Symmetry group	Regular tiling	Comment
LET	p4m	4^4	
LET	p6m	3^6	
LET	p6m	6^3	
Switchback	cmm	-	non regular tiles
Switchback	p4	4^4	
Switchback	p4g	4^4	mirror tiles
Switchback	p31m	3^3	mirror tiles
Switchback	p6	3^6	
Switchback	p6	6^3	
Coil	cmm	4^4	
Skew coil	p6	6^3	skew $+30°$
Skew coil	p6	6^3	skew $-30°$

Table 4.1: List over new flexure patterns

[1]Switchback cmm is only observed with one switchback. The general version is therefore presented here as a new flexure.

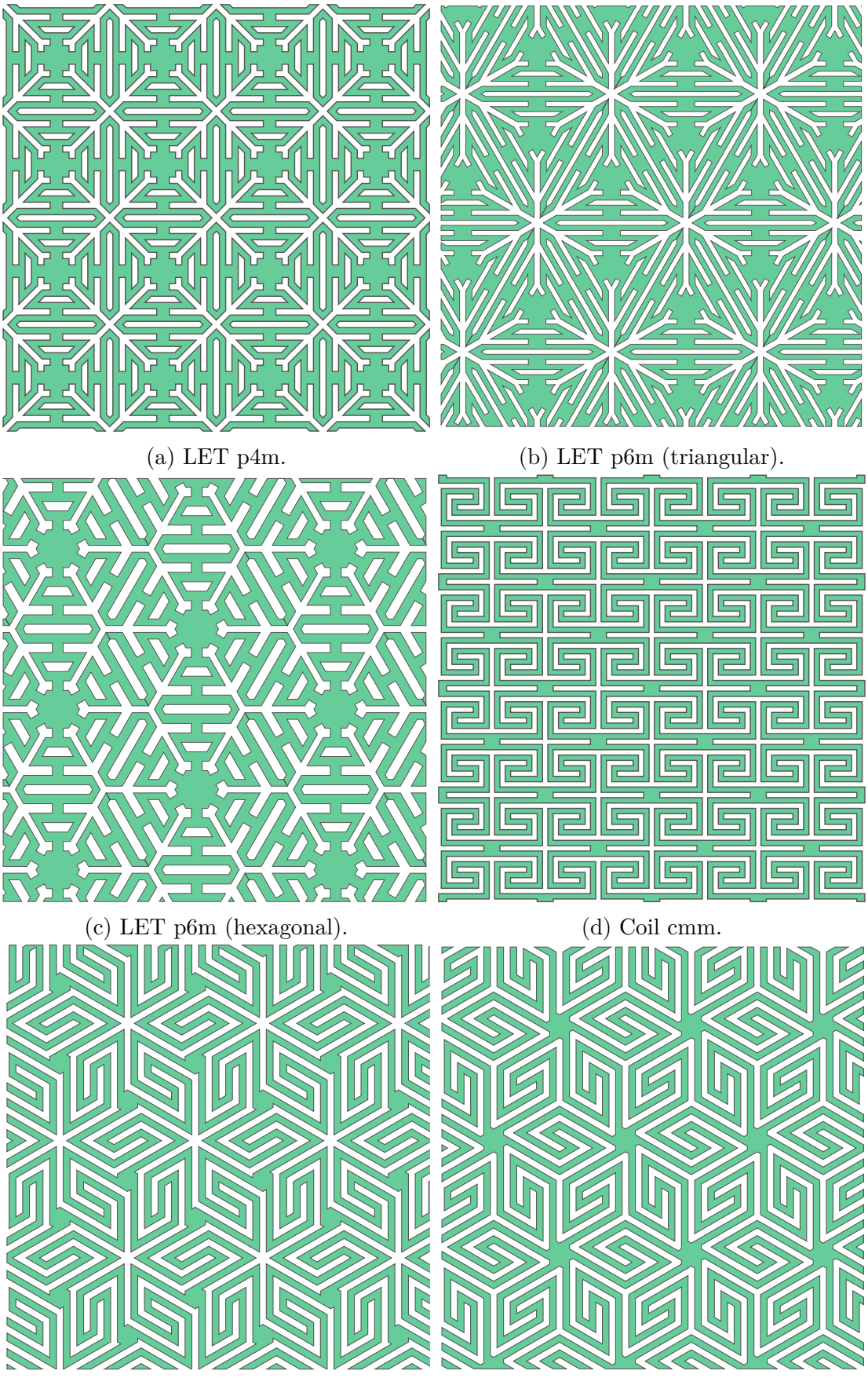

(a) LET p4m.

(b) LET p6m (triangular).

(c) LET p6m (hexagonal).

(d) Coil cmm.

(e) Coil p6 (skew −30°).

(f) Coil p6 (skew +30°).

Figure 4.1: New flexure patterns corresponding to table 4.1.

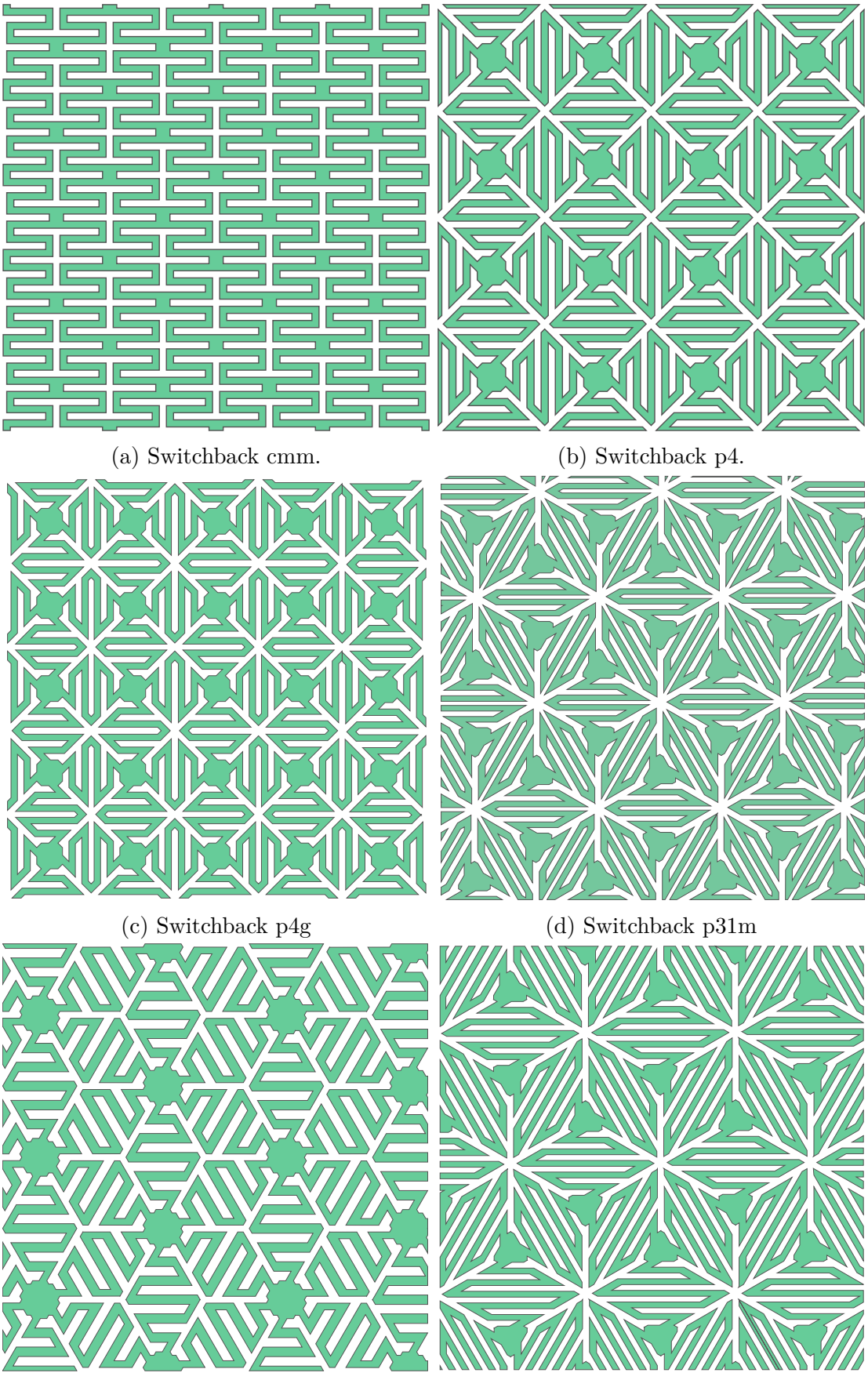

(a) Switchback cmm.

(b) Switchback p4.

(c) Switchback p4g

(d) Switchback p31m

(e) Switchback (hexagonal) p6

(f) Switchback (triangular) p6

Figure 4.2: New flexure patterns corresponding to table 4.1.

4.2 Mechanical behaviour

The stiffness matrix of the flexure patterns in table 4.4 are calculated with the method described in section 3.2. The results are presented in terms of anisotropy and the variation of geometrical parameters. In addition, some special behaviour and properties of the stiffness matrices are highlighted. The simulated thickness is set to 1, if not else is commented, and gives the relationship $[A] = [Q]$.

4.2.1 Principal deformation mechanisms

The relations between basic geometrical parameters of flexures and the principal equations for determining the properties of the laminate stiffness matrix is showed for a LET cmm. The simulations are done with the values and variables for given in table 4.2 and a description of the measurements are found in figure 4.3.

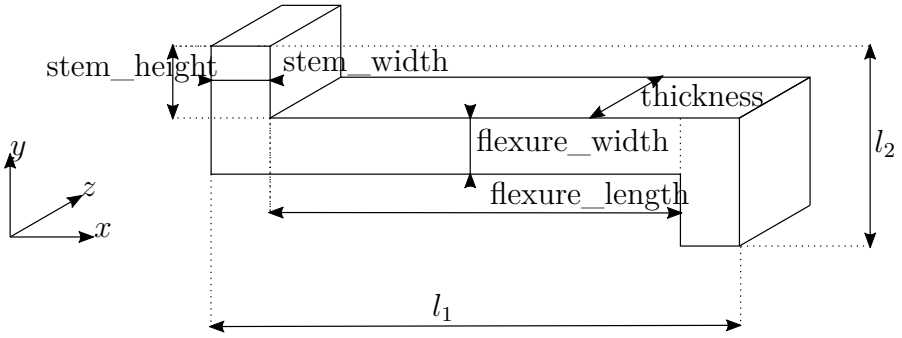

Figure 4.3: Dimensions of the generating region for the LET.

Simulation	Flexure length	Flexure width	Stem length	Stem width	Thickness	Data points
1	[1.0, 32.0]	1.0	1.0	1.0	1.0	6
2	5.0	[0.2, 3.0]	1.0	1.0	1.0	10
3	1.0	1.0	[1.0, 6.0]	1.0	1.0	6
4	1.0	1.0	1.0	[1.0, 6.0]	1.0	6
5	5.0	1.0	1.0	1.0	[0.5, 8.0]	8

Table 4.2: Dimensions of the simulated LET cmm. Variation of parameters is given in an interval [-].

A plot of the results from simulation 1 is shown in figure 4.4. Simulation 5 is shown in figure 4.5. All plots are found in Appendix C. A complete table of the estimated slope of the linear- or logarithmic regression line is shown in table 4.3 together with the statistical R^2 values. The table show only the values for the best fitted regression method.

A proportional increase of all parameters while keeping the thickness constant was simulated on a YdX pattern and is seen in figure 4.6.

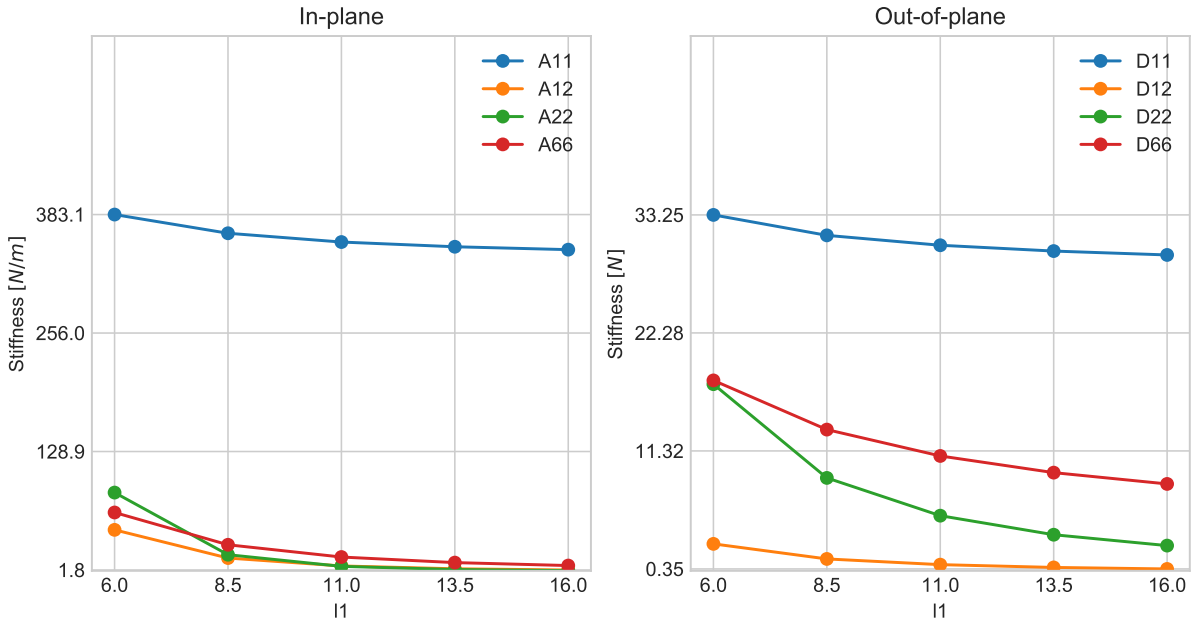

(a) Linear plot.

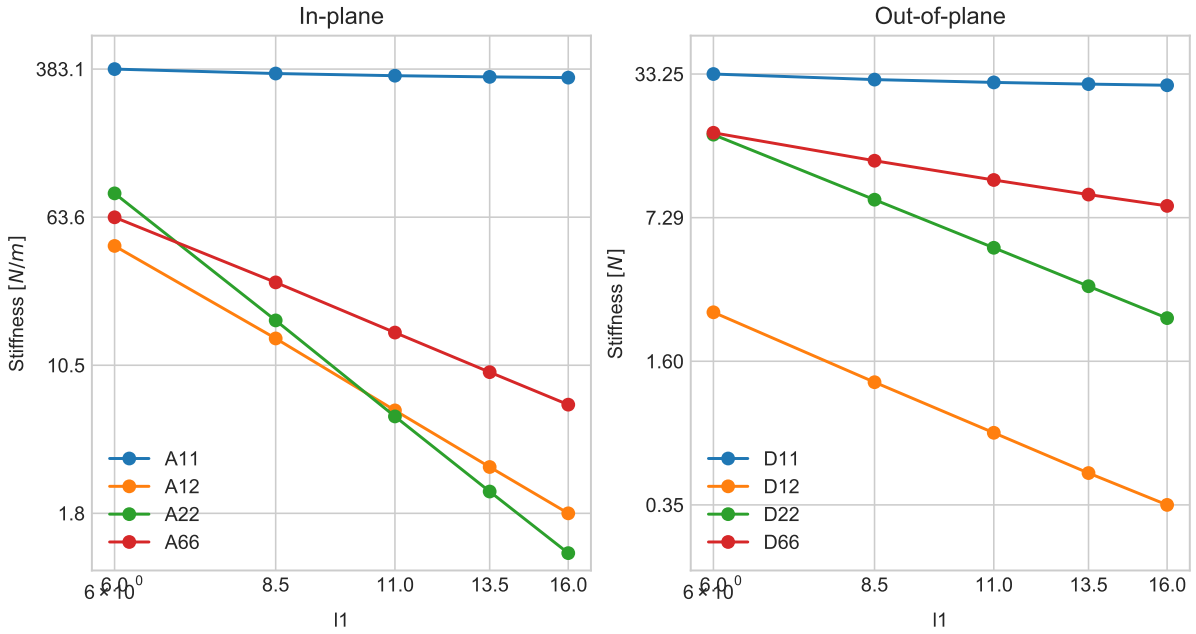

(b) Logarithmic plot.

Figure 4.4: The change of stiffness when flexure length is increased of LET cmm. Variable $l1$ in the plot is proportional to flexure length.

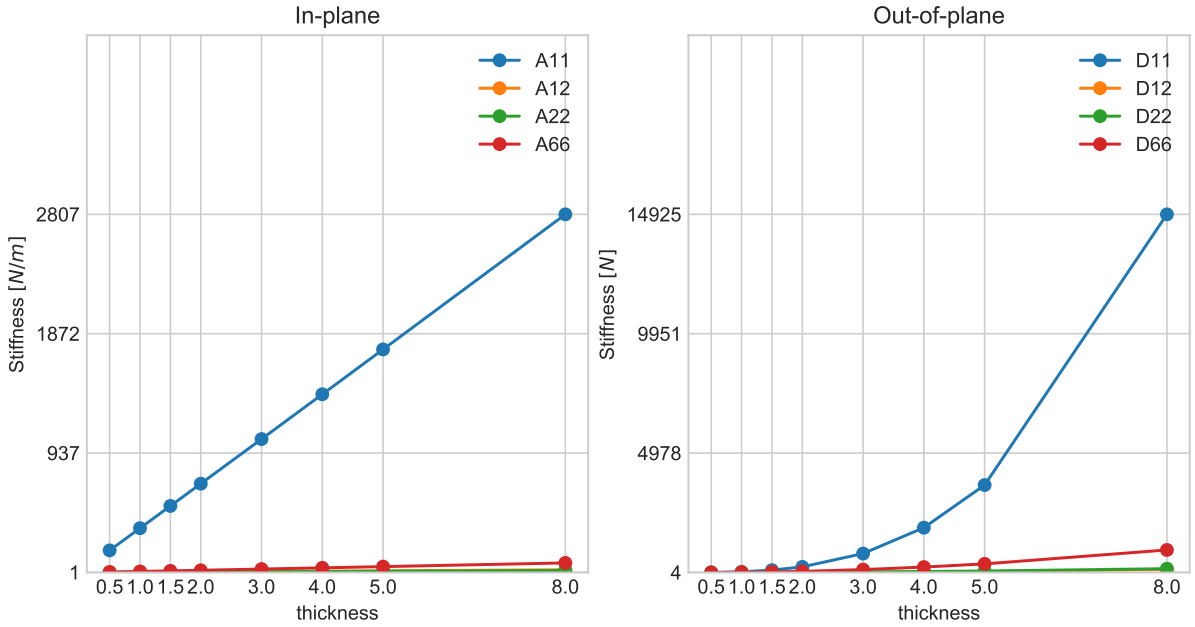

(a) Linear plot.

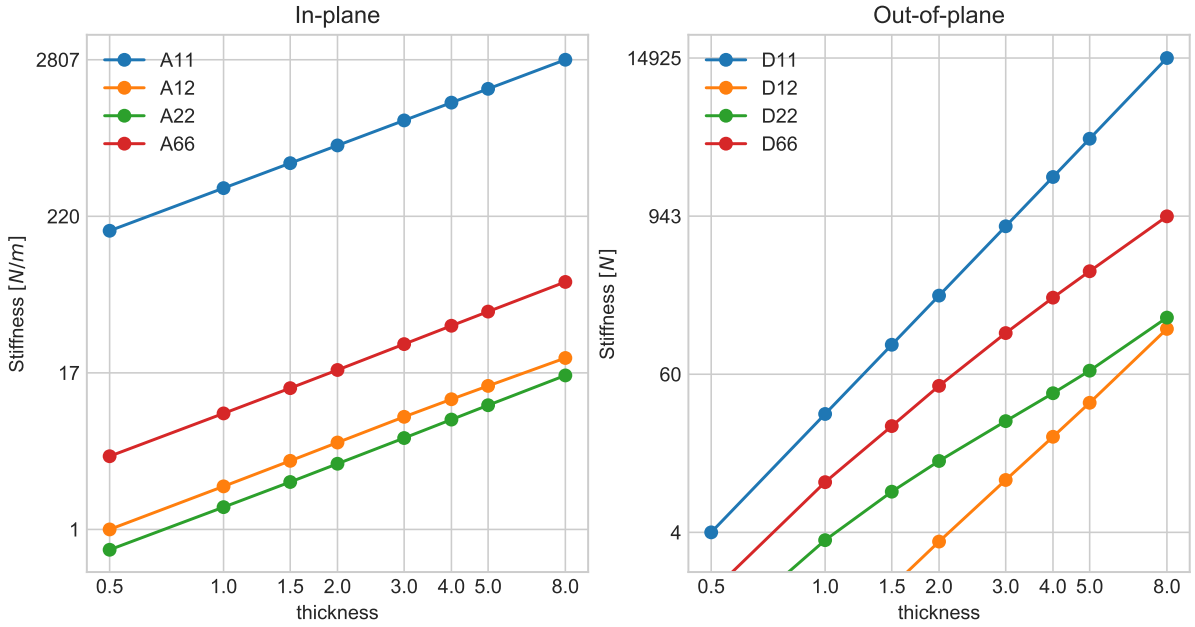

(b) Logarithmic plot.

Figure 4.5: The change of stiffness when flexure thickness is increased of a LET cmm .

Simulation 1	Slope	R-value	Reg
A_{11}	-0.045	0.94185	log
A_{22}	-2.868	0.97837	log
A_{66}	-1.475	0.98010	log
D_{11}	-0.055	0.97146	log
D_{22}	-1.284	0.97697	log
D_{66}	-0.457	0.99495	log

Simulation 2	Slope	R-value	Reg
A_{11}	0.658	0.98584	log
A_{22}	2.849	0.99973	log
A_{66}	1.947	0.96521	log
D_{11}	0.642	0.98439	log
D_{22}	1.921	0.95164	log
D_{66}	1.138	0.98655	log

Simulation 3	Slope	R-value	Reg
A_{11}	-0.837	0.99793	log
A_{22}	0.478	0.99794	log
A_{66}	-1.258	0.98631	log
D_{11}	-0.822	0.99779	log
D_{22}	0.187	0.98629	log
D_{66}	0.851	0.99129	linear

Simulation 4	Slope	R-value	Reg
A_{11}	0.215	0.99721	log
A_{22}	-0.951	0.99995	log
A_{66}	-5.455	0.57298	linear
D_{11}	0.205	0.99117	log
D_{22}	-0.688	0.97774	log
D_{66}	-1.918	0.44502	linear

Simulation 5	Slope	R-value	Reg
A_{11}	351.112	0.99999	linear
A_{22}	2.078	0.99980	linear
A_{66}	9.509	0.99987	linear
D_{11}	2.987	0.99999	log
D_{22}	1.968	0.99361	log
D_{66}	2.355	0.99620	log

Table 4.3: Slope, R-value and best fitted regression model for variation of different stiffness components when parameters are variation of the LET cmm flexure pattern.

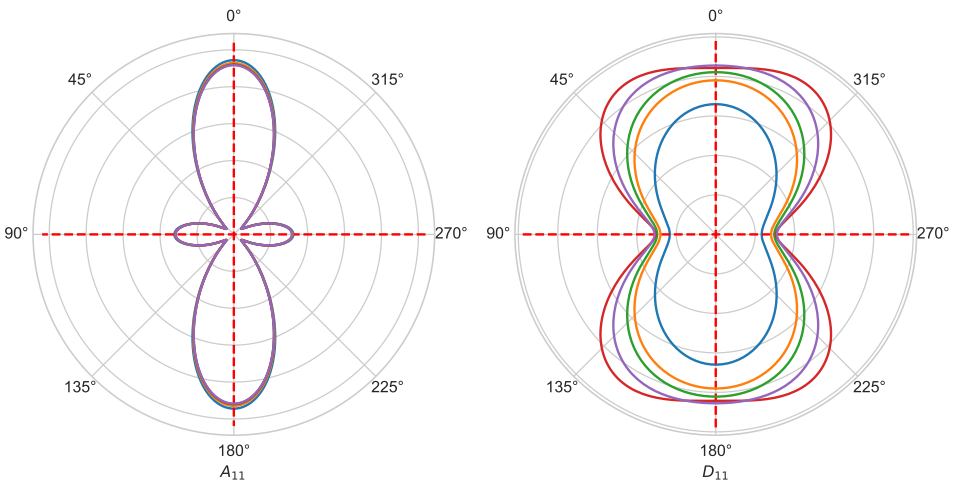

Figure 4.6: A YdX pattern scaled proportionally, while keeping the thickness constant.

4.2.2 Elastic anisotropy

With the rotation matrices given in section 2.2.1, considering an angular rotation θ of the unit cell from its internal reference coordinate system, around the out-of-plane axis. The change in the elastic stiffness matrix with coordinate rotations was observed for the stiffness matrix for the patterns in table 4.4. More detailed results are found in appendix C.

The periodic anisotropy is discussed for matrix $[A]$, but the same periodicity is present for matrix $[D]$ in not else is mentioned. The polar plots are given for matrix components A_{11} and D_{11} respectively.

The term $n = 0, 1, 2, 3...$ describes the n-fold rotation in which a term in the stiffness matrix is repeated. The phase-shift is denoted by ϕ.

Flexure type	Symmetry group
Misc	p1
Misc	p2
Misc	pm
Misc	pg
LET	cmm
Switchback	cmm
Ydx	cmm
Coil	cmm
Switchback	p4
Coil	p4
LET	p4m
Switchback	p4g
LET	p6m

Table 4.4: List over simulated flexure patterns

A *p1* pattern

The simulated p1 pattern is done mainly to observe the response of a pattern with only translative symmetry. The stiffness matrix of the *p1* pattern is:

$$\left[\begin{array}{ccc|ccc} A_{11} & A_{12} & A_{16} & 0 & 0 & 0 \\ A_{12} & A_{22} & A_{26} & 0 & 0 & 0 \\ A_{16} & A_{26} & A_{66} & 0 & 0 & 0 \\ \hline 0 & 0 & 0 & D_{11} & D_{12} & D_{16} \\ 0 & 0 & 0 & D_{12} & D_{22} & D_{26} \\ 0 & 0 & 0 & D_{16} & D_{26} & D_{66} \end{array}\right] \tag{4.1}$$

The simulated unit and a polar plot for A_{11} and D_{11} values is seen in 4.8. The values of the rotated stiffness matrix is seen in figure 4.7 with the following observed response:

- A_{11}, A_{22}, A_{16} and A_{26} repeat with a $180°n$ period, A_{12} and A_{66} repeat with a $90°n$ period.
- A_{12} and A_{66} are symmetric with $45°n$ period.

- A_{11} and A_{22} have the same magnitude with a phase shift of $\phi = 90°$.

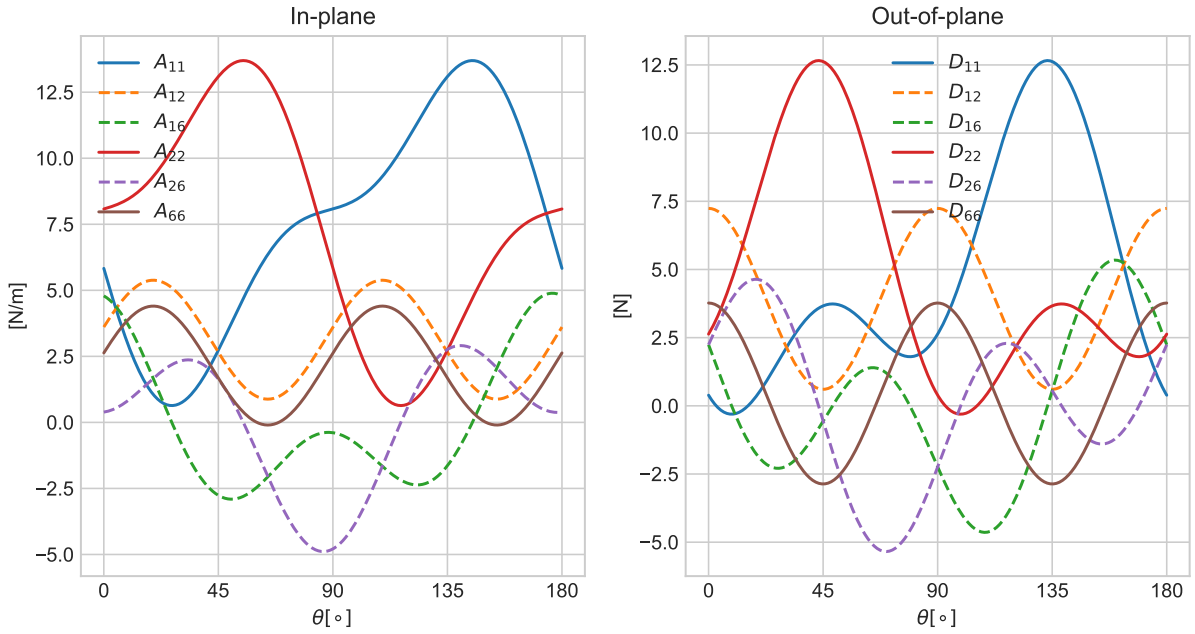

Figure 4.7: The anisotropic response of a rotated stiffness matrix of the *p1* pattern.

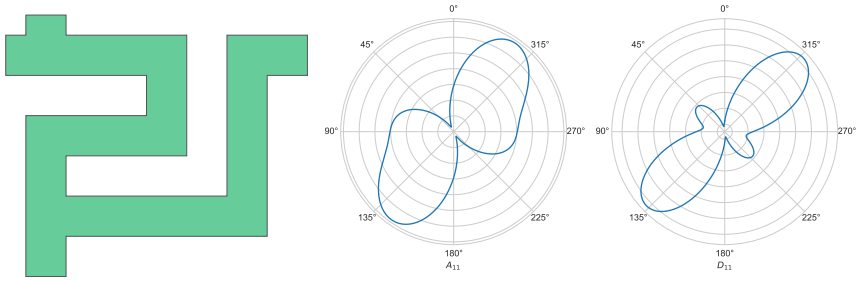

(a) Simulated unit. (b) A_{11} and D_{11}.

Figure 4.8: A *p1* flexure pattern.

A *p2* pattern

The simulated p2 pattern is done mainly to observe the response of a pattern with only translative and 2-fold rotational symmetry. The simulated unit and a polar plot is seen in 4.9. The properties of the stiffness matrix are in principal the same as for the *p1* pattern.

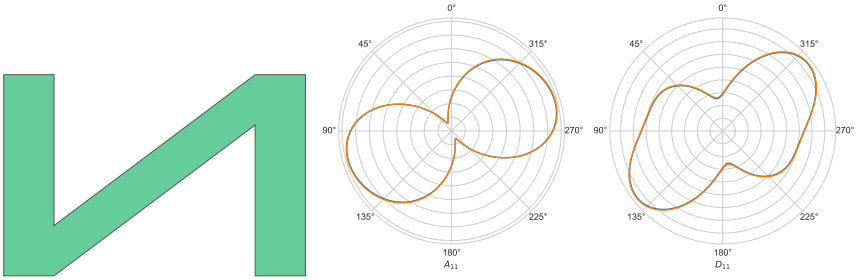

(a) Simulated unit. (b) A_{11} and D_{11}.

Figure 4.9: A *p2* flexure pattern.

A *pm* pattern

The simulated pm pattern is done mainly to observe the response of a pattern with only translative and mirror symmetry. The stiffness matrix for a pm pattern is observed to be:

$$\left[\begin{array}{ccc|ccc} A_{11} & A_{12} & 0 & 0 & 0 & 0 \\ A_{12} & A_{22} & 0 & 0 & 0 & 0 \\ 0 & 0 & A_{66} & 0 & 0 & 0 \\ \hline 0 & 0 & 0 & D_{11} & D_{12} & 0 \\ 0 & 0 & 0 & D_{12} & D_{22} & 0 \\ 0 & 0 & 0 & 0 & 0 & D_{66} \end{array}\right] \tag{4.2}$$

The simulated unit and a polar plot for A_{11} and D_{11} values is seen in 4.11. The values of the rotated stiffness matrix is seen in figure 4.10 with the following observed response:

- A_{16} and A_{26} appear for $\theta \neq 90°n$.
- A_{11}, A_{22}, A_{16} and A_{26} repeat with a $180°n$ period, A_{12} and A_{66} repeat with a $90°n$ period.
- A_{11} and A_{22} have the same magnitude with a phase shift of $\phi = 90°$.
- Extreme values are symmetric for A_{11}, A_{22} and found at $\theta = 90°n$
- When $A_{16} = 0$ an extreme value of A_{22} is found, and when $A_{26} = 0$ an extreme value of A_{11} is found.

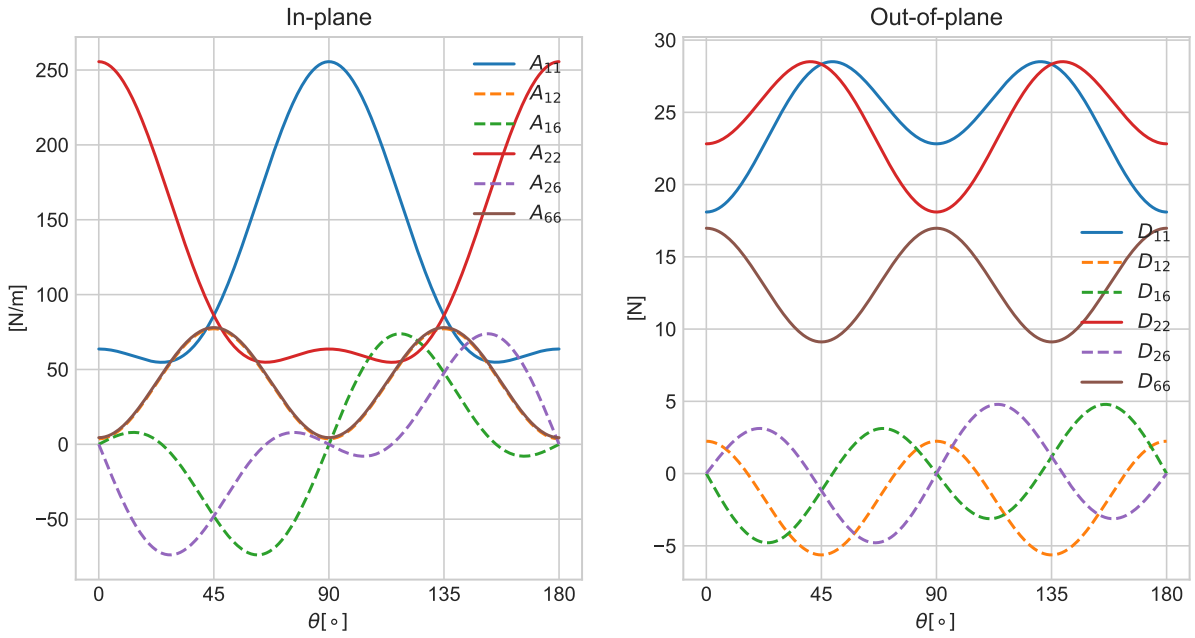

Figure 4.10: The anisotropic response of a rotated stiffness matrix of the *pm* pattern.

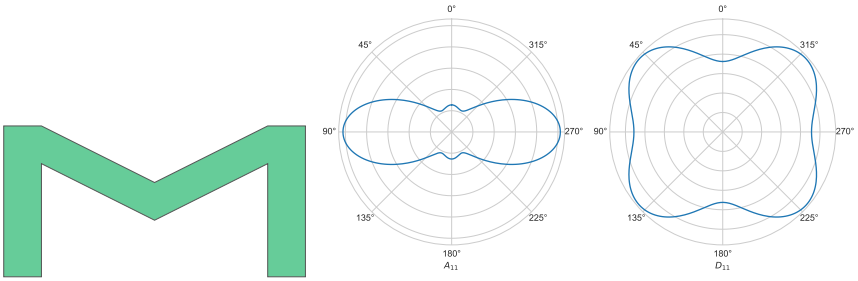

(a) Simulated unit. (b) A_{11} and D_{11}.

Figure 4.11: A *pm* flexure pattern.

A *pg* pattern

The simulated pm pattern is done mainly to observe the response of a pattern with only translative and glide-reflection symmetry. The simulated unit and a polar plot is seen in 4.12 and repeats with 180° intervals. There are two axes of symmetry.

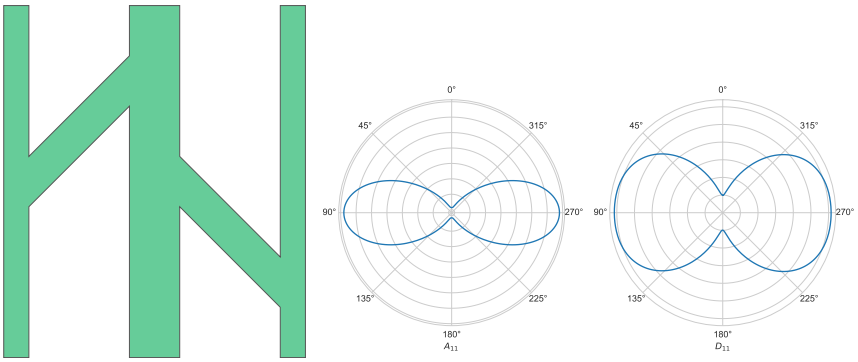

(a) Simulated unit. (b) A_{11} and D_{11}.

Figure 4.12: A *pg* flexure pattern.

cmm patterns

The stiffness matrix for a typical *cmm* is the same as given in matrix 4.2. Polar plots for A_{11} and D_{11} and some additional graphs are given for the following flexure patterns:

LET cmm with flexure length as free variable is given in figure 4.13. A more detailed study of the parameters is seen in figure C.9 for increased flexure length and in figure C.8 for increased flexure width.

Switchback cmm with cut width as free variable is given in figure 4.14.

Coil cmm with cut width as free variable is given in figure 4.16

YdX cmm with flexure angle as free variable is given in figure 4.15.

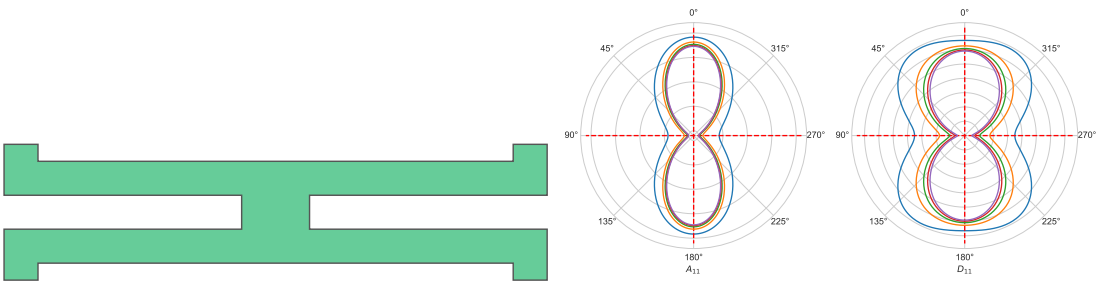

(a) Simulated unit. (b) A_{11} and D_{11}.

Figure 4.13: A *LET cmm* flexure pattern where *flexure length* is increased.

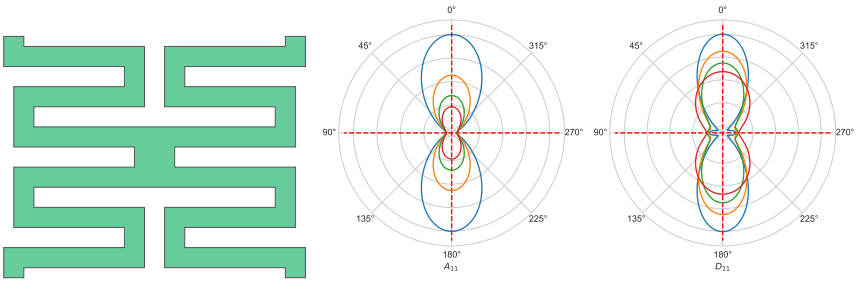

(a) Simulated unit. (b) A_{11} and D_{11}.

Figure 4.14: A *Switchback cmm* flexure pattern where *cut width* is increased.

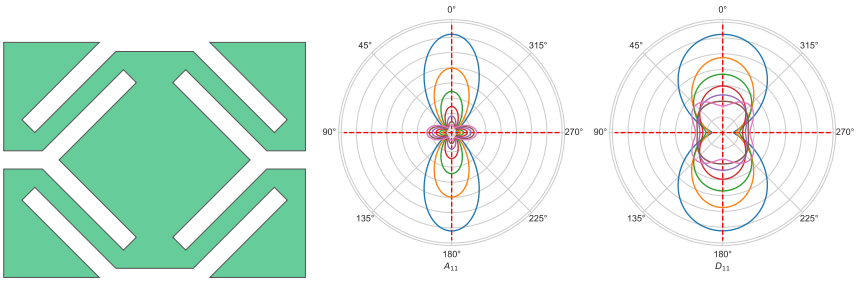

(a) Simulated unit. (b) A_{11} and D_{11}.

Figure 4.15: A *YdX cmm* flexure pattern where *flexure angle* is increased.

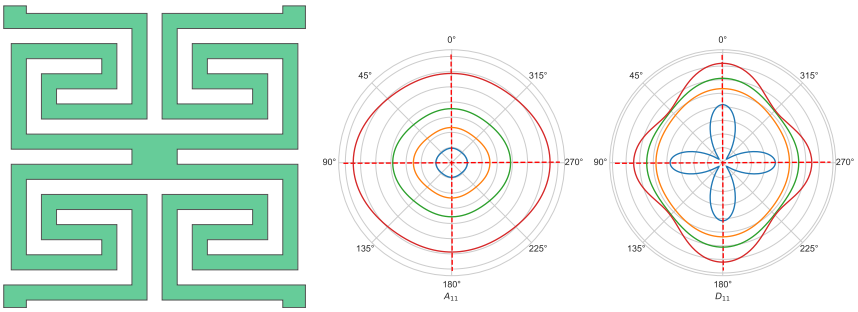

(a) Simulated unit. (b) A_{11} and D_{11}.

Figure 4.16: A *Coil cmm* flexure pattern where *cut width* is increased.

p4 patterns

A *p4* flexure pattern that is parallel with its principal axes has the stiffness matrix

$$\left[\begin{array}{ccc|ccc} A_{11} & A_{12} & 0 & 0 & 0 & 0 \\ A_{12} & A_{11} & 0 & 0 & 0 & 0 \\ 0 & 0 & A_{66} & 0 & 0 & 0 \\ \hline 0 & 0 & 0 & D_{11} & D_{12} & 0 \\ 0 & 0 & 0 & D_{12} & D_{11} & 0 \\ 0 & 0 & 0 & 0 & 0 & D_{66} \end{array}\right] \tag{4.3}$$

An anisotropic response is seen in figure 4.17 and is from a *switchback p4*. The following properties are observed for the rotated stiffness matrix:

- All properties repeat with a $90°n$ period.
- All components are symmetric about its extreme values which repeat with a $45°n$ period.
- The extreme values are shifted with an angle ϕ for A_{11}, A_{12}, A_{22} and A_{66} where $A_{16} = A_{26} = 0$, and $\phi + 22.5°$ for $A_{16} = A_{26}$
- There is a change of ϕ with a change of geometry.
- A_{16} and A_{26} are non-zero for $\theta \neq \phi + 45°n$

Polar plots for A_{11} and D_{11} is given together with the principal axes for the following flexure patterns:

Switchback p4 with cut width as free variable is given in figure 4.18. The simulated unit is parallel with the flexures, but the stiffness matrix is shifted an angle ϕ.

Coil p4 with cut width as free variable is given in figure 4.19

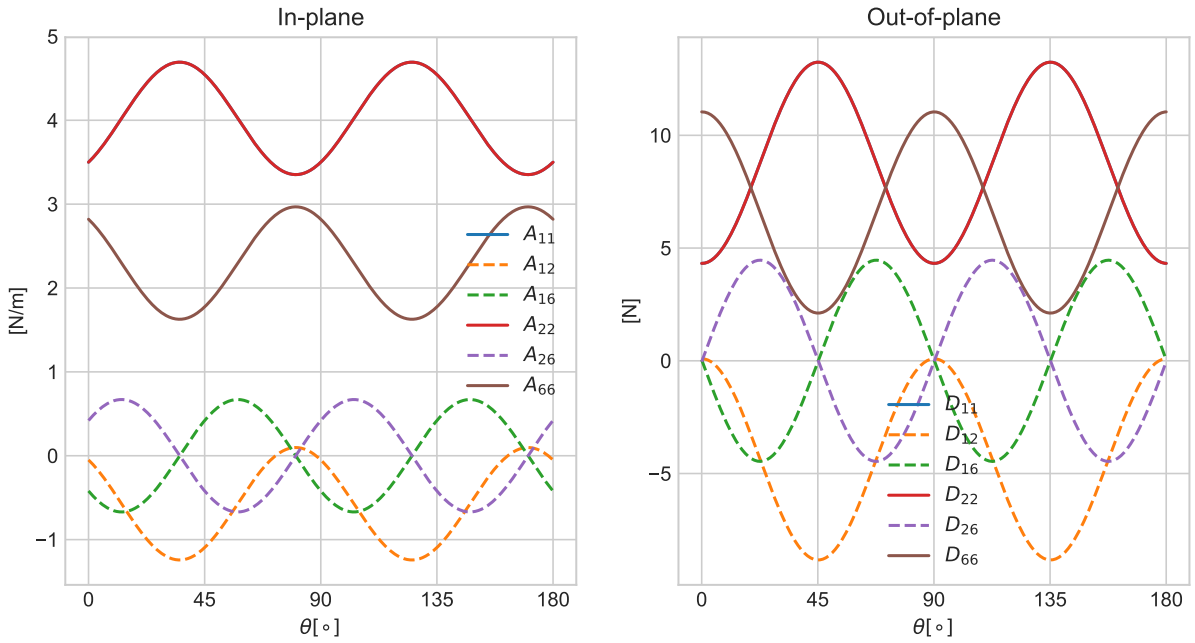

Figure 4.17: Anisotropic in-plane stiffness components for a *p4 switchback* .

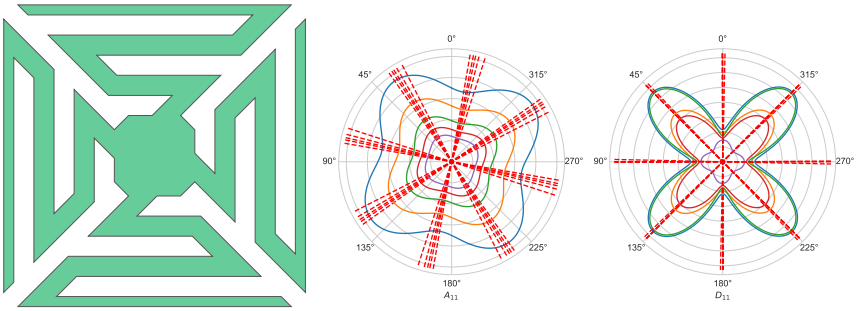

(a) Simulated unit. (b) A_{11} and D_{11}.

Figure 4.18: A *switchback p4* flexure pattern where *cut width* is increased.

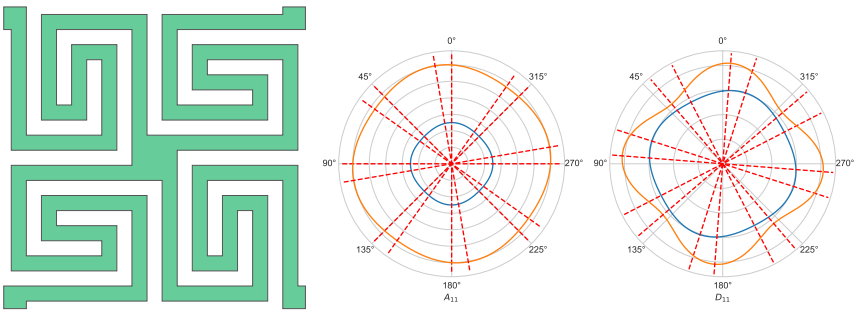

(a) Simulated unit. (b) A_{11} and D_{11}.

Figure 4.19: A *Coil p4* flexure pattern where *cut width* is increased.

A *p4m* pattern

The stiffness matrix for a typical *p4m* flexure pattern with coordinate system parallel to two of the reflection symmetry lines is the same as for the *p4* flexure pattern but with no shift of phase angle ϕ. When the parameters of the geometry is varied, the results show that only the amplitude changes, and no phase shift angle is observed.

Polar plots for A_{11} and D_{11} is given for the LET p4m with junction length as free variable is given in figure 4.20.

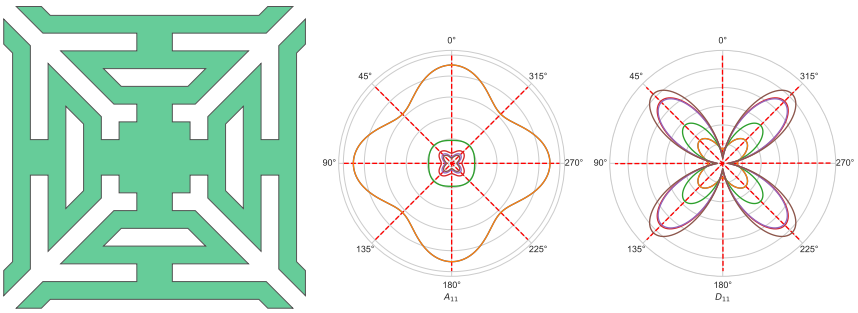

(a) Simulated unit. (b) A_{11} and D_{11}.

Figure 4.20: A *LET p4m* flexure pattern where *junction length* is increased.

A *p4g* pattern

The stiffness matrix for a typical *p4g* flexure pattern with with coordinate system 45° offset from the reflection symmetry lines is the same as for the *p4* flexure pattern but with no shift of phase angle ϕ.

Polar plots of A_{11} and D_{11} with flexure width as free variable for Switchback p4g is given in figure 4.21. When the parameters of the geometry is varied, the results show that only the amplitude of all components of the stiffness matrix shifts scales, and no phase shift angle is observed.

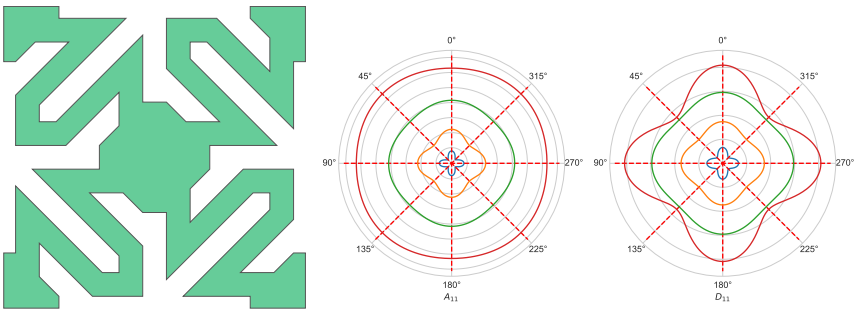

(a) Simulated unit. (b) A_{11} and D_{11}.

Figure 4.21: A *switchback p4g* flexure pattern where *junction length* is increased.

A *p6m* pattern

The stiffness matrix for a typical *p6m* flexure pattern with coordinate system parallel with two perpendicular lines of reflection symmetry is

$$\left[\begin{array}{ccc|ccc} A_{11} & A_{12} & 0 & 0 & 0 & 0 \\ A_{12} & A_{11} & 0 & 0 & 0 & 0 \\ 0 & 0 & \frac{A_{11}-A_{12}}{2} & 0 & 0 & 0 \\ \hline 0 & 0 & 0 & D_{11} & D_{12} & 0 \\ 0 & 0 & 0 & D_{12} & D_{11} & 0 \\ 0 & 0 & 0 & 0 & 0 & \frac{D_{11}-D_{12}}{2} \end{array}\right] \tag{4.4}$$

Figure 4.22 shows the transformed properties of the LET *p6m* flexure pattern. This shows little variation in the transformed stiffness and a transverse isotropic behaviour. Figure 4.23 shows the simulated unit and a polar plot of the rotated stiffness.

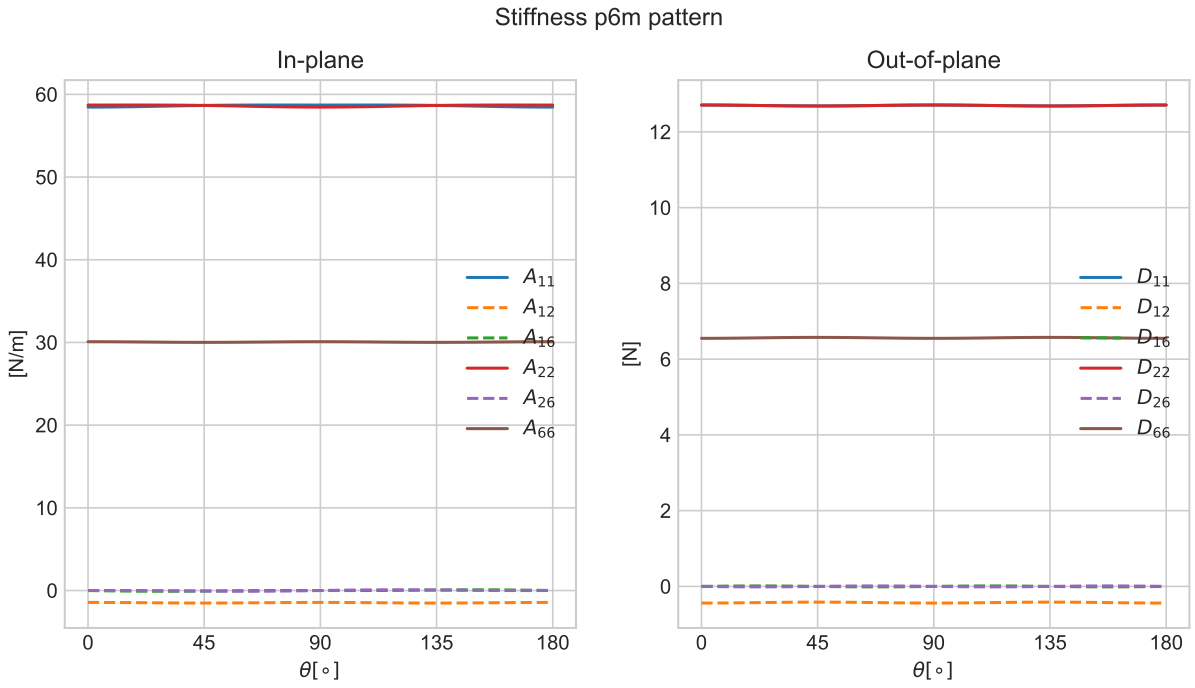

Figure 4.22: Isotropic stiffness for a *LET p6m*.

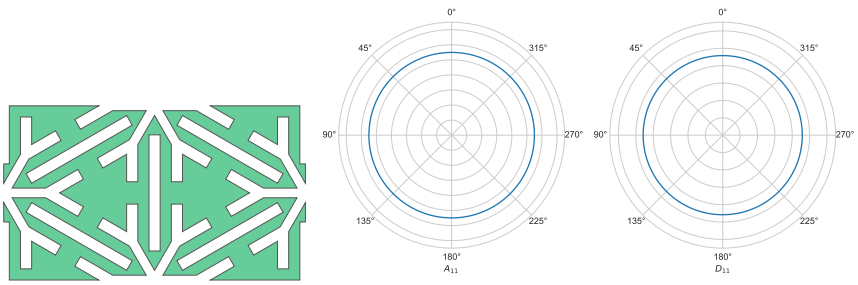

(a) Simulated unit. (b) A_{11} and D_{11}.

Figure 4.23: A *LET p6m* flexure pattern.

Negative Poisson's ratio

The YdX pattern showed great increase of the negative Poisson's ratio when the angle of the flexure was changed as shown in figure 4.24. The result can be seen in table 4.5.

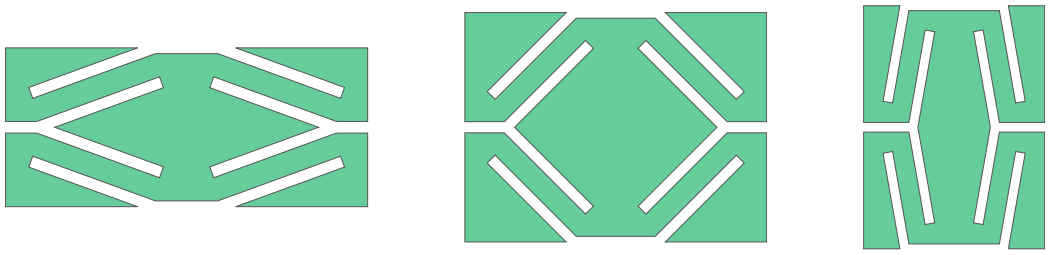

Figure 4.24: YdX cmm where interior angle is varied.

θ	ν_{xy}	ν_{yx}
20	-0.12	-5.22
30	-0.24	-3.08
40	-0.41	-1.90
50	-0.64	-1.21
60	-0.95	-0.78
70	-1.33	-0.50
80	-1.71	-0.30

Table 4.5: Change of Negative Poisson's ratio with change of angle of the internal flexure in YdX cmm.

Degree of anisotropy

Degree of anisotropy η_A and η_D for in-plane and out-of-plane anisotropy is calculated as the ratio between the maximal and minimal value of the 11-component for the rotated stiffness matrix for A_{11} and D_{11}.

$$\eta_A = \frac{A_{11}^{min}}{A_{11}^{max}} \qquad \eta_D = \frac{D_{11}^{min}}{D_{11}^{max}} \tag{4.5}$$

As seen by the polar plots, the degree of anisotropy varies for the different patterns. Table 4.6 shows the maximum and minimum degree of anisotropy for different patterns for all simulated variations for values of the $[A]$ and $[D]$ matrix.

Flexure pattern	η_A	η_D
LET cmm	[4.5, 11000]	[2.0, 200.5]
Switchback cmm	[1.14, 137.6]	[1.1, 1064.6]
Ydx cmm	[9.0, 2.8]	[1.3, 9.0]
Coil cmm	[1.1]	[1.1, 1.4]
Switchback p4	[1.1, 1.4]	[1.5, 3.7]
Coil p4	[1.1]	[1.1, 1.4]
LET p4m	[1.1, 4.1]	[2.3, 23.6]
Switchback p4g	[1.1, 1.2]	[1.1, 1.4]
LET p6m	[1.0]	[1.0]

Table 4.6: Some calculated values of η for different flexure patterns.

Detailed variation of geometry

Some variation of parameters are shown in the polar plots. But to capture the complete variation of the stiffness, all terms in the stiffness matrix most be considered. The following graphs in figure 4.25 show the anisotropic response of a YdX cmm flexure pattern where the flexure angle is varied. For more detailed variations, see appendix C.

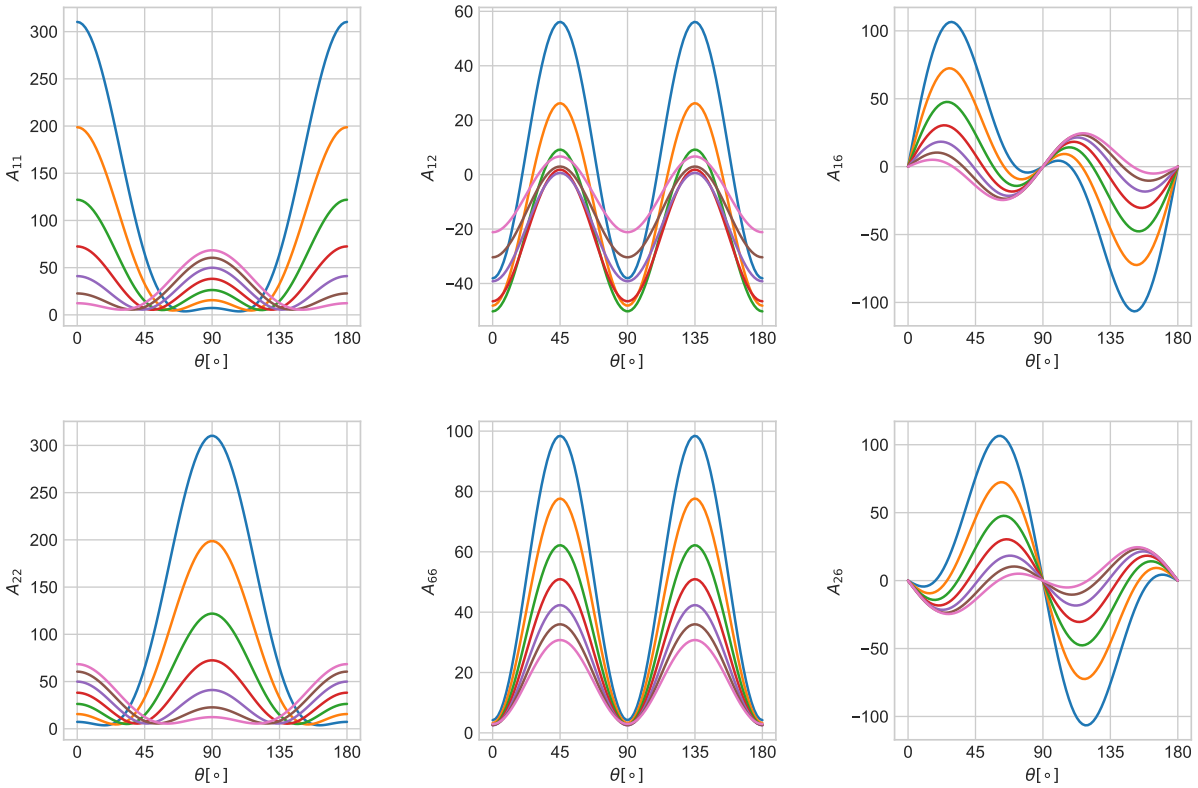

(a) In-plane components.

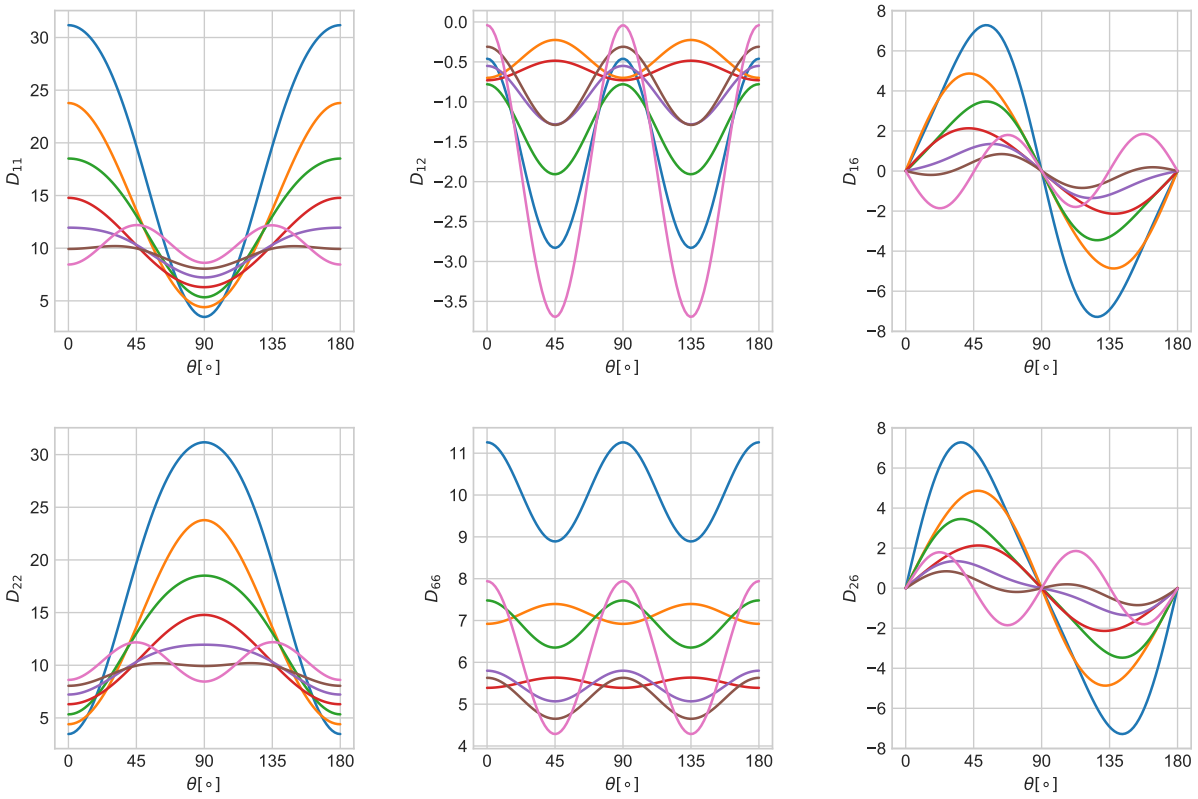

(b) Out-of-plane components.

Figure 4.25: Anisotropic stiffness for a *YdX cmm* flexure pattern where *flexure angle* is varied from 20° to 80°.

4.3 Flexure pattern design tool

A Python program that generates flexure patterns according to user input is made. The program has the following capabilities:

- Generate the geometry of 11 unique flexure patterns where all parameters can be varied.
- Methods for generating units from 7 of the plane symmetry groups are implemented
- Generate a flexure pattern with the desired number of units.
- Output a *.svg* file that can be used for manufacturing.

The capabilities of the Python program is demonstrated in appendix B.1. The class methods `plot()`, `set_unit_para()`, `make_pattern()` and `save_svg()` are important methods (functions) for manipulating the Unit object. The lattice related attributes (variables) are important for making the pattern and to determine the boundaries when the is sent to a simulation in a FEA program.

A list of attributes and methods is found in table 4.7 and 4.8.

The full code is found on the GitHub page `https://github.com/oddvinostmo/patterns-code` [40] and is free and open source.

Attributes	Comment
`unit.name`	unit name
`unit.unit`	geometry of unit
`unit.generating_region`	geomety of generating region
`unit.para`	parameters for geometry
`unit.lattice_type`	
`unit.center`	center of lattice
`unit.l1`	lattice length 1-direction
`unit.l2`	lattice length 2- direction
`unit.angle`	lattice angle
`unit.flexure_pattern`	geometry of flexure pattern

Table 4.7: Central attributes of the Unit class.

Methods	Comment
`unit.set_unit_name()`	sets custom name
`unit.plot()`	plots unit in coordinate system
`unit.set_unit_para()`	changes parameters and updates geometry
`unit.make_pattern()`	creates a flexure pattern
`unit.save_svg()`	creates a .svg file of the flexure pattern
`unit.batch_save_svg()`	

Table 4.8: Central methods of the Unit class.

Chapter 5

Discussion

5.1 Definition

The new term *flexure pattern* describes the same concept as *living hinge[26], lattice hinge[7], kerf bend [26]* and *compliant array[25]*, but in a broader sense. *Flexure* refers to the basic building component that is a fundamental way of introducing flexibility into a material. *Pattern* refers to the concept of something being repeated in the plane according to some rules. Subjectively speaking, the term flexure pattern is more catchy and I argue that this term is better than the other names found.

Living hinge is originally the term for a thin flexible hinges that connect two rigid pieces together in a pivoting motion. It is extensively used in injection molding of plastics containers, but have been adopted as a term to describe a flexure pattern as well.

Lattice hinge creates the notion of a *lattice structure* of strips usually arranged to form a diagonal pattern of open spaces between the strips [4] and hinge being the motion of pivoting.

Kerf bend is originally the term for the concept where slots are almost cut through the material in order to let it be bent.

Compliant array consists of compliance which is synonymously with flex and array being "a regular order or arrangement; series" [4]. It refers to the usual rectangular arrangement of shapes in rows and columns. I argue the word pattern is a better word as it does not lay any restrictions of how it is repeated. This means it can include periodic patterns but also aperiodic or non-periodic patterns and gives the possibility of bottom-up metamaterials that have changing structure according to the desired properties in the specific region.

This thesis characterizes a flexure pattern as a 2 dimensional mechanical metamaterial that consists of flexures configured in a pattern that increase the compliance compared to the bulk material of which it has been made. The flexures are patterned onto the plane according to a set of rules.

The reason that patterned is specified as "according to a set of rules" is because this does not constrain it do be done in a repetitive manner. One can imagine a complex

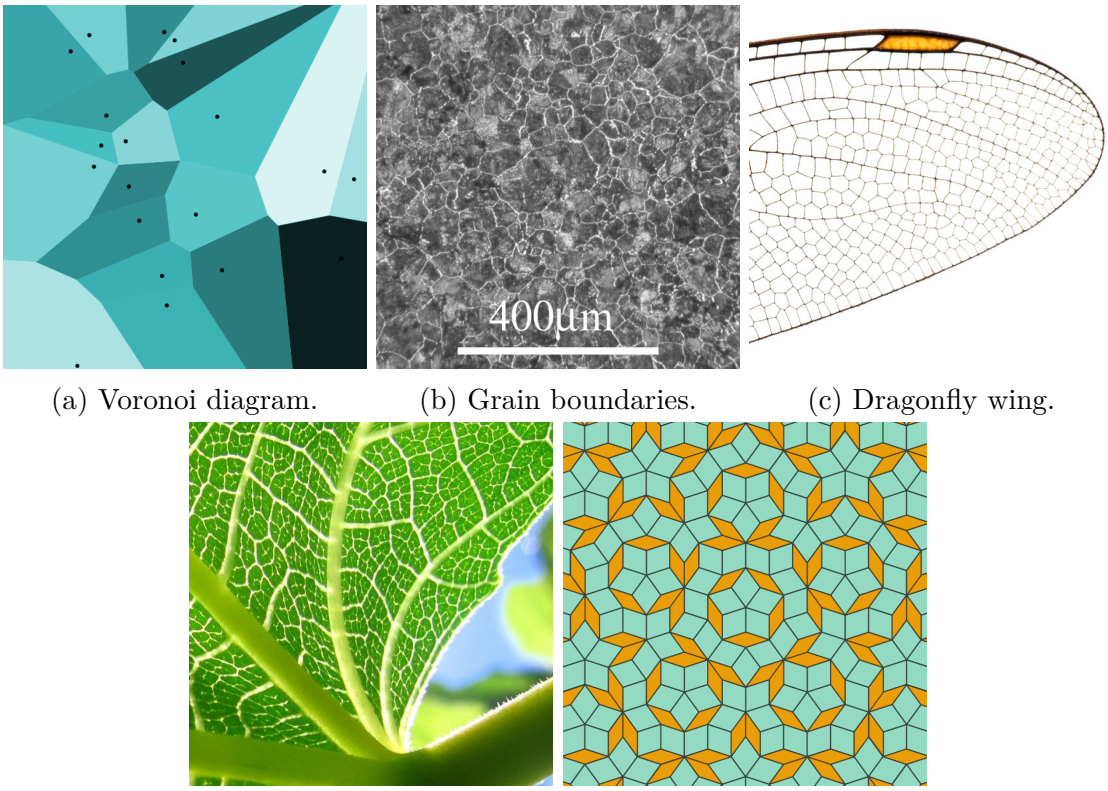

(a) Voronoi diagram. (b) Grain boundaries. (c) Dragonfly wing.

(d) Leaf structure. (e) Penrose tiling.

Figure 5.1: Various patterns that are not not periodic, but occurring in nature as a localized optimization.

surface where local variations of the stiffness are desirable, and this pattern needs to be patterns according to some rules that describes the local geometry and not just the global.

This local customization also fits good with the definition of a *bottom up meta material*. Other ways to pattern the plane according to other rules are Voronoi tiling and aperiodic tiling. Voronoi tiling, as seen in figure 5.1, is popular in some optimization problems and occur spontaneously in nature.

Mechanical metamaterials is an interesting due to their high strength to weight ratios. Flexure patterns are in many ways related to the flexible 2D truss lattice which is defined as a meta material [8].

5.1.1 New flexure patterns

The criterion to call the proposed flexure patterns *new* are: they are unique to any other flexure patterns I have found after research on the internet. Due to long traditions for making decorative patterns, there are numerous different motifs and some might be of the same design claimed to be new in this thesis.

5.2 Interpretation of results

5.2.1 Principal deformation mechanisms and numerical results

By comparing the expected values from the equations 3.16 with the simulated values in table 4.3, one can discuss the relations between the geometric parameters and the stiffness components of the LET cmm.

When the flexure length was varied in *simulation 1* one could see from the graph in figure 4.4 a logarithmic relationship between the flexure length and the stiffness. When w and t is held constant, the expected relations are:

$$A_{11} \propto L^0, \quad A_{22} \propto L^{-3}, \quad D_{11} \propto L^0, \quad D_{22} \propto L^{-1} \tag{5.1}$$

The simulated results versus the analytically expected values are seen table 5.1. The only differing significantly is D_{22} which is the torsion mode of a flexure strip. As commented in section 2.3.1 other effects like warping may occur for rectangular cross-sections.

Component	Simulated slope	Expected slope	Difference
A_{11}	-0.04	0	0.04
A_{22}	-2.97	-3	0.03
D_{11}	-0.05	0	0.05
D_{22}	-1.28	-1	0.28

Table 5.1: Logarithmic regression slope from simulations and the analytically expected for some stiffness components when the flexure length is varied.

When the flexure width was increased in *simulation 2*, is was expected that all stiffness components increase as seen in appendix C. The simulated results compared to the analytically expected values are seen table 5.2. When L and t is constant, the expected relations are:

$$A_{11} \propto w, \quad A_{22} \propto w^3, \quad D_{11} \propto w, \quad D_{22} \propto J(w) \tag{5.2}$$

Component	Simulated slope	Expected slope	Difference
A_{11}	0.66	1	0.34
A_{22}	2.85	3	0.15
D_{11}	0.64	1	0.36
D_{22}	1.92	-	-

Table 5.2: Logarithmic regression slope from simulations and the analytically expected for some stiffness components when the flexure width is varied.

The simplification predicts a slope of 1 fore A_{11} and D_{11} components. A more realistic estimate is related to the proportion of the simulated unit containing a flexure $w/l_2 \to 1$ and will therefore asymptotically approach a limit in the stiffness. With an exponent of 0.64 and 0.66 gives an asymptotic curve for the values < 1.

A_{22} is expected to behave like a beam with the second moment of inertia increasing in a cubic fashion with the increased height. For D_{22} the approximations in section 2.3.1 on J have to be considered. This contains several higher order terms that gives it an non-trivial logarithmic relation. The contention $w > t$ in the formula should result that the smallest gets increases the stiffness by a power of three and the largest increases the stiffness by a power of one. Tho regression shows however that a power of 2.18 fits the results good.

When the thickness increases in *simulation 5*, all A- components increases linearly with the slope of the stiffness; hence a doubling in the thickness doubles the in-plane stiffness. For the D-components the stiffness increases logarithmic with a factor 3 for D_{11} . This is similar behaviour of what we would expect as seen in table 5.3. For D_{22} varying the thickness results in the same conclusion as for the increased flexure width. Both simulations gives a slope close to 2 which means that the results corresponds with each other.

The opposite case of changing the stiffness and remaining the other dimensions constants is to keep the thickness constant and scale the unit. The expected outcome will then be that the in-plane stiffness remains the same, while the out-of-plane stiffness increases with the same factor. This was observed for the YdX cmm and is seen in figure 4.6..

$$A_{11} \propto t, \quad A_{22} \propto t, \quad D_{11} \propto t^3, \quad D_{22} \propto J(t) \tag{5.3}$$

Component	Simulated slope	Expected slope	Difference
A_{11}	1.00	1	0.00
A_{22}	1.02	1	0.02
D_{11}	2.99	3	0.01
D_{22}	1.97	-	-

Table 5.3: Logarithmic regression slope from simulations and the analytically expected for some stiffness components when the flexure thickness is varied.

The stem width and stem height are categorized as "stiff areas" in the analytically models and would not contribute to any stiffness reduction from increased deformation modes. The results points in the direction that the parameters have opposite effects on the stiffness, but the mechanisms are not self evident at this point. Increase of stem width contributes to a wider unit, which means that the resultant forces will distribute over a longer length and results in a less stiff unit. This is also consistent with the results as A_{11} and D_{11} decreases for increased stem width and A_{22} and D_{22} decreases with a longer stem width.

It must however be commented that D_{22} proportion to $J(t)$ is expected a linear relation for the simplest approximation when the thickness or the width of the flexure is increased and is investigated through the graph in figure 2.20. Both simulations showed close to a quadratic relationship which was not predicted by the model. Further work could focus on describing these relationship further.

More sophisticated models for the flexure strip, that encounter non-linearities are investigated analytically in other studies [23]. A full derivation of the stiffness of the LET is also done by [17] where the results are compared with physical experiments.

5.2.2 Anisotropic elasticity

The results indicates that most flexure patterns inhibit anisotropic elasticity and some inhibit isotropic elasticity. This is best seen when the stiffness matrix is rotated about an angle and reveals the change of properties. The fact that many of the stiffness matrices had the same form, point in the direction that there are some general cases that gives similar properties.

The question about anisotropy is essentially a question about the mathematical eigenvalues of the stress tensors and are thoroughly studied on a mathematical level since L.A Cauchy. This is done by defining a set of invariants that the general Hooke's law must satisfy. A derivation of the 2D cases is done [37], but without referencing it to the plane symmetry groups.

The 2D stress tensors accept only four symmetry classes [31] *diagonal (Z_2), orthogonal (D_2), tetragonal (D_4) and isotropic ($O(2)$)* and correspond to the crystallographic groups: triclinic, orthotropic (and monoclinic), tetragonal and hexagonal.

The criterion for being an orthotropic material in 3D is stated as having three mutually, perpendicular planes of reflective symmetry. The case for the 2D case is maybe surprisingly only one plane of reflective symmetry. But as the simulation show, a glide-reflection gives the same result. While not being an of crystallography and not having complete overview, the result of a glide reflection being enough symmetry to make an orthogonal 2D material is something I have not found in the literature.

The minimal symmetries present in a pattern for becoming an other category is presented in figure 5.2.

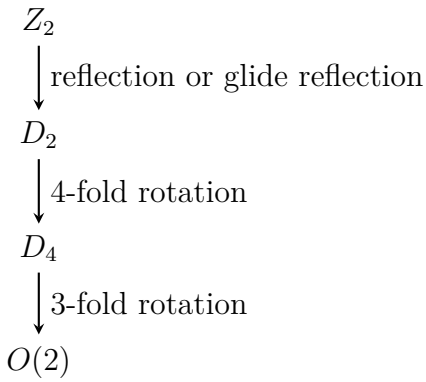

Figure 5.2: Minimal symmetries for tensor category.

Symmetry group	Symbol	Category	Simulated
p1	Z_2	Diagonal	Yes
p2	Z_2	Diagonal	Yes
pm	D_2	Orthogonal	Yes
pg	D_2	Orthogonal	Yes
cm	D_2	Orthogonal	No
pmm	D_2	Orthogonal	No
pmg	D_2	Orthogonal	No
pgg	D_2	Orthogonal	No
cmm	D_2	Orthogonal	Yes
p4	D_4	Tetragonal	Yes
p4m	D_4	Tetragonal	Yes
p4g	D_4	Tetragonal	Yes
p3	$O(2)$	Isogonal	No
p3m1	$O(2)$	Isogonal	No
p31m	$O(2)$	Isogonal	No
p6	$O(2)$	Isogonal	No
p6m	$O(2)$	Isogonal	Yes

Table 5.4: Categorization of tensor properties from symmetry group.

Diagonal

The tested flexure patterns belonging to *p1* and *p2* fitted this category. These showed 180° periodicity and had no principal axes. The observed stiffness matrices for a diagonal material has five independent terms for both $[A]$ and $[D]$ matrices

$$\begin{bmatrix} A_{11} & A_{12} & A_{16} \\ A_{12} & A_{22} & A_{26} \\ A_{16} & A_{26} & A_{66} \end{bmatrix} \tag{5.4}$$

A physical interpretation of the 180° periodicity is that all forces must have an equal counter force in the opposite direction. By rotating anything by 180° you are basically measuring the specimen upside down.

The 180° periodicity being the minimal form for symmetry for any flexure pattern can be seen from the transformation operation in equation 2.20. From this one can see $cos(\theta)$ and $sin(\theta)$ is 360° periodic while $cos^3(\theta)sin(\theta)$ and $cos(\theta)sin^3(\theta)$ are 180° periodic, and $cos^2(\theta)sin^2(\theta)$ are 90° periodic. A visualization is seen in figure 5.3.

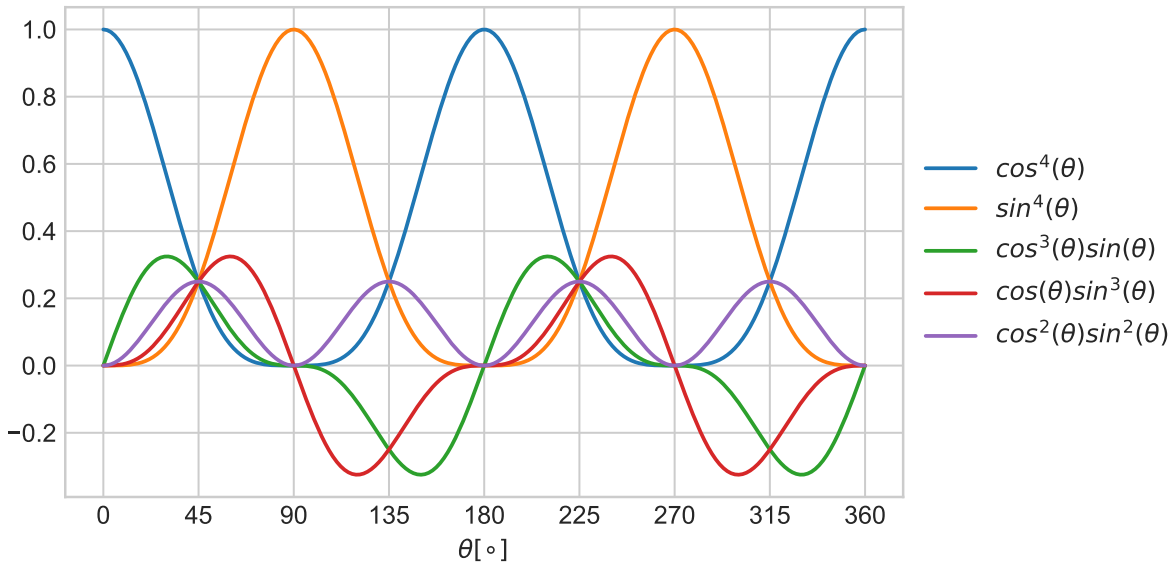

Figure 5.3: The terms of the transformation matrix visualized.

Orthogonal

The tested flexure patterns belonging to *pm*, *pg* and *cmm* fitted this category with only one reflection or glide reflection present. Since these patterns has a reflection the principal axes will follow these and no offset was observed. The observed stiffness matrices for these are consistent with an orthogonal material will have the form

$$\begin{bmatrix} A_{11} & A_{12} & 0 \\ A_{12} & A_{22} & 0 \\ 0 & 0 & A_{66} \end{bmatrix} \tag{5.5}$$

Tetragonal

The tested flexure patterns belonging to *p4*, *p4m* and *p4g* fitted this category. The symmetry groups with reflective symmetry had a natural basis parallel to to the reflection axes.

The tetragonal stiffness tensor parallel to the natural basis has the form with three independent variables.

$$\begin{bmatrix} A_{11} & A_{12} & 0 \\ A_{12} & A_{11} & 0 \\ 0 & 0 & A_{66} \end{bmatrix} \tag{5.6}$$

As [A] and [D] matrices are related to different bending modes, they do not need to have the principal axes in the same directions. The phase angle ϕ is calculated by [8].

$$\tan(4\phi^{D4}) = 2\sqrt{2}\frac{C_{16}}{C_{11} - C_{66} - C_{12}} \tag{5.7}$$

From the switchback p4 in table 5.5 one can see that the equation fits the results shown in figure 5.4 good. An interesting thing to note is that the natural basis for in-plane properties and out-of-plane properties are different for the same geometry.

$\phi^{D4}_{[A]}$	$\phi^{D4}_{[D]}$
$-14.60°$	$-0.23°$
$-11.70°$	$-0.49°$
$-9.683°$	$-0.25°$
$-7.667°$	$-0.48°$
$-6.209°$	$0.67°$

Table 5.5: Phase shift $\phi^{D4}_{[A]}$ and $\phi^{D4}_{[A]}$ for switchback p4.

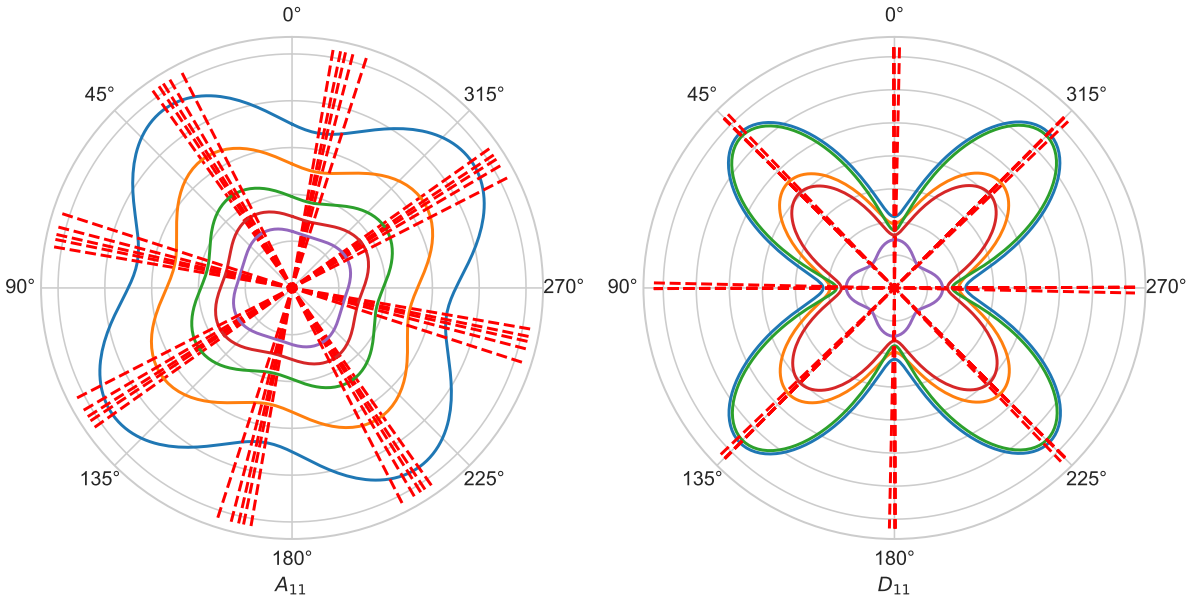

Figure 5.4: A_{11} and D_{11}

Isogonal

Isogonal in 2D corresponds to transverse isotropic in 3D. The finding that *p6m* patterns had an isotropic behaviour for both stretching and bending was an interesting result. This makes it a preferred choice when the goal is to equally reduce the stiffness of a plate in all directions.

It is however not likely that the material strength of the material is isotropic. Other studies found on symmetric lattice structures showed that the structures that showed isotropic stiffness also showed anisotropic strength [6].

The expected for a transverse isotropic material is 5 independent constant in 3D and 2 in 2D [35]. The stiffness matrix is:

$$\begin{bmatrix} A_{11} & A_{12} & 0 \\ A_{12} & A_{11} & 0 \\ 0 & 0 & (A_{11} - A_{12})/2 \end{bmatrix} \tag{5.8}$$

A numerical check for a simulated stiffness matrix,

$$\left[\begin{array}{ccc|ccc} 58.46 & -1.44 & 0 & 0 & 0 & 0 \\ -1.44 & 58.71 & 0 & 0 & 0 & 0 \\ 0 & 0 & 30.09 & 0 & 0 & 0 \\ \hline 0 & 0 & 0 & 12.71 & -0.44 & 0 \\ 0 & 0 & 0 & -0.44 & 12.71 & 0 \\ 0 & 0 & 0 & 0 & 0 & 6.55 \end{array}\right] \tag{5.9}$$

$$A_{66} = \frac{58.46 - -1.44}{2} = 29.95 \approx 30.09 \quad D_{66} = \frac{12.71 - -0.44}{2} = 6.58 \approx 6.55 \tag{5.10}$$

which is a very close fit with the predicted characteristic.

Even though there are many symmetry groups with 3-fold rotations that was not simulated, these are expected to be 2D isotropic as well. This is from the fact that all except one (p3) has three planes of symmetry, which is a criterion for transverse isotropic materials and they have no reason to be any of the other categories like diagonal, orthogonal and tetragonal.

Anisotropic differences for $[A]$ and $[D]$

The deformation mechanisms for the two cases are different, but share much of the anisotropic behaviour. In-plane components for $[A]$ only rely on tension and bending, while $[D]$ rely on torsion and bending.

The simulations show that the principal axes are the same for the in-plane and out-of-plane properties when a reflection or glide reflection is present, but does not have to be true for the p4 pattern as seen in the figures 4.18 and 4.19. It is hard foresee where these axes will occur, but there is no reason for them to occur at the same place, as they are dependent on different deformation modes and the geometry does not have any reflection symmetries.

The anisotropic behaviour differs also with the proportional scaling of the geometry where the thickness is constant. This results in a change in $[D]$ while $[A]$ is constant, as seen in figure 4.6.

5.2.3 Special behaviour

Coupling A_{12} and D_{12}

The coupling terms [1] describe the interaction between the deformations and the forces (and moments) in the lateral direction when a plate is subjected to a unidirectional strain or curvature. With unidirectional strain, the coupling component A_{12} describe the transverse stress components and with unidirectional curvature D_{12} describe the transverse bending moment. The related terms in the compliant matrix S describes the same but for the transverse strain or curvature when subjected to an axial force or moment.

The different relations for what effect the coupling terms have on a plate deformed axially with tension or curvature is summarized in table 5.6. Pictures of the zero- (devalopable), postive- (synclacstic) and negative (anticlastic) Gaussian curvatures is shown in figure 2.13.

	Close to zero	Negative	Positive
A_{12}	No lateral strain	Lateral expansion	Lateral contraction
D_{12}	Zero Gaussian curvature	Positive Gaussian curvature	Negative Gaussian curvature

Table 5.6: Response of a material when subjected to pane starain or curvature in axial direction for with different values of A_{12} and D_{12}.

It must be pointed out that A_{12} and D_{12} is anisotropic for diagonal, orthogonal and tetragonal patterns and change with rotation. In other directions than the principal directions shear or twist coupling terms, A_{16}, A_{26}, D_{16} and D_{26} will appear and introduce shear forces or twist moments.

No coupling A flexure pattern having close to zero coupling (and therefore close to zero Poisson's ratio) has little, or non-existing strain and stress coupling. These can be interesting for applications where the different forces and deformations in different directions should not effect each other. They also make good specimens for tensile testing of plates, as no lateral strain will influence the stiffness.

Poisson's ratio For a material with no present shear coupling terms, A_{16} and A_{26}, the coupling term A_{12} describe the same as the Poisson's ratio for isotropic and orthotropic materials.

Normal values for the Poisson's ratio are within the range [0.1, 0.5]. Materials that exhibit a negative, near to zero or above 0.5 Poisson's ratio can be characterized as special and negative Poisson's ratio materials are often classified as a subset of mechanical metamaterials. Table 5.7 shows a summary of the Poisson's ratios that are found in some of the flexure patterns studied and shows special behaviour.

The YdX cmm pattern showed an extreme Poisson's ratio when subjected to stretching. A closer look at the geometry reveal similarities with a reentrant honeycomb pattern as seen in figure 5.5. The reentrant honeycomb pattern is vastly studied and a version more similar to the modified version that also contains stiff regions is found in [22]. It is however

[1] The described terms should not be confused with the $[B]$ matrix for a laminate that is called the coupling matrix. Since the simulated patterns are both symmetric and balanced, $[B] = 0$ and no coupling is present between in-plane and out-of-plane deformations.

Pattern	ν_{12}	ν_{21}
LET cmm	[0.01, 0.12]	[0.53, 1.62]
LET p4m	[0.00, 0.05]	
LET p6m	[-0.02]	
Switchback cmm	[-0.13, 0.29]	[-0.14, 0.01]
Switchback p4	[0.00]	
Switchback p4g	[-0.62, 0.01]	
Coil cmm	[-0.03, -0.08]	
Coil p4	[-0.08, -0.04]	
YdX cmm	[-1.70, -0.20]	[-5.20, -0.30]

Table 5.7: Poisson ratio of some flexure patterns pattern. Where ν_{21} is not listed, the value is the same as for ν_{12}.

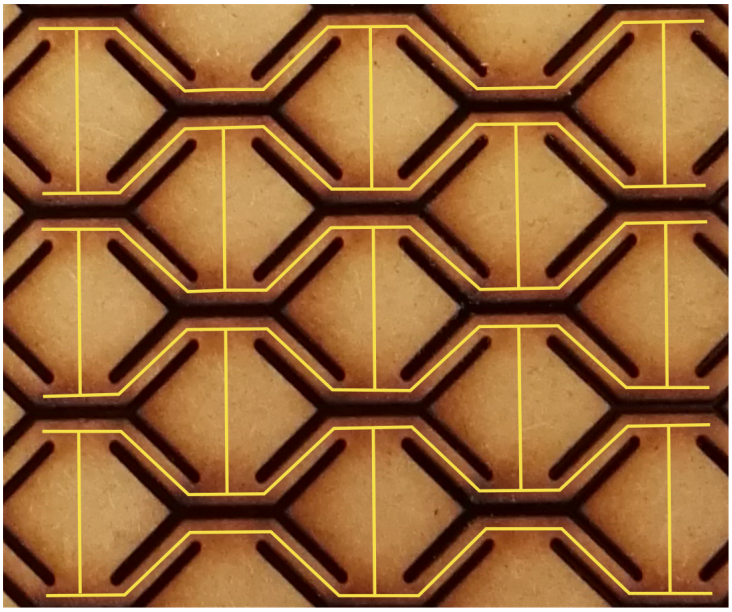

Figure 5.5: The YdX pattern with the modified reentrant honeycomb pattern drawn for visualization.

a good chance that the knowledge of this property being present in the pattern is unknown for most users and it has not been seen in the context of a pattern cut in plates.

The other auxetic patterns are not found in review articles [5], but some show similarities like the Coil cmm.

Degree of anisotropy

Table 4.6 is generated on the basis of the database of results from the other simulations and not as a designed experiment to compare the degree of anisotropy and can not be compared quantitatively in between. There exists most likely many variation of the patterns that shows higher or smaller degree of anisotropy.

Practically speaking, large degree of anisotropy results in distinctive compliant and stiff directions, while small degree of anisotropy results in more similar properties in all directions and behaves close to an isotropic material. These properties can be utilized in

different applications depending on what you need.

The results point, however out some interesting trends of some of the different patterns:

- Patterns with *with tension axes* can achieve very high degree of anisotropy because the deformation mode changes from tensile to bending for A_{11} and changes from torsion to bending for D_{11}. An example of this is the LET cmm.
- Coil and switchback flexure configurations show very little degree of anisotropy and behave close to isotropic in some special cases like for the Coil p4, Coil cmm and switchback p4g. This can be a result from the flexure mechanisms having few restricted DOFs.
- LET flexure configurations show high degree of anisotropy and can come from the fact that the LET joint has a symmetric flexure configuration that restricts many DOFs. A good example of this is the LET p4m that show relative large anisotropy for D_{11}.

5.2.4 Numerical error

The results from all simulations will have numerical noise. This comes from various sources like numerical integration, interpolations, bad shaped elements, and the fact that the FE model has finite precision in describing numbers. The simulated geometries are in most cases different from the one in the convergence test in section 3.2.2 and variations of the same model will have different meshes. This means that the error will also be different for the different components. The requirement of minimum two C3D20 elements across a cross-section is however maintained though out all simulations, but the number is in many cases larger. This can be a source to some error seen in the regression analysis.

5.3 Design principles

The following principles are proposed to achieved target properties:

- Increase compliance: reduce flexure width increase flexure length, reduce plate thickness.
- Keeping in-plane stiffness, but increase out-of-plane compliance: proportionally scale the geometry while remaining the same thickness of the plate.
- Axis of compliance different for in-plane and out-of-plane: choose a p4 pattern with only rotations present.
- Have orthogonal stiffness: choose a pattern with at least one axis of reflection or glide reflection (pm, pg, cm, pmm, pmg, pgg, cmm).
- Have transverse isotropic stiffness: choose pattern with 3-fold symmetry or more (p3, p3mi, p31m, p6 or p6m).
- Low degree of anisotropy: chose a flexure configuration with many DOFs like the Switchback or Coil.

- High degree of anisotropy: choose a flexure configuration with few DOFs like the LET.

When the same length of a flexure mechanism is considered in an natural extension (see section 3.1.3), the switchback will allow larger travel distances than the LET, because it has longer flexure length as discussed in section 2.22. This makes it generally a better alternative for making compliant patterns.

The authors recommended patterns for introducing compliance in different directions:

- Orthogonal, one compliant axis: LET cmm
- Tetragonal, two compliant axes: switchback p4g
- Isotropic: switchback p6

5.4 Objectives and approach

The objectives defined in the preface tries to cover different aspects of the use and utilizing of flexure patterns and demand different approaches. Part of the difficulty in choosing an appropriate approach for studying the different objectives is to make it coherent with a the other objectives and to find common ground.

Part of the difficulty in choosing an appropriate approach for studying the relations between symmetry, geometry and mechanical behaviour of a flexure pattern is the variation of methods of the fields of crystallography, mathematics and physics, that try to describe the principles for determining properties of material structures.

In general, this thesis tries to describe the fundamentals from a mathematical and physical point of view but does not carry a detailed discussion from the stress tensors. I will give some comments with the chosen approaches with respect to the given objectives.

Establish the geometry-symmetry conditions in order to -

(a) understand patterns This objective focuses on the qualitative aspects of flexure patterns and want to describe the governing theories, concepts and terms that can be used to describe flexure patterns. To accommodate this, a search in the literature is necessary to find relevant fields and research that can supplement and be build upon for flexure patterns. When the classification methods for flexure patterns are implemented, an effort is made to make it coherent with the related fields. Fields that have been found to be related and useful for describing flexure patterns are: plane symmetry groups, compliant mechanisms, metamaterial and crystallography. The background for these fields are presented in the background before elaborated on in the method. For describing the different unique patterns the 17 wallpaper groups and the different compliant mechanisms has served as useful concepts to classify by.

(b) create new patterns This objective is fundamentally a creative problem-solving process of searching for an original and previously unknown solution to a problem. This problem, has no limit to the number of possible patterns solutions as there are infinitely possibilities for repeating motifs.

My solution to the objective is the procedure of creating compatible compliant tiles which builds on the definition, and the obtained knowledge about compliant mechanisms and concepts within group theory. The method opens up for new patterns by considering other shapes and symmetries than the repetitive rectangular element often presented as a pattern.

As recognized, the unit of the pattern defined by the wallpaper groups don't serve as an intuitive repeating cell because it might partition the flexure mechanism at strange places. For this reason the method uses tilings that serve as a better way of looking at the patterns of compliant mechanisms.

Establish a numerical model to quantify the properties of any given pattern The objective focuses on quantifying aspects of flexure patterns, meaning gathering data. The chosen approach takes basis in plate theory to describe the different behaviour in order to make a FE model that could calculate the properties of various geometries. The plate theory is in many ways a better way of describing the behaviour of flexure patterns as it captures the coupling between axial and transverse properties, which is missed by other authors [25].

Make a tool for adjusting parameters of new flexure patterns efficiently to make it easier for people to make and utilize the patterns. Where the previous objectives focuses on expanding the knowledge of flexure patterns, this objective focuses on the utility of the thesis. Integrating flexure patterns into a design is, a laborious process of drawing the desired patterns and is suitable for automating. The approach chosen is to parameterize some patterns so they can be generated according to the required specifications. In order to utilize the patterns, an output vector file (`.svg`) need to be created in order to export it to the software that is used to manufacture the flexure patterns.

On the choice of different approaches for the objectives, I must admit that there are several other ways of answering the objectives. The resulted methods are a result of making a choice upon the information obtained within the semester and the synthesis of this.

5.5 Relevance

Over all this study contribute to clarify the concept and basic behaviour of flexure patterns. The wish is that this will serve as an inspirational source for other people to make innovative and aesthetic products with functionality. It can ultimately be whatever the designer can produce, from jewelry pieces to clothing, toys, games, or artistic designs.

More industrial applications can be within packaging, shelters but also more general as a technique for manipulating properties of a plate that can be useful for prototyping with only one material available in stock.

5.6 Critics

The stress tensor theory is often presented by group theory experts for the crystallographic groups [3], while the development of new non-symmetric structures are driven by the

potential of making metamaterials with special properties are driven by scientists and engineers without this expertise [24]. This can lead to confusion and incorrect use of the theory.

The theory for fully understand the relationship between crystallographic restrictions and mechanical properties is the essence for understanding the properties of different flexure patterns. To give a complete description of the consequences of the mechanical properties of all symmetry groups is extensive work that should be given to persons with such expertise. This study is limited to discuss some findings for some flexure patterns classified by the plane symmetry groups and not an extensive deduction of the criterions.

Part of the difficulty in reading from various sources on a diverse topic, is the variation of terminology used by the authors. Not only are different terms used to identify the same object, but sometimes the same terms are employed to identify different objects. I have tried to use the correct terms when referencing to other studies and to point out what terms that are used synonymously.

It can also be relevant to mention that flexible materials are not always the answer to creating flexible products, especially when the designer is also looking to create a product that is also very strong.

5.7 Further work

Whereas some progress has been made since the start of this thesis, a lot of open issues are yet to be tackled within flexure patterns:

- Strength analysis
- Topology optimization
- Making numerical models for parallelogrammic shaped units and compliant tiles of other shapes to calculate the stiffness properties of all repeating patterns.
- Make a program for end user
- Custom flexure patterns for bottom up metamaterials

Chapter 6

Conclusions

Through geometrical modelling, FEM simulations and by studying the possible symmetries, a classification, the mechanical behaviour and design principles for achieving extreme stretchability and flexibility in stiff plates via the introduction of flexure patterns, has been explored.

The term *flexure pattern* has been established for describing the concept of introducing compliant properties to stiff plates by manufacturing a pattern of flexures. It is characterized as a 2D meta material that consists of flexures patterned according to a set of rules, increasing the compliance compared to the bulk material. It is categorized by the flexure configuration and the two dimensional symmetry groups which have been the basis on which they have been studied in this thesis. The elastic behaviour is favourably described by a stiffness matrix on which the anisotropy is studied.

Design principles

The design principles are summarized by the method of making *compatible compliant tiles* that are compliant, continuous and connected. The method borrows concepts from compliant mechanisms, tiling, and the plane symmetry groups and synthesize some of the physical constraints with the vast opportunities for making new unique designs. Facilitating for bending or torsion modes in the pattern showed to be the most effective method for achieving in-plane and out-of-plane compliance, while the method of making a continuous and connected pattern address some of the geometrical constraints.

To demonstrate the design principles, new flexure patterns with different geometries that belonged to different plane symmetry groups were created. These showed favorable compliant properties in multiple directions and distinguishes from previously found flexure patterns as better alternatives when compliance is required along multiple axes.

Mechanical behaviour

The computational homogenization technique using the finite element method was successfully implemented for obtaining the elastic stiffness matrix of different patterns. Furthermore, the continuum approach was utilized to study the anisotropic characteristics of the flexure patterns by transforming the reference coordinate system. The elastic response was found to be highly dependent upon the geometrical orientation and loading directions. According to these observations, the following conclusions are made:

1. The elastic behavior of flexure patterns are generally orientation dependent. This dependency is directly related to the geometric configuration of the flexures, as well as the topological symmetry of the pattern

2. Flexure patterns have generally an ordinarily anisotropic (diagonal) behavior. However, symmetries of the pattern change the response:

   - One glide reflection or reflective symmetry leads to an orthogonal response.
   - A 4-fold rotation symmetry leads to a tetragonal response.
   - A flexure pattern is isotropic when six reflective symmetries exist[1].

3. There is no obvious dependency between in-plane and out-of-plane stiffness and the principal axes can be offset by an angle for patterns with no reflective or glide reflection symmetry.

4. The compliance of a flexure pattern is increased by making the flexures more slender and is achieved by increasing the length/width or length/thickness ratio. Logarithmic regression models fit many of the changes of compliance we variation of some of the between geometrical parameters and the compliance is present when the variation of one parameter is studied seems to describe the . The compliance is also increased when there are fewer flexures present per length of the unit of the pattern.

Computational resources

Python code program able to generate 11 different flexure patterns based on the method described is presented. It can output a `.svg` file with the requested parameters that can be used for manufacturing. A compatible finite element script can determine the stiffness matrix of all square or rectangular lattice flexure patterns. The simulated data can be used to make a choice of the right pattern for an application.

The design principles proposed in this work can be applied to a wide range of flexure pattern and help to get a conceptual understanding of how the concept can be further developed. The quantification of the characteristics is of importance for engineering applications but a strength analysis should be conducted before using it in critical applications. I believe this work can expand the potential applications of flexure patterns.

[1]The not simulated flexure patterns with 3-fold rotation symmetry is expected to be the same

Appendix A

Metamaterials

Inverse approach of creating materials

When talking about invert design of materials, we also have to look at the conventional way of design. The conventional way of designing is to pick a material and then make a product with the desired properties. This approach also uses trial and error to iterative towards a optimum solution of the design of the product that is desired.

Inverse design first declare the functionality that is needed for an application, and then find the material that has that functionality. The inverse design approach takes benefits of being able to predict the behaviour of a certain material configurations or structures and then use data computation to investigate numerous possibilities for making such new materials as shown in figure A.1. The predicting of properties builds on the fundamental understanding that was developed in order to understand the materials used in the conventional way for designing applications. The exploration of possibilities is done thorough different algorithms that can run through a large amount of solutions. Some much used algorithms are topology optimization or genetic algorithms.

A third important aspect of the inverse approach is to test its validity. As the results are new materials with a desired functionality it is essential to test if it actually behaves according to the models.

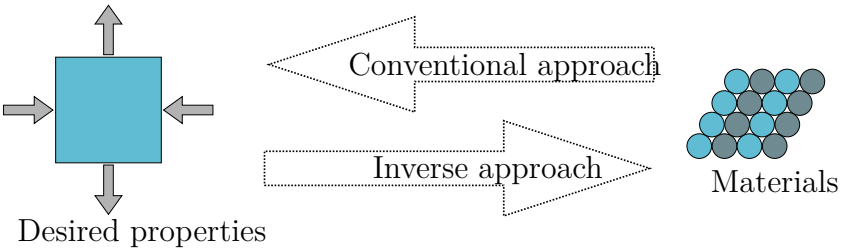

Figure A.1: A comparison between the traditional and inverse approach for material properties.

Appendix B

Code

B.1 Flexure pattern design tool

```
from patternGeneratorClass import Unit

# Set initial parameters
flexure_type = 'switchback'
wallpaper_group = 'p4g'
unit = Unit(flexure_type, wallpaper_group)

# Display name
unit.name
>>'switchback_p4g'

# Set name
unit.set_name('test')
unit.name
>>'switchback_p4g-test'

# Display svg representation of object geometry
unit.unit
>>

# Plot object with dimensions
unit.plot()
>>

# Display parameters
>>unit.para
  {'cut_width': 1.0,
   'flexure_width': 1.0,
   'junction_length': 2.0,
   'num_flex': 1,
   'side_cut': 'default',
   'stem_width': 'default'}
```

```
# Set new parameters, name must match
unit.set_unit_para(cut_width=0.5)
>>{'cut_width': 0.5,
   'flexure_width': 1.0,
   'junction_length': 2.0,
   'num_flex': 1,
   'side_cut': 'default',
   'stem_width': 'default'}

# Various variables can be accessed through
unit.lattice_type
>>'square'
unit.l1 # lattice length 1-direction
>>10.606801717798216
unit.l2 # lattice length 2-direction
>>10.606801717798216
unit.angle # lattice angle
>>90
unit.center # center tuple
>>(-1.1124368670764584, 1.210786437626905)
unit.unit_coords # corner coordinates
>>[(-6.415837725975567, -4.092614421272203),
   (4.190963991822651, -4.092614421272203),
   (4.19096399182265, 6.514187296526013),
   (-6.415837725975566, 6.514187296526013)]
unit.unit.area # area of unit
>>82.34255857559613
unit.unit.length # contour length of unit
>>141.3153084989848
list(unit.unit.exterior.coords) # access list of all geometry coordinates
>>[(-5.165637725975566, 2.4608864376269066),
   (-4.8122257567385285, 2.4608864376269066),
   (-1.3623368670764584, 5.910775327288978),
   ...]

# Creates a 3-column, 2-rows flexure pattern
unit.make_pattern(3,2)
unit.flexure_pattern
>>

# Save flexure pattern as SVG
unit.save_svg()
>>

# Save flexure pattern, unit and generating region as SVG
unit.batch_save_svg()
```

>>

B.1.1 Geometrical representation

Polygon object

The basic object is the shapely Polygon object. This supports geometrical manipulations are provided by the Shapely library. The pseudo code describes the syntax of the relevant operations on a Polygon object.

```
from shapely.geometry import Polygon
from shapely.affinity import affine_transform, rotate, scale, translate
from shapely.obs import unary_union
# Creates a Polygon object
geom = Polygon(coords)
# Transforms polygon
transformed = affine_transform(geom, matrix)
transformed = scale(geom, xfact=, yfact=, origin=())
transformed = translate(geom, xoff=xoff, yoff=yoff)
transformed = rotate(geom, angle=, origin=())
# Union of
union = shapely.obs.unary_union([geom_list])
```

B.1.2 GeneratingRegion object

The Polygon object is implemented in the GeneratingRegion object for representing the geometry.

```
import shapely.geometry

def make_generating_region(flex_para):
    # create the x and y coordinates of the desired pattern
    x = [x1, x2, ..., xn]
    y = [y1, y2, ..., yn]
    # make a list of coordinate tuples
    coords = list(zip((x,y)))
    # create a shapely polygon object
    return shapely.geometry.Polygon(coords)
```

B.1.3 Unit object

The repeating unit consists of a generating region in which have been copied through transformation functions. To make one unit cell out of several regions a union operator is used.

The transformation library from shapely are accessed though the header `import shapely.affinity`

An example of the method for generating a p4m unit is given. The unit has attribute `self.unit`.

```
def p4m(self):
    generating_unit = self.generating_region
    xmin, ymin, xmax, ymax = generating_unit.bounds
    # reflect the generating region along a line paralell to the y-axis
    mirrored_y = shapely.affinity.scale(generating_unit, xfact=-1, yfact=1, origin=(x
    # create a list for polygons to union
    poly_list = []
    # 4-fold rotation on the original and mirrored generating region
    for i in range(0,4):
        poly_list.append(shapely.affinity.rotate(generating_unit,angle=(90*i), origin
        poly_list.append(shapely.affinity.rotate(mirrored_y,angle=(90*i), origin=(xma
    # union the list of polygons into one object
    self.unit = shapely.ops.cascaded_union(poly_list)
```

B.1.4 Handling numerical precision

A problem encountered when working with numerical geometric representation is that the the union of polygons will not always create a continuous geometry. This happens when the geometry is represented through irrational numbers like $\sqrt{2}$ or $\sqrt{3}$.

```
# sqrt(2)^2 should be perfectly 2
(2**0.5)**2
>>>> 2.0000000000000004

# sqrt(3)^2 should be perfectly 3
(3**0.5)**2
>>>> 2.9999999999999996
% # Square root of two
% 2**0.5
% >>>> 1.4142135623730951
% In[3]:  3**0.5
% Out[3]: 1.7320508075688772
```

An example of this is illustrated by the following code where a hexagon is created from a union of six equilateral triangles. The code results in the polygon shown in B.1 where some of the sides don't align. The solution to this is to extend the geometry so that it becomes a little larger, making the unconnected regions connect. The function *buffer* increases the polygon so it gets rid of the numerical flaws in the geometry.

```
from shapely.affinity import rotate
from shapely.ops import cascaded_union
from shapely.geometry import Polygon

# Create an equilateral triangle
triangle = Polygon([(0,0), (1,0), (0.5, 3**0.5/2)])
# Creates an empty list for storing transformed triangles
triangles = []
# Rotate it six times and appends to list
```

```
for i in range(6):
    triangles.append(rotate(triangle, angle=60*i, origin=(0,0)))
# Union the list of rotated triangles
hexagon = cascaded_union(triangles)

# .bounds returns the boundary coordinates xmin, ymin, xmax, ymax of the object
# Size of flawed geometry
hexagon.bounds
>>>>
(-0.9999999999999999,
-0.8660254037844389,
1.0,
0.8660254037844387)
#Increase boundaries with buffer
hexagon.buffer(0.00001, resolution=1).bounds
>>>>
(-1.0000086602540377,
 -0.8660354037844389,
 1.000008660254038,
 0.8660354037844387)
```

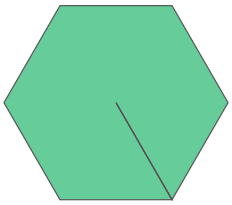

Figure B.1: Imperfect polygon created with a union of equilateral triangles where numerical imperfection counteracts the formation of a perfect hexagon.

B.2 Abaqus RVE program

The important parts of the main code that is run is the following:

```
def runLoadCases(abaqus_para, unit):
    # Creates model and part
    RVEModel, RVEPart = makePartFromShapely(abaqus_para, unit)
    # Set material properties
    setMaterialProperties(RVEModel, RVEPart, abaqus_para)
    # Mesh part and create instance
    meshPart(RVEModel, RVEPart, abaqus_para, unit)
    # Create assembly sets
    createAssemblySets(RVEModel, abaqus_para, unit)
    # Create step and boundart conditions
    stepAndBC(RVEModel, abaqus_para, unit)
```

```
    # Create loadcases
    loadcases = [
                 (1, 0, 0, 0, 0, 0),
                 (0, 1, 0, 0, 0, 0),
                 (0, 0, 1, 0, 0, 0),
                 (0, 0, 0, 1, 0, 0),
                 (0, 0, 0, 0, 1, 0),
                 (0, 0, 0, 0, 0, 1)
                 ]
    resultArray = list()
    for num, loadcase in enumerate(loadcases):
        # Make new model name
        newModelName = abaqus_para['modelName']+'-'+str(num)
        # Copy model
        copyModel(RVEModel, newModelName)
        # Create constraint equations
        constraintEquations(newModelName, loadcase, abaqus_para, unit)
        # Create job
        jobName = createJob(newModelName, submit=True)
        # Calulate stiffness matrix
        resultArray.append(getLoadCaseResult(jobName+'.odb', workdir, unit))
        # Create a countour picture of the model
        printModel(abaqus_para, jobName, workdir, components=False)
    # Write result to file
    writeResultToFile(resultFileName, resultArray, abaqus_para, unit)

# SYSTEM SETUP
workdir = 'C:/Temp/'
os.chdir(workdir)
resultFileName = 'Result-test.txt'

# UNIT SETUP
unit = Unit('let', 'cmm')

# ABAQUS PARAMETERS
# Set up abaqus simulation parameters
abaqus_para = {}
abaqus_para['modelName'] = 'RVE'+unit.name
abaqus_para['partName'] = 'RVEPart'
abaqus_para['instanceName'] = 'RVEInstance'
abaqus_para['elementSize'] = 0.5
abaqus_para['elementType'] = C3D20
abaqus_para['tolerance'] = abaqus_para['elementSize']*0.1
abaqus_para['youngsModulus'] = 1000.0
abaqus_para['poissonsRatio'] = 0.3
abaqus_para['thickness'] = 1.0
abaqus_para['contourComponent'] = 'E'
```

```
# Run main program
runLoadCases(abaqus_para, unit)
```

Appendix C

Additional results

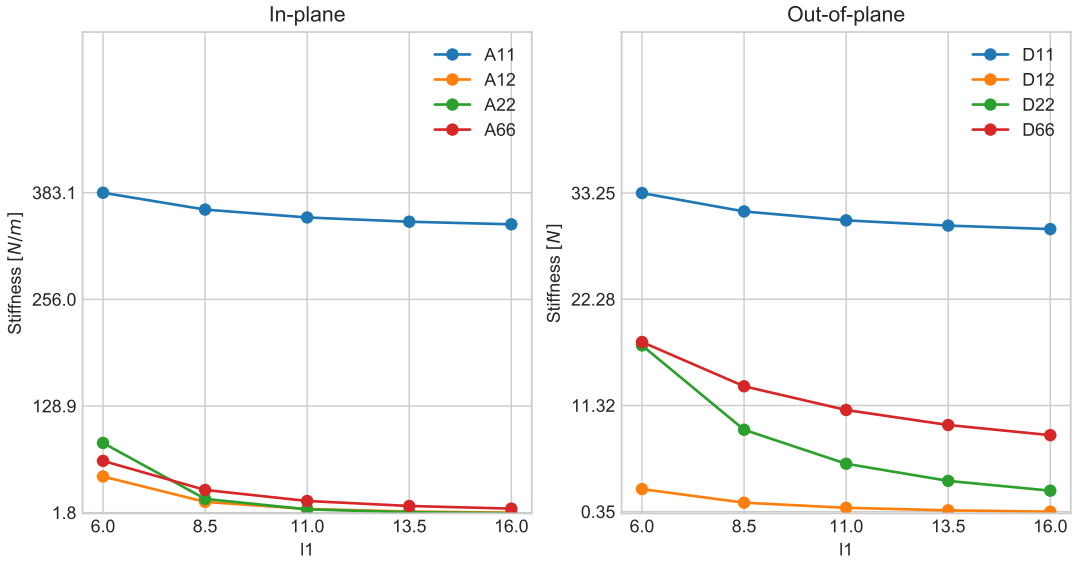

(a) Linear plot of LET cmm with varied flexure length.

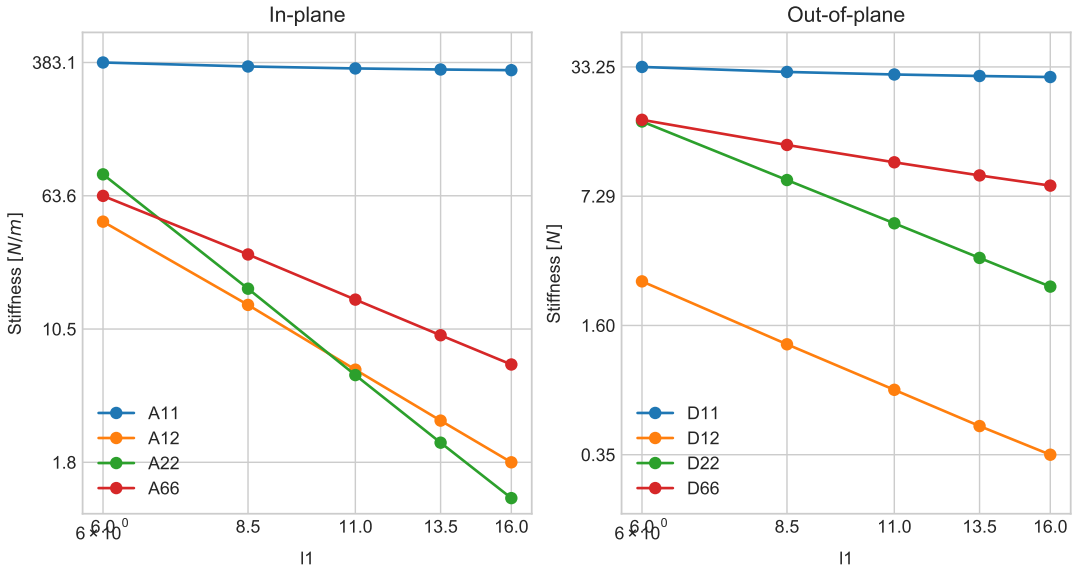

(b) Log plot of LET cmm with varied flexure length.

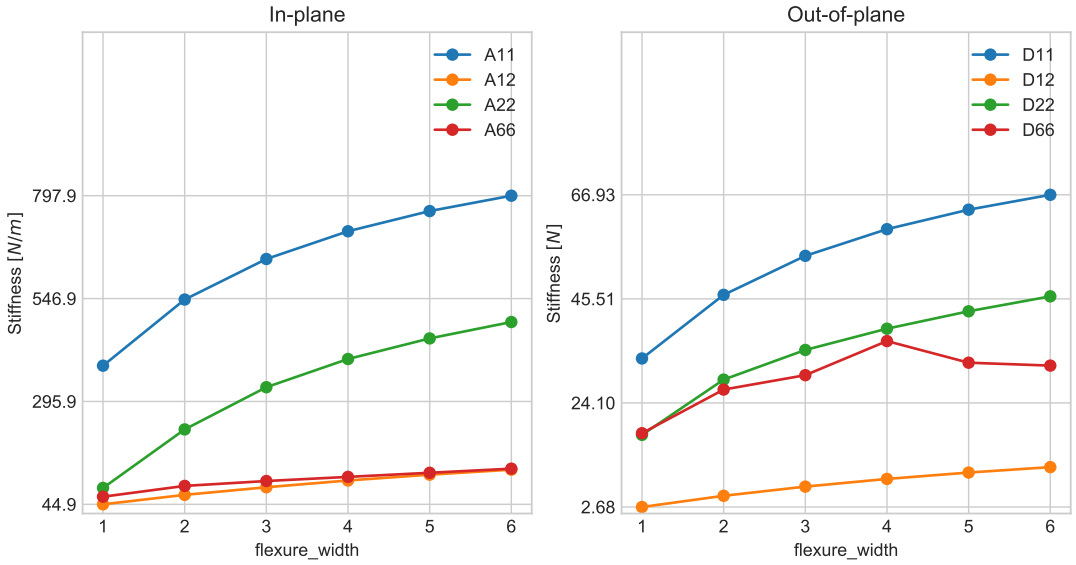

(c) Linear plot of LET cmm with varied flexure width.

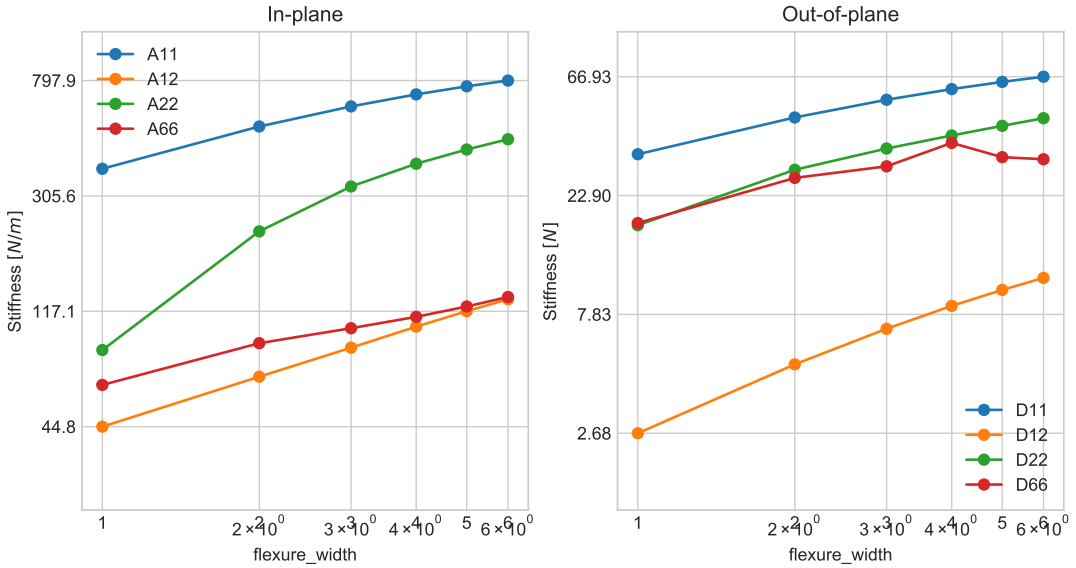

(a) Log plot of LET cmm with varied flexure width.

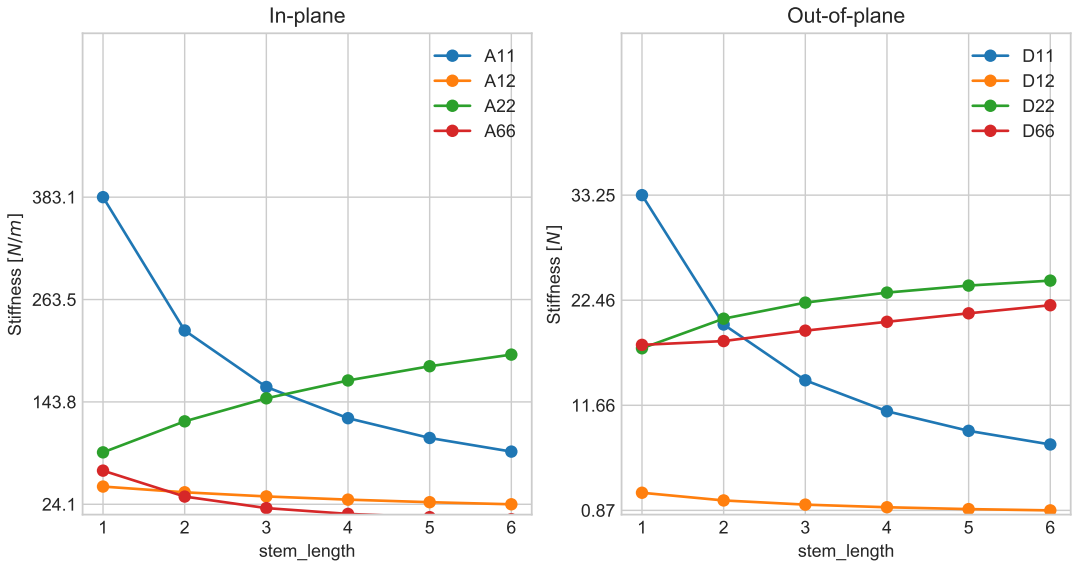

(b) Linear plot of LET cmm with varied stem length.

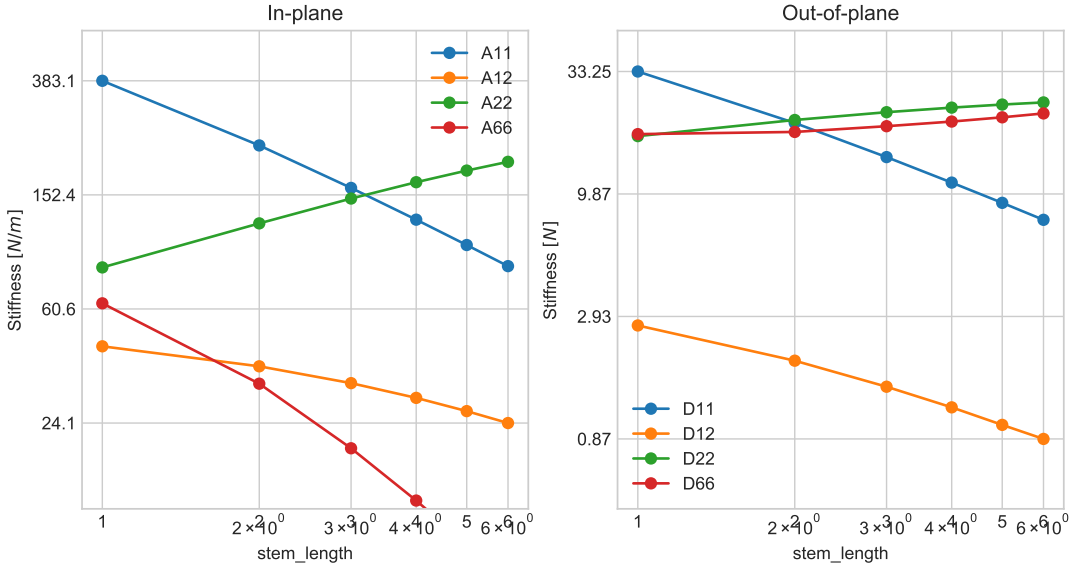

(c) Log plot of LET cmm with varied stem length.

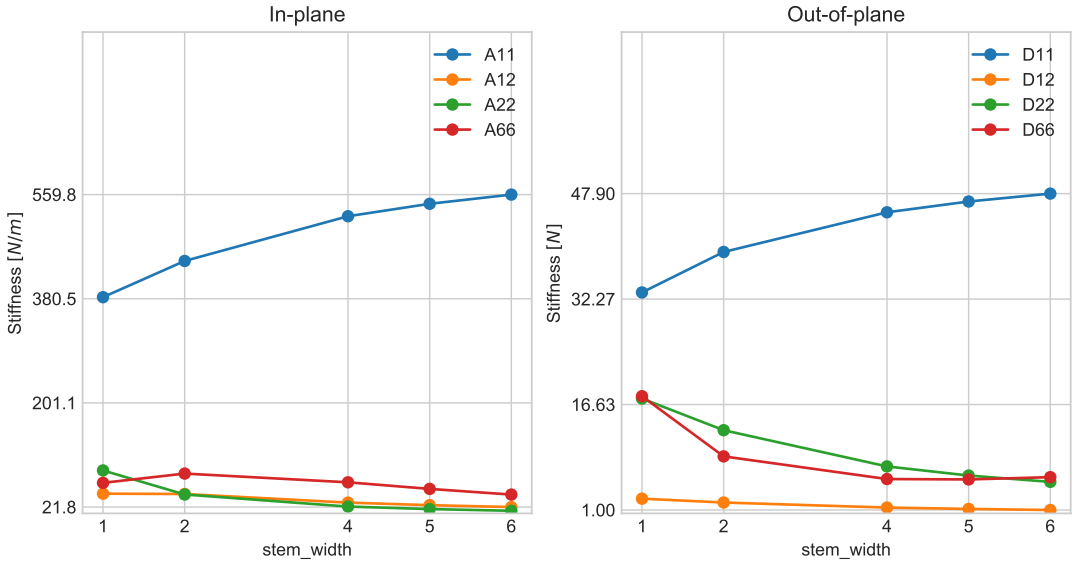

(a) Linear plot of LET cmm with varied flexure length.

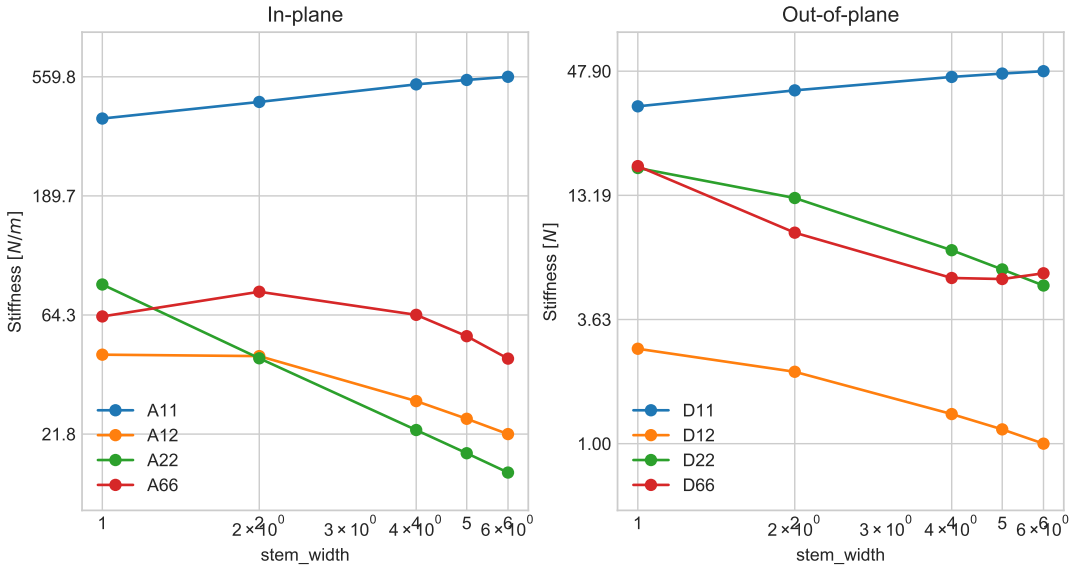

(b) Log plot of LET cmm with varied flexure length.

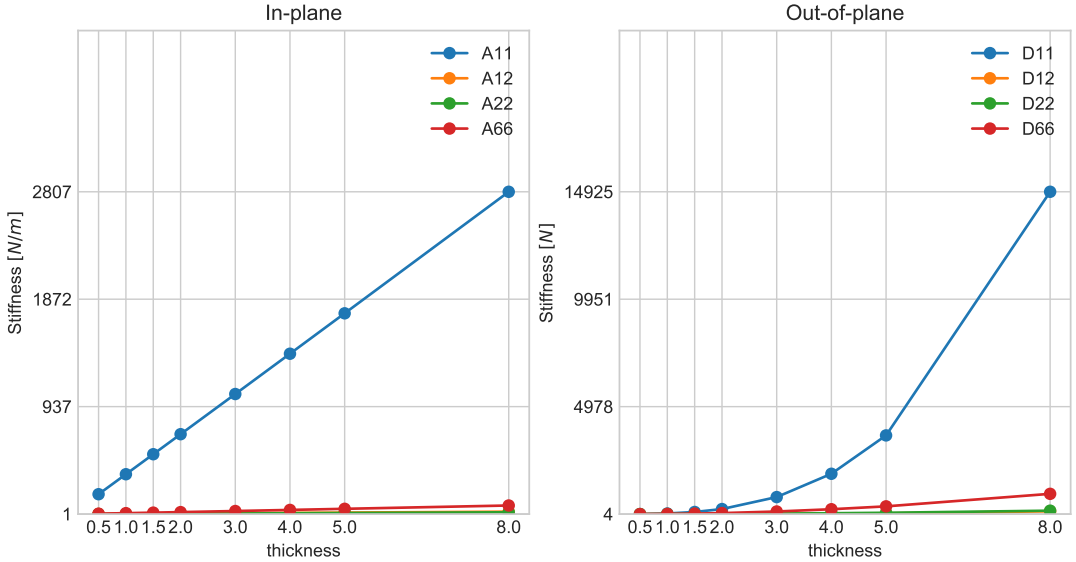

(c) Linear plot of LET cmm with varied flexure thickness.

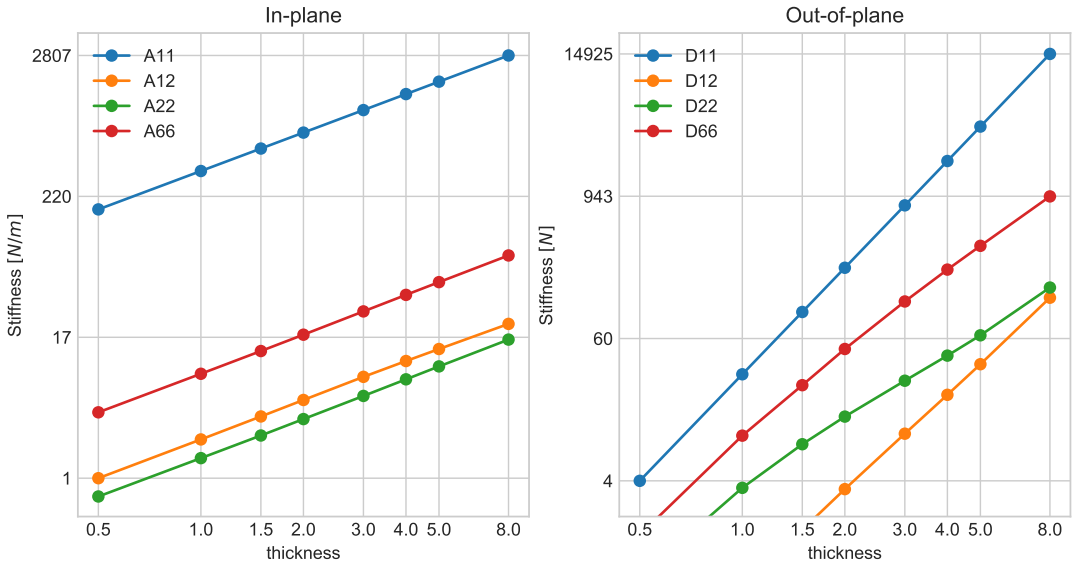

(a) Log plot of LET cmm with varied flexure thickness

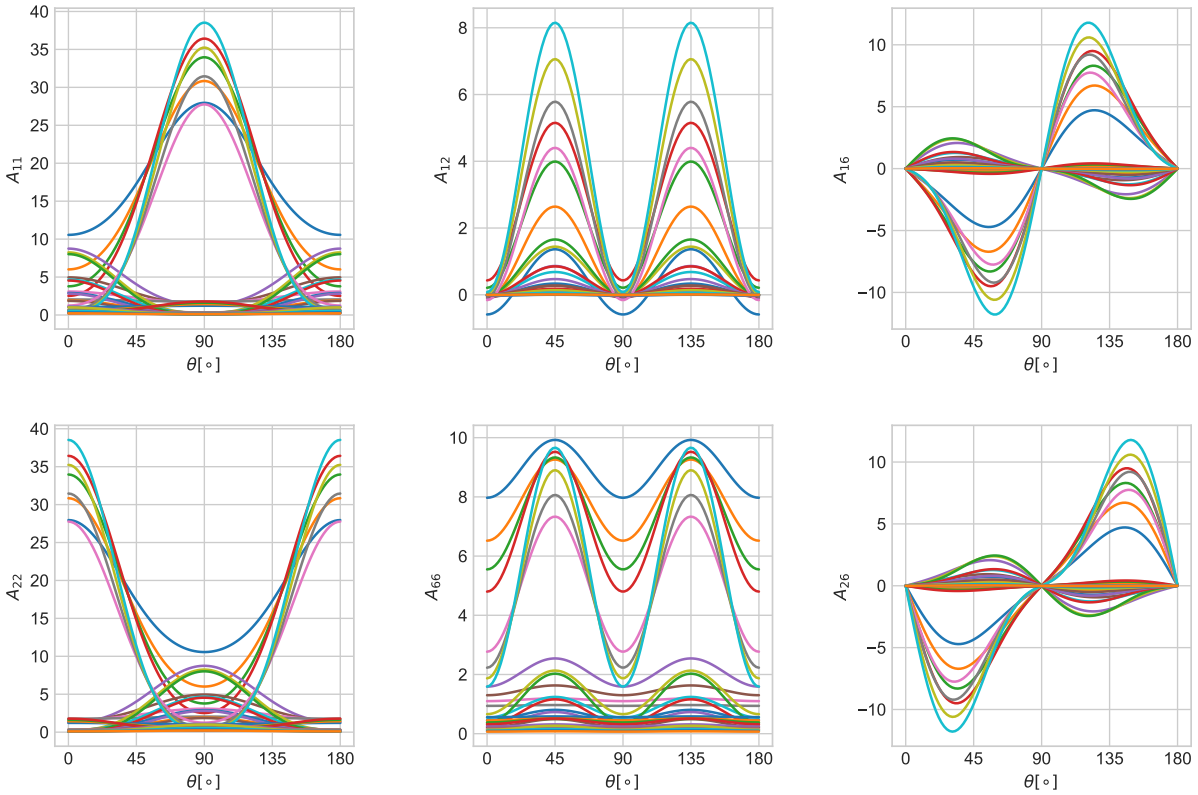

(a) In-plane components.

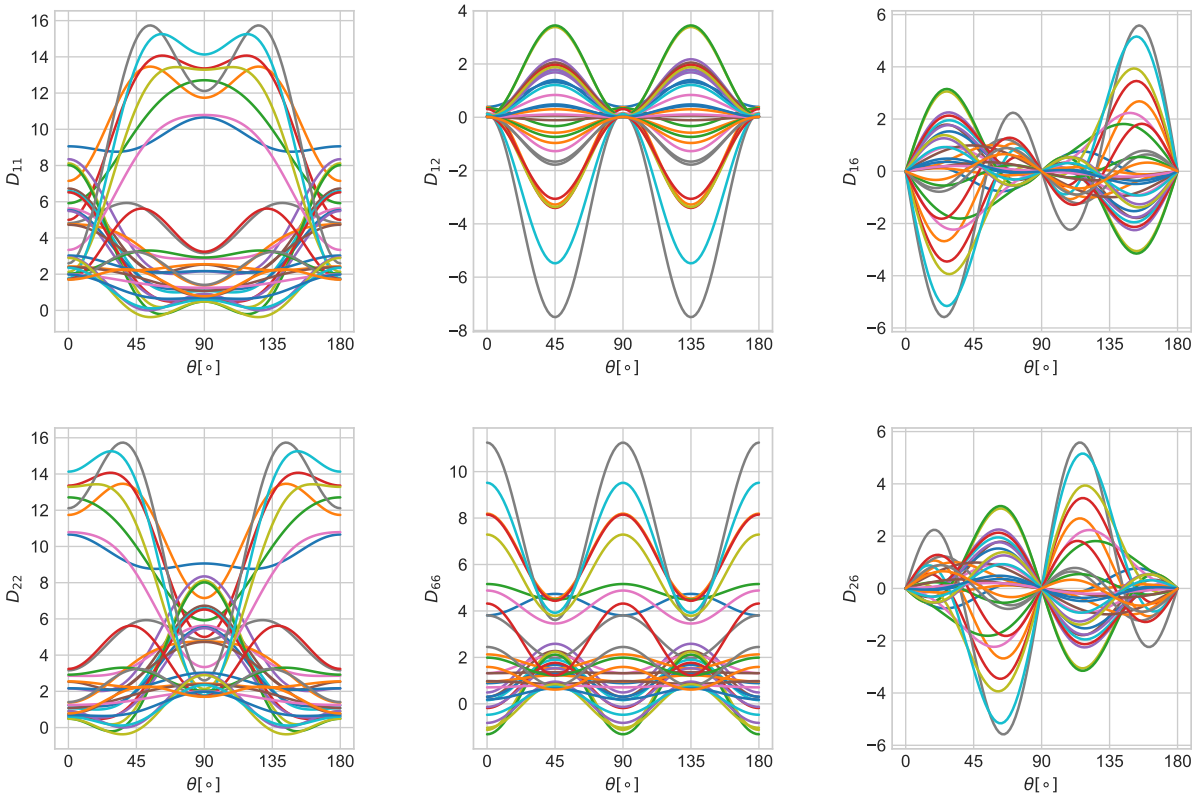

(b) Out-of-plane components.

Figure C.5: Anisotropic stiffness for a *Switchback cmm* flexure pattern where all geometrical parameters are varied.

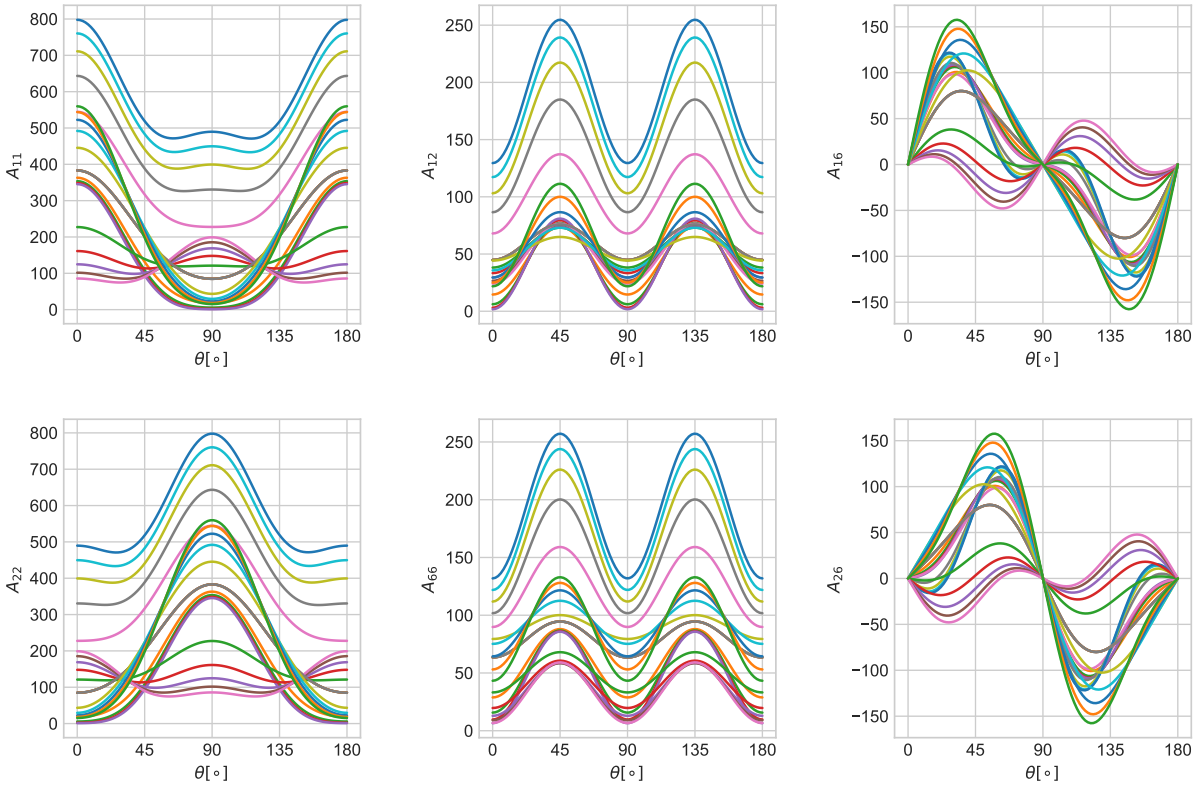

(a) In-plane components.

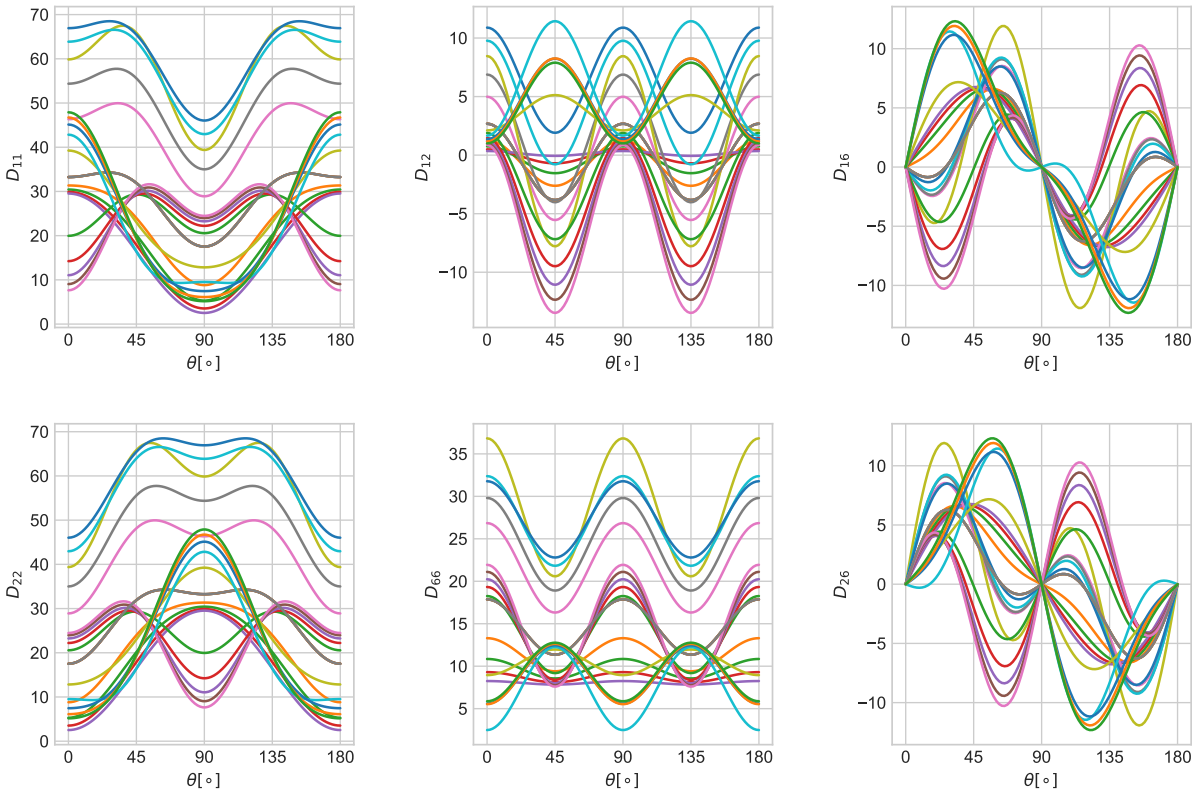

(b) Out-of-plane components.

Figure C.6: Anisotropic stiffness for a *LET cmm* flexure pattern where all geometrical parameters are varied.

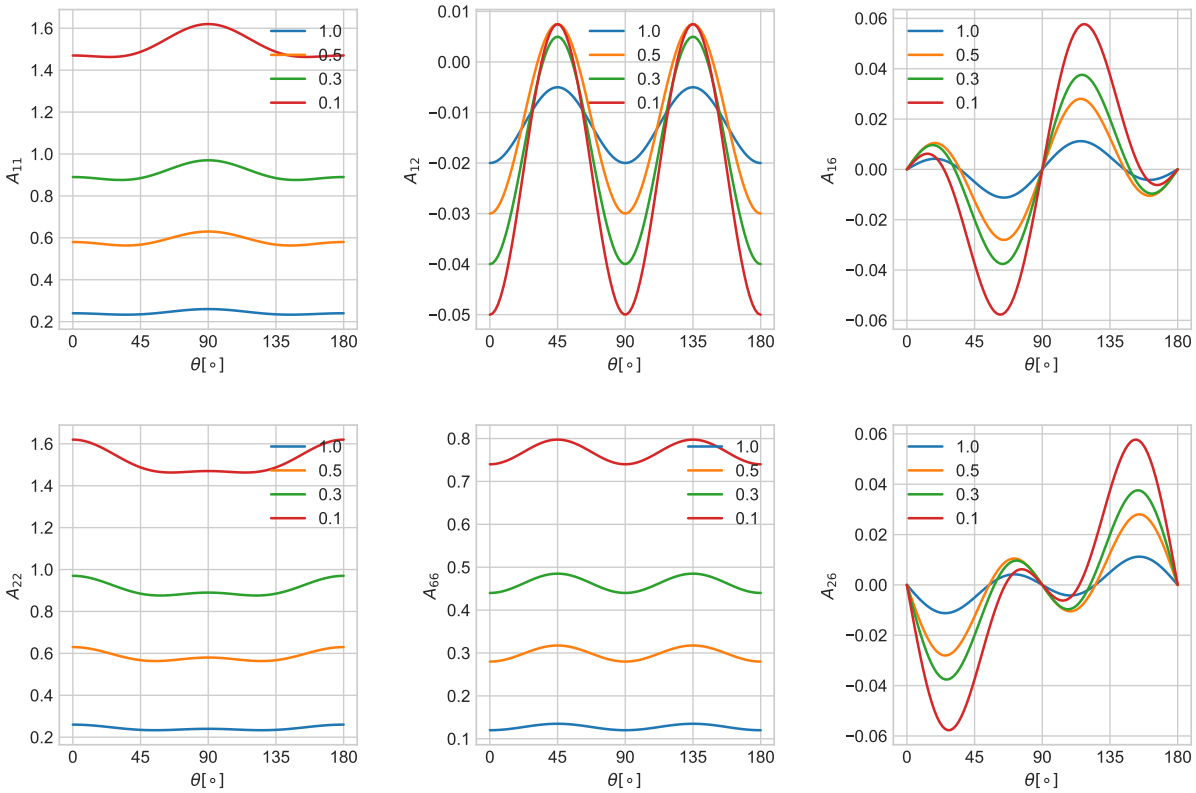

(a) In-plane components.

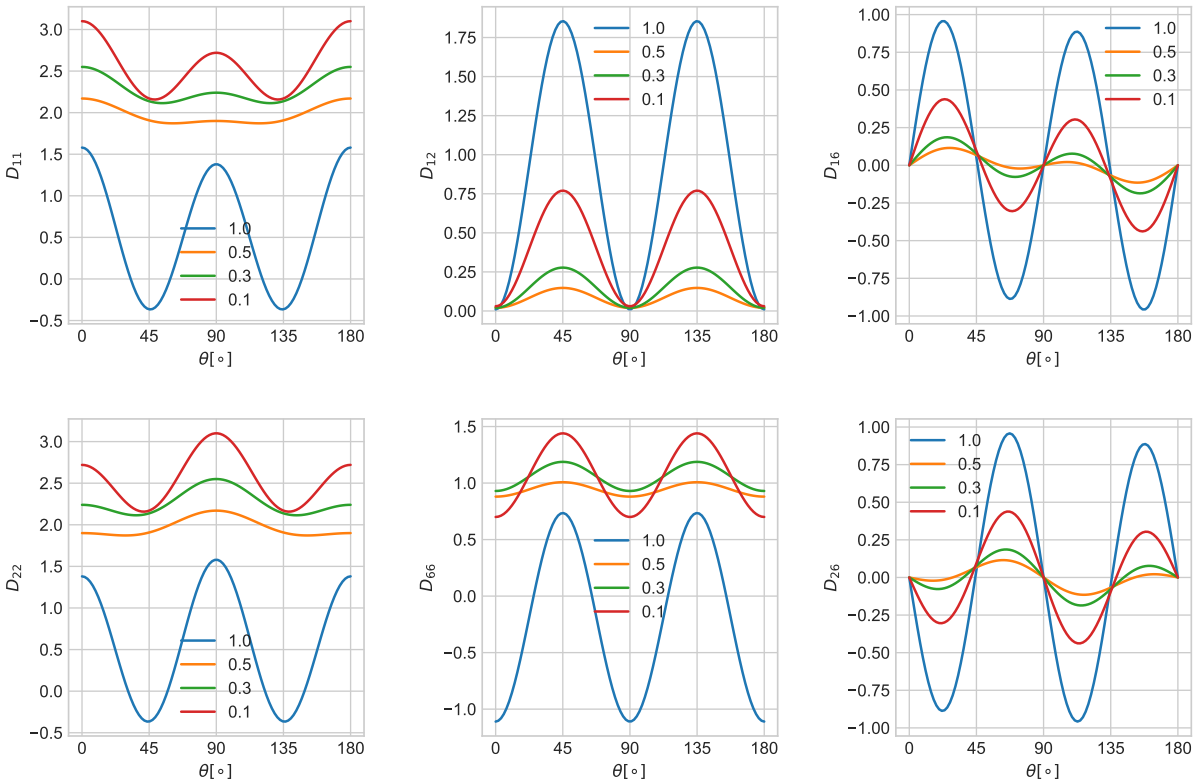

(b) Out-of-plane components.

Figure C.7: Anisotropic stiffness for a *Coil cmm* flexure pattern where *cut width* is increased.

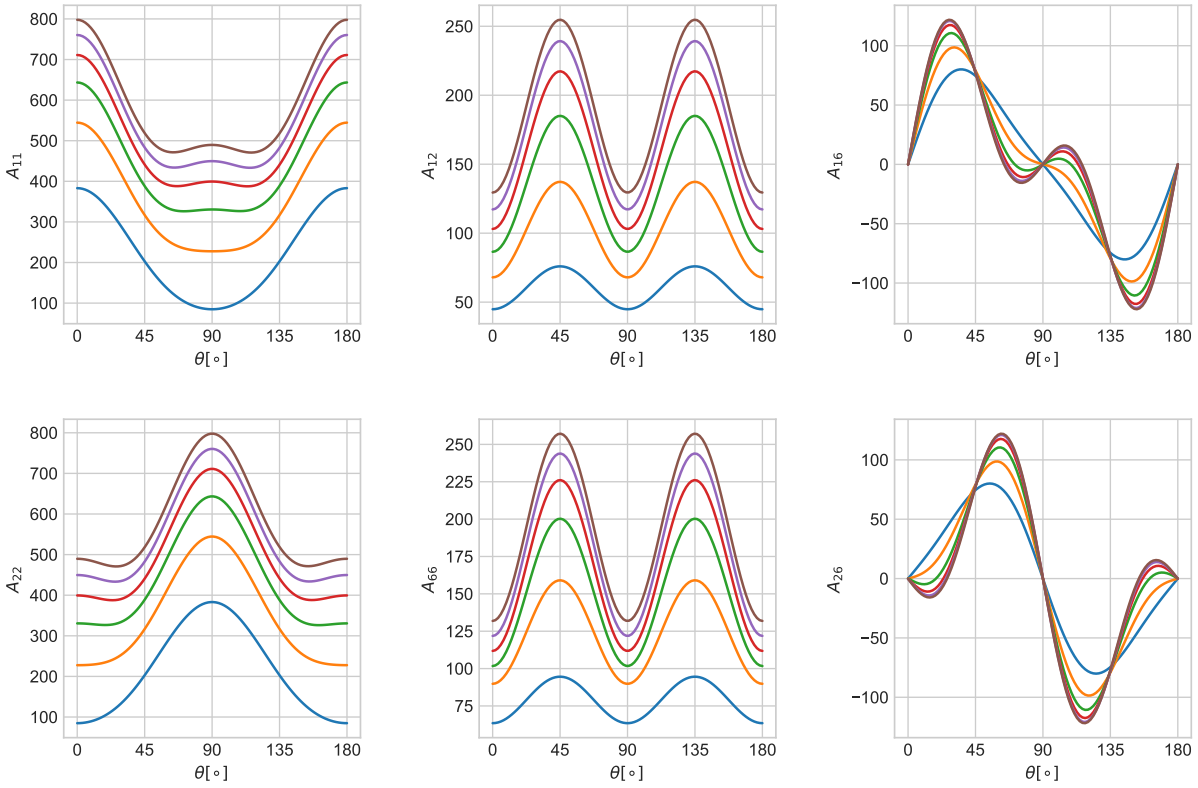

(a) In-plane components.

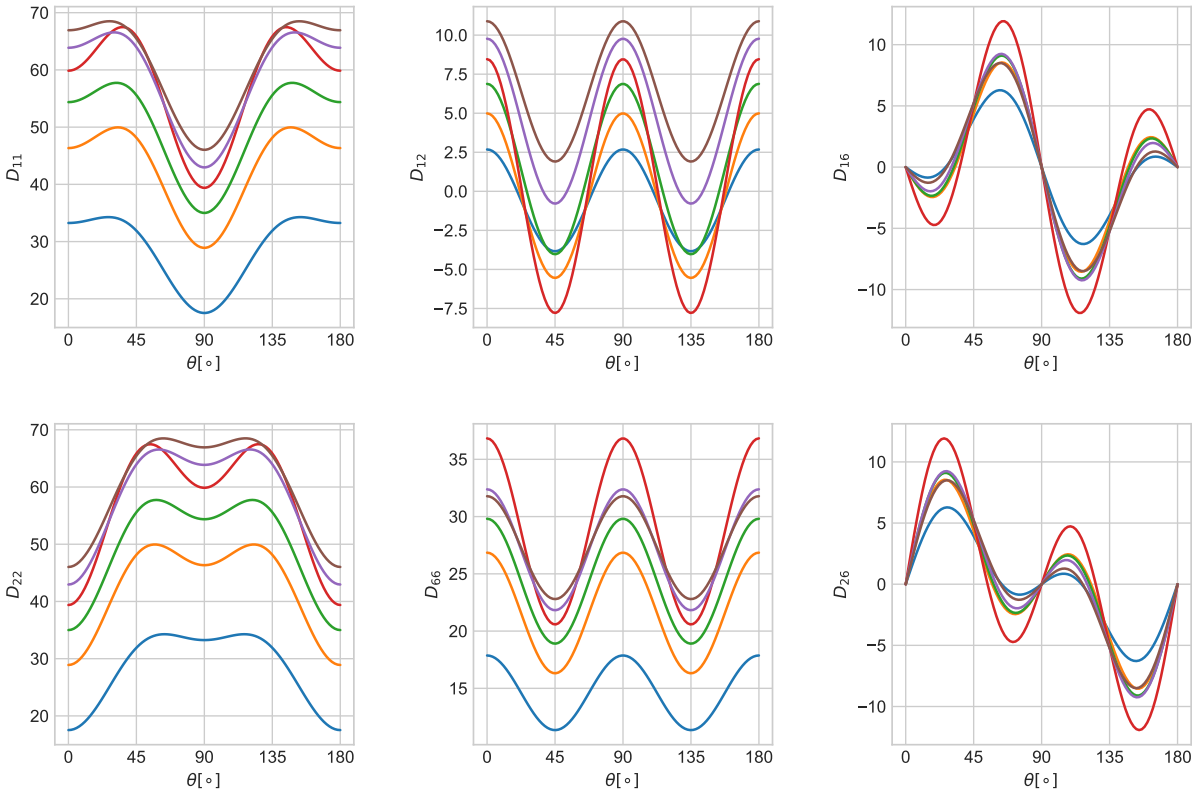

(b) Out-of-plane components.

Figure C.8: Anisotropic stiffness for a *LET cmm* flexure pattern where *flexure width* is decreased.

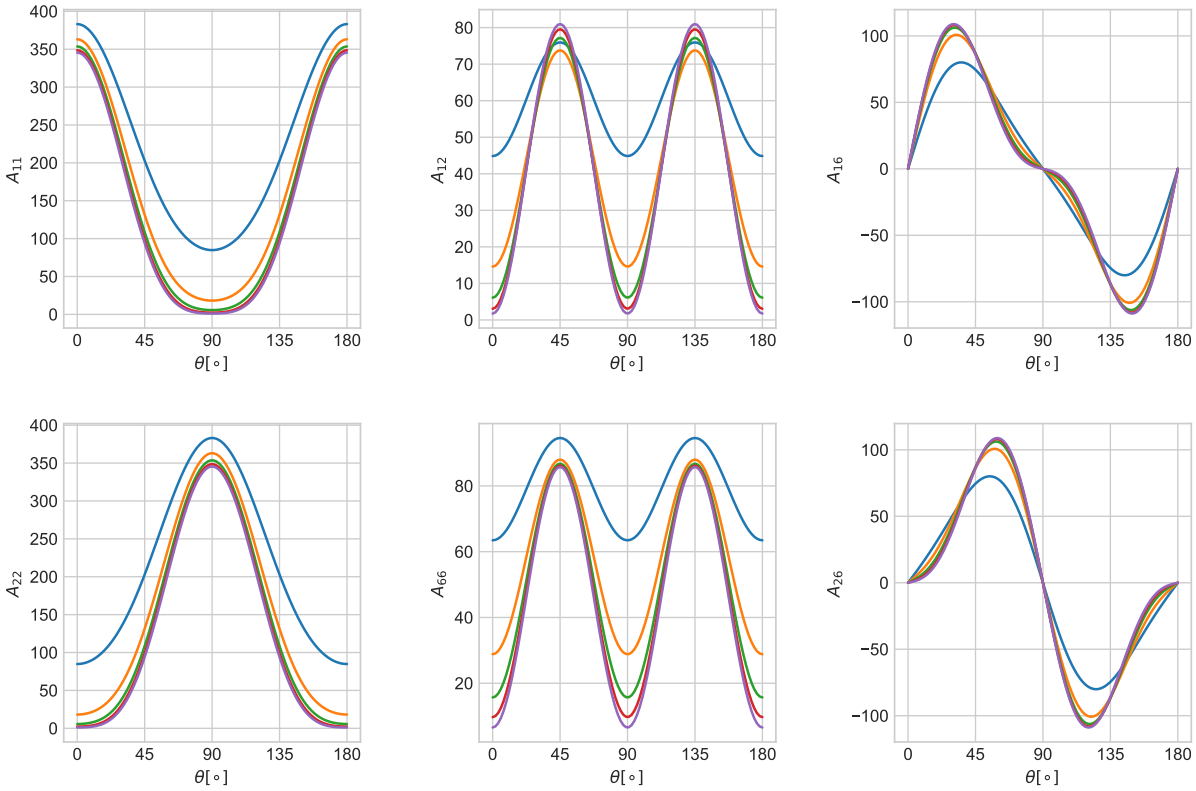

(a) In-plane stiffness components.

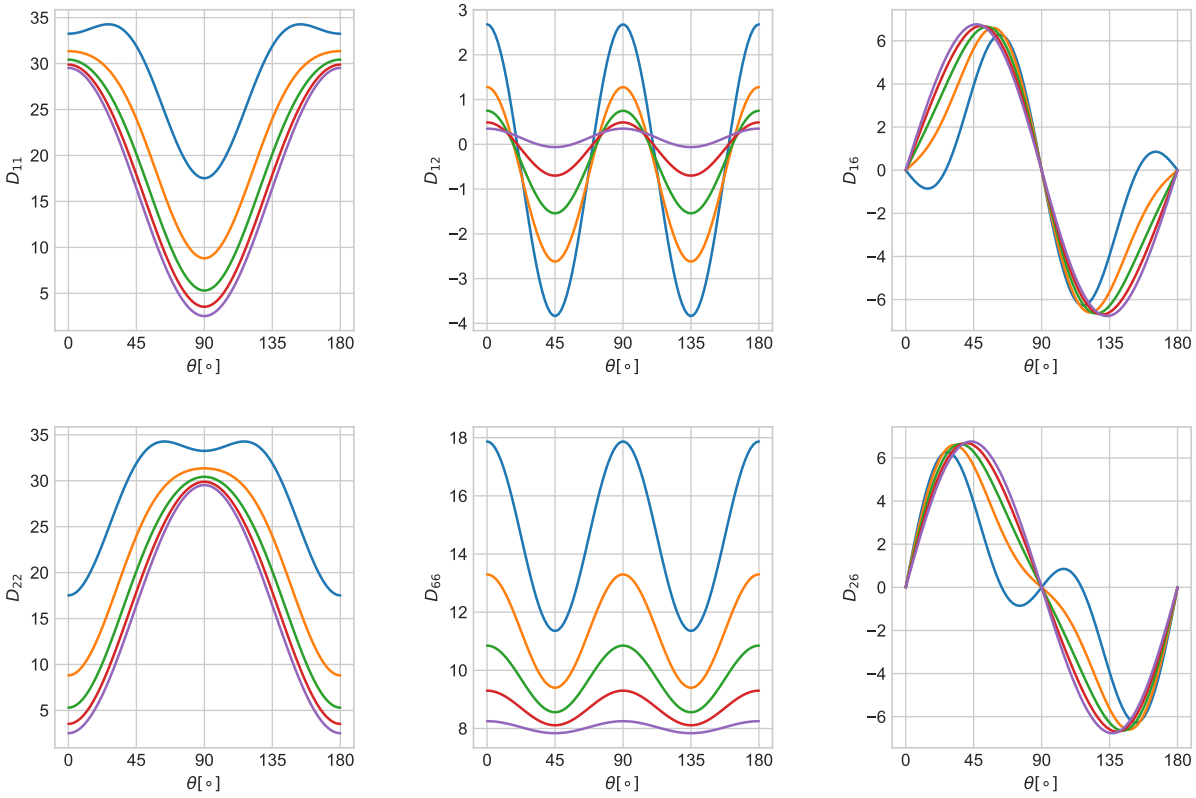

(b) Out-of-plane components.

Figure C.9: Anisotropic stiffness for a *LET cmm* flexure pattern where *flexure length* is increased.

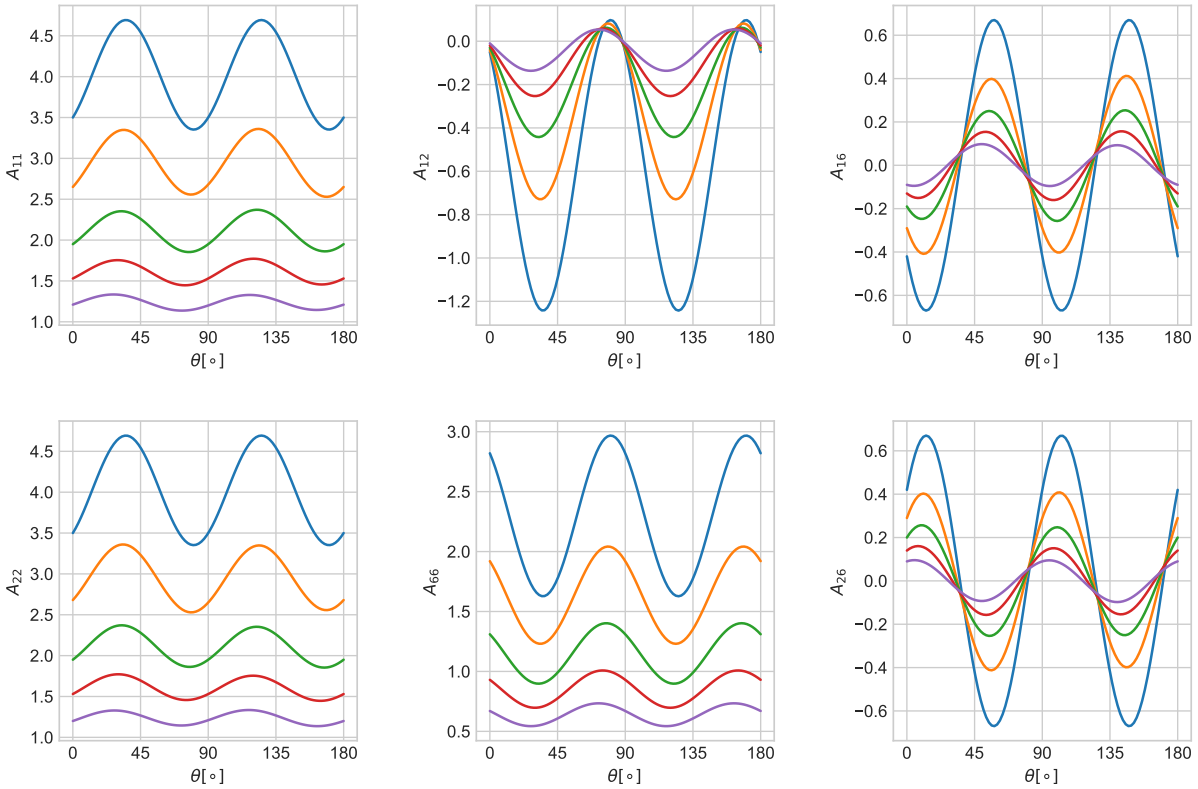

(a) In-plane stiffness components.

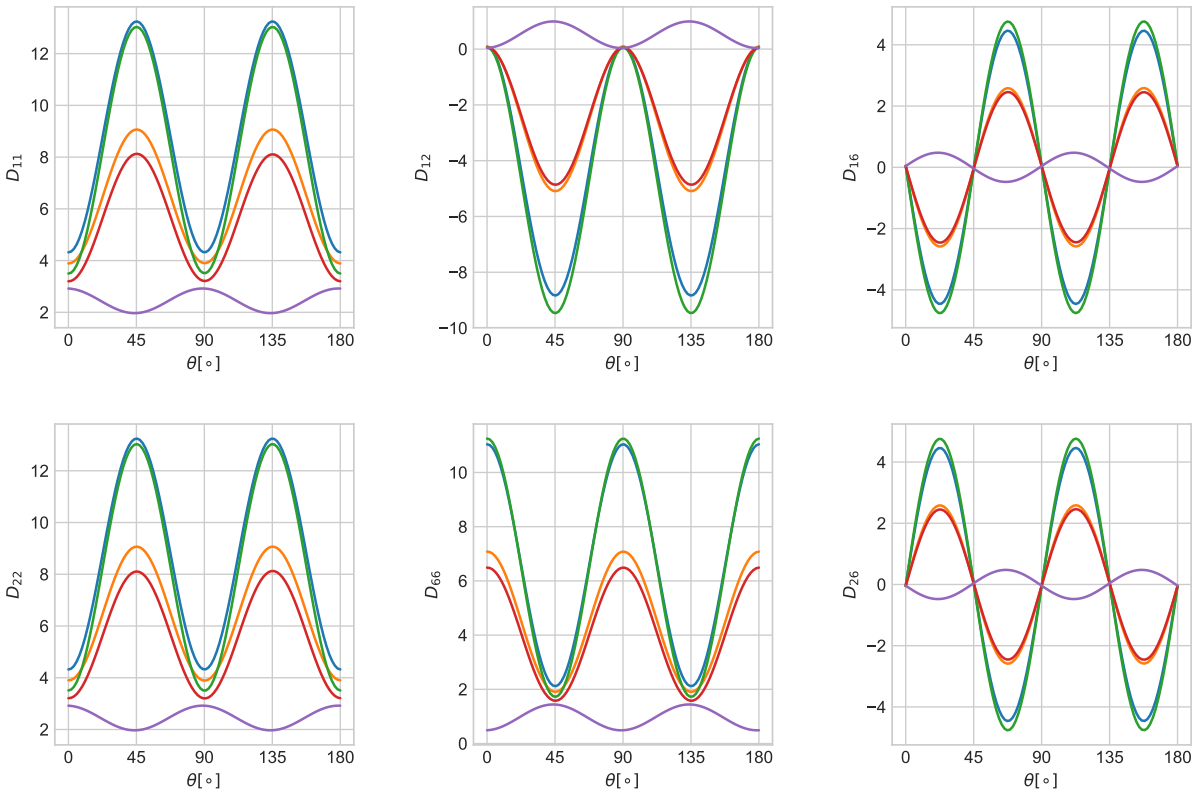

Figure C.10: Anisotropic stiffness components for a *p4 switchback* when flexure length is increased.

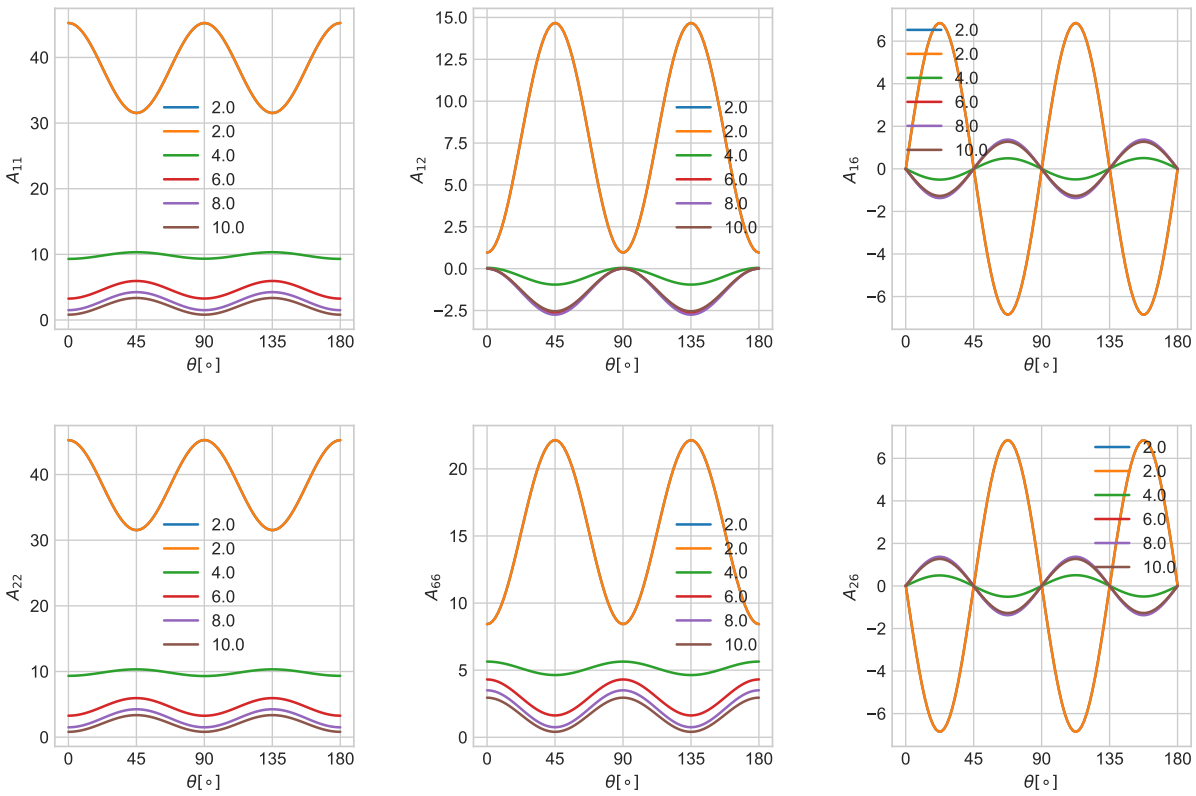

(a) In-plane components.

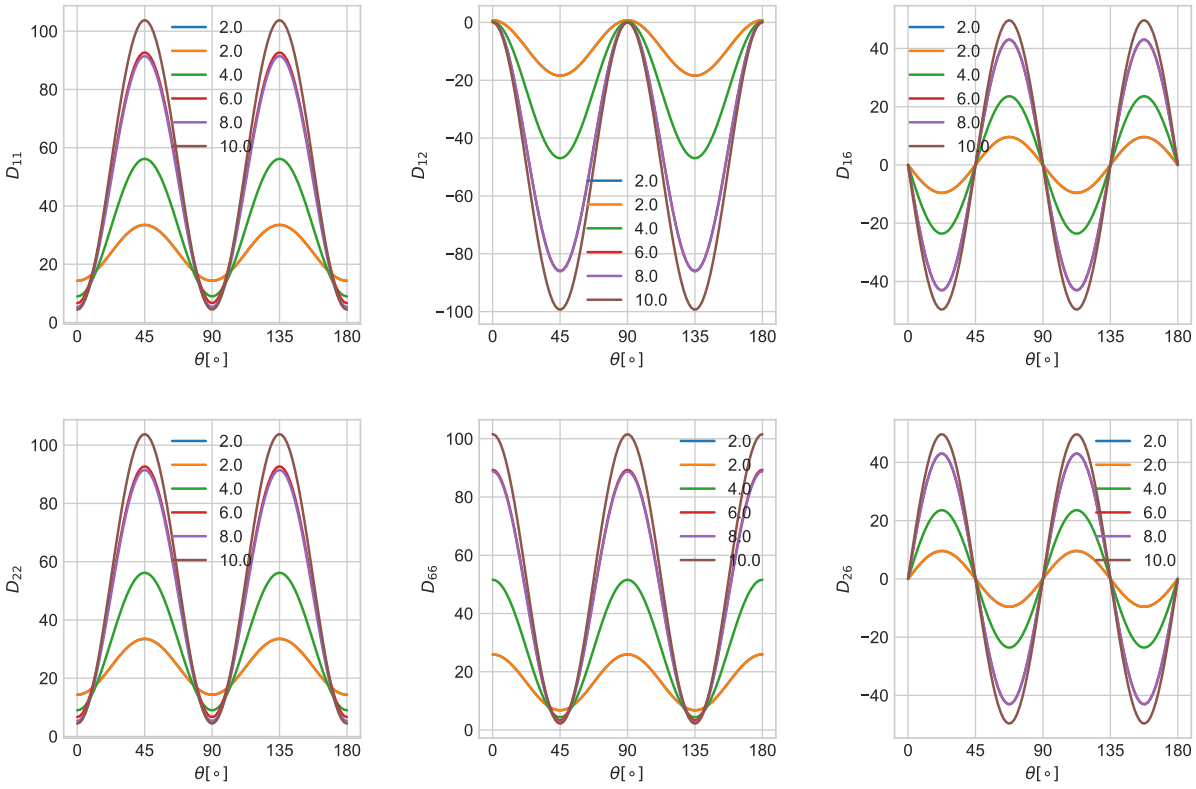

(b) Out-of-plane components.

Figure C.11: Anisotropic stiffness for a *LET p4m* flexure pattern where *flexure length* is increased.

Bibliography

[1] Nathan B. Albrechtsen, Spencer P. Magleby, and Larry L. Howell. "Using Lamina Emergent Mechanisms to Develop Credit-Card-Sized Products". In: 54839 (2011). 10.1115/DETC2011-48420, pp. 223–231. DOI: 10.1115/DETC2011-48420. URL: http://dx.doi.org/10.1115/DETC2011-48420http://proceedings.asmedigitalcollection.asme.org/data/conferences/idetc/cie2011/70657/223_1.pdf.

[2] Hong-Ji Chen and Stephen W. Tsai. "Analysis and Optimum Design of Composite Grid Structures". In: *Journal of Composite Materials* 30.4 (1996), pp. 503–534. ISSN: 0021-9983. DOI: 10.1177/002199839603000405. URL: https://doi.org/10.1177/002199839603000405.

[3] A. P. Cracknell. "Tables of the irreducible representations of the 17 two-dimensional space groups and their relevance to quantum mechanical eigenstates for surfaces and thin films". In: *Thin Solid Films* 21.1 (1974), pp. 107–127. ISSN: 0040-6090. DOI: https://doi.org/10.1016/0040-6090(74)90095-9. URL: http://www.sciencedirect.com/science/article/pii/0040609074900959.

[4] *Dictionary.com the world's leading digital dictionary*. Web Page. 2018.

[5] Juan Carlos Álvarez Elipe and Andrés Díaz Lantada. "Comparative study of auxetic geometries by means of computer-aided design and engineering". In: *Smart Materials and Structures* 21.10 (2012), p. 105004. ISSN: 0964-1726.

[6] H. L. Fan and D. N. Fang. "Anisotropic Mechanical Properties of Lattice Grid Composites". In: *Journal of Composite Materials* 42.23 (2008), pp. 2445–2460. ISSN: 0021-9983. DOI: 10.1177/0021998308095888. URL: https://doi.org/10.1177/0021998308095888.

[7] Patrick Fenner. *Lattice Hinge Design — Minimum Bend Radius*. Web Page. Nov, 9, 2012. URL: https://www.defproc.co.uk/blog/2012/minimum-bend-radius/.

[8] M. L. M. François, L. Chen, and M. Coret. "Elasticity and symmetry of triangular lattice materials". In: *International Journal of Solids and Structures* 129 (2017), pp. 18–27. ISSN: 0020-7683. DOI: https://doi.org/10.1016/j.ijsolstr.2017.09.019. URL: http://www.sciencedirect.com/science/article/pii/S0020768317304298.

[9] Paul Garcia, B. Grunbaum, and G. C. Shephard. "Tilings and Patterns: An Introduction". In: *The Mathematical Gazette* 74.468 (1990), p. 207. ISSN: 00255572. DOI: 10.2307/3619416.

[10] M. G. D. Geers, V. G. Kouznetsova, and W. A. M. Brekelmans. "Multi-scale computational homogenization: Trends and challenges". In: *Journal of Computational and Applied Mathematics* 234.7 (2010), pp. 2175–2182. ISSN: 0377-0427. DOI: https://doi.org/10.1016/j.cam.2009.08.077. URL: http://www.sciencedirect.com/science/article/pii/S0377042709005536https://www.sciencedirect.com/science/article/pii/S0377042709005536?via%3Dihub.

[11] Ruslan Guseinov, Eder Miguel, and Bernd Bickel. "CurveUps: shaping objects from flat plates with tension-actuated curvature". In: *ACM Transactions on Graphics (TOG)* 36.4 (2017), pp. 1–12. ISSN: 0730-0301. DOI: 10.1145/3072959.3073709.

[12] Norman F. M. Henry, Kathleen Lonsdale, and Crystallography International Union of. *International tables for x-ray crystallography : 1 : Symmetry groups*. [3rd edition]. Vol. 1. Birmingham: Kynoch Press, 1969.

[13] Carl T. Herakovich. *Mechanics of fibrous composites*. New York: Wiley, 1998. ISBN: 0471106364.

[14] Larry L. Howell. *Compliant mechanisms*. New York: Wiley, 2001. ISBN: 047138478X.

[15] Joseph O. Jacobsen, Larry L. Howell, and Spencer P. Magleby. "Components for the Design of Lamina Emergent Mechanisms". In: 43041 (2007). 10.1115/IMECE2007-42311, pp. 165–174. DOI: 10.1115/IMECE2007-42311. URL: http://dx.doi.org/10.1115/IMECE2007-42311http://proceedings.asmedigitalcollection.asme.org/data/conferences/imece2007/71573/165_1.pdf.

[16] Joseph O. Jacobsen et al. "Lamina Emergent Mechanisms and Their Basic Elements". In: *Journal of Mechanisms and Robotics* 2.1 (2009). 10.1115/1.4000523, pp. 011003–011003–9. ISSN: 1942-4302. DOI: 10.1115/1.4000523. URL: http://dx.doi.org/10.1115/1.4000523http://mechanismsrobotics.asmedigitalcollection.asme.org/data/journals/jmroa6/27989/011003_1.pdf.

[17] Joseph O. Jacobsen et al. "Lamina Emergent Torsional (LET) Joint". In: *Mechanism and Machine Theory* 44.11 (2009), pp. 2098–2109. ISSN: 0094-114X. DOI: http://dx.doi.org/10.1016/j.mechmachtheory.2009.05.015. URL: http://www.sciencedirect.com/science/article/pii/S0094114X09001116.

[18] J. H. Jang et al. "Combining Pattern Instability and Shape-Memory Hysteresis for Phononic Switching". In: *Nano Letters* 9.5 (2009). Cited By :70 Export Date: 19 February 2018, pp. 2113–2119. DOI: 10.1021/nl9006112. URL: https://www.scopus.com/inward/record.uri?eid=2-s2.0-66449109397&doi=10.1021%2fnl9006112&partnerID=40&md5=19940723c26b56b7be86fcab3b927d2dhttps://pubs.acs.org/doi/pdf/10.1021/nl9006112.

[19] Mina Konaković et al. "Beyond developable: computational design and fabrication with auxetic materials". In: *ACM Transactions on Graphics (TOG)* 35.4 (2016), pp. 1–11. ISSN: 0730-0301. DOI: 10.1145/2897824.2925944.

[20] Robert J Lang et al. "Facilitating Deployable Mechanisms and Structures Via Developable Lamina Emergent Arrays". In: (2016).

[21] Jae-Hwang Lee, Jonathan P. Singer, and Edwin L. Thomas. "Micro-/Nanostructured Mechanical Metamaterials". In: *Advanced Materials* 24.36 (2012), pp. 4782–4810. ISSN: 1521-4095. DOI: 10.1002/adma.201201644. URL: http://dx.doi.org/10.1002/adma.201201644http://onlinelibrary.wiley.com/store/10.1002/adma.201201644/asset/4782_ftp.pdf?v=1&t=jdpugz5m&s=7435d81a690930c355252434dc4e63//onlinelibrary.wiley.com/store/10.1002/adma.201201644/asset/4782_ftp.pdf?v=1&t=jegtac5e&s=001192395bf9d3d2381b5e4d4a741b7ee4eaf587.

[22] Yanping Liu and Hong Hu. "A review on auxetic structures and polymeric materials". In: *Scientific Research and Essays* 5.10 (2010), pp. 1052–1063. ISSN: 1992-2248.

[23] Fulei Ma and Guimin Chen. "Bi-BCM: A Closed-Form Solution for Fixed-Guided Beams in Compliant Mechanisms". In: *Journal of Mechanisms and Robotics* 9.1 (2016). 10.1115/1.4035084, pp. 014501–014501–8. ISSN: 1942-4302. DOI: 10.1115/1.4035084. URL: http://dx.doi.org/10.1115/1.4035084http://mechanismsrobotics.asmedigitalcollection.asme.org/data/journals/jmroa6/935905/jmr_009_01_014501.pdf.

[24] Florian Maurin et al. "Probability that a band-gap extremum is located on the irreducible Brillouin-zone contour for the 17 different plane crystallographic lattices". In: *International Journal of Solids and Structures* 135 (2018), pp. 26–36. ISSN: 0020-7683. DOI: https://doi.org/10.1016/j.ijsolstr.2017.11.006. URL: http://www.sciencedirect.com/science/article/pii/S0020768317305103.

[25] Todd G. Nelson et al. "Material selection shape factors for compliant arrays in bending". In: *Materials and Design* 110 (2016), pp. 865–877. ISSN: 0264-1275. DOI: https://doi.org/10.1016/j.matdes.2016.08.056. URL: http://www.sciencedirect.com/science/article/pii/S0264127516311194https://www.sciencedirect.com/science/article/pii/S0264127516311194?via%3Dihub.

[26] Donald Papp. *3D printing flexible surfaces out of non-flexible material*. Web Page. 2017. URL: https://hackaday.com/tag/living-hinge/.

[27] X. Q. Peng and J. Cao. "A continuum mechanics-based non-orthogonal constitutive model for woven composite fabrics". In: *Composites Part A* 36.6 (2005), pp. 859–874. ISSN: 1359-835X. DOI: 10.1016/j.compositesa.2004.08.008. URL: https://www.sciencedirect.com/science/article/pii/S1359835X04002593?via%3Dihub.

[28] C. P. Quaglia, A. J. Dascanio, and A. P. Thrall. "Bascule shelters: A novel erection strategy for origami-inspired deployable structures". In: *Engineering Structures* 75 (2014), pp. 276–287. ISSN: 0141-0296. DOI: 10.1016/j.engstruct.2014.06.003.

[29] Raymond J. Roark. *Roarks formulas for stress and strain*. 8th ed. New York: McGraw-Hill, 2012. ISBN: 9780071742474.

[30] Enrique Sanchez-Palencia and A. Zaoui. *Homogenization techniques for composite media : lectures delivered at the CISM International Center for Mechanical Sciences, Udine, Italy, July 1-5, 1985*. Vol. 272. Lecture notes in physics. Berlin: Springer, 1987. ISBN: 3540176160 0387176160.

[31] Géry de Saxcé and Claude Vallée. "Invariant Measures of the Lack of Symmetry with Respect to the Symmetry Groups of 2D Elasticity Tensors". In: *Journal of Elasticity* 111.1 (2013), pp. 21–39. ISSN: 1573-2681. DOI: 10.1007/s10659-012-9392-3. URL: https://doi.org/10.1007/s10659-012-9392-3.

[32] Doris Schattschneider. "The Plane Symmetry Groups: Their Recognition and Notation". In: *The American Mathematical Monthly* 85.6 (1978), pp. 439–450. ISSN: 00029890, 19300972. DOI: 10.2307/2320063. URL: http://www.jstor.org/stable/2320063.

[33] Andreas Sebastian. *Mesostrctured cellular materials*. Web Page. URL: http://www.andreasbastian.com/Mesostructured-Cellular-Materials.

[34] Zeming Song et al. "Kirigami-based stretchable lithium-ion batteries". In: *Scientific Reports* 5 (2015), p. 10988. DOI: 10.1038/srep10988https://www.nature.com/articles/srep10988#supplementary-information. URL: http://dx.doi.org/10.1038/srep10988https://www.ncbi.nlm.nih.gov/pmc/articles/PMC4463940/pdf/srep10988.pdf.

[35] George H. Staab. "2 - A review of stress–strain and material behavior". In: *Laminar Composites (Second Edition)*. Butterworth-Heinemann, 2015, pp. 17–36. ISBN: 978-0-12-802400-3. DOI: https://doi.org/10.1016/B978-0-12-802400-3.00002-7. URL: https://www.sciencedirect.com/science/article/pii/B9780128024003000027.

[36] Christian Strobl. "Dimensionally Extended Nine-Intersection Model (DE-9IM)".

[37] M Vianello. "An integrity basis for plane elasticity tensors". In: *Archives of Mechanics* 49.1 (1997), pp. 197–208. ISSN: 0373-2029.

[38] S. Yang, Is Choi, and R. D. Kamien. "Design of super-conformable, foldable materials via fractal cuts and lattice kirigami". In: *MRS Bull.* 41.2 (2016), pp. 130–137. ISSN: 0883-7694. DOI: 10.1557/mrs.2016.5.

[39] Shannon Zirbel et al. "Accommodating Thickness in Origami-Based Deployable Arrays1". In: *Journal of Mechanical Design (Transactions of the ASME)* 135.11 (2013), []–[]. ISSN: 1050-0472. DOI: 10.1115/1.4025372.

[40] Oddvin Agnalt Østmo. *Python code for generating flexure patterns*. Web Page. 2018. URL: https://github.com/oddvinostmo/patterns-code.